

AD-773 025

DESIGN, FABRICATION, AND FLIGHT TEST
OF THE ACTIVE ARM EXTERNAL LOAD
STABILIZATION SYSTEM FOR CARGO
HANDLING HELICOPTERS

J. H. Smith, et al

Boeing Vertol Company

Prepared for:

Army Air Mobility Research and Development
Laboratory

September 1973

DISTRIBUTED BY:

NTIS

National Technical Information Service
U. S. DEPARTMENT OF COMMERCE
5285 Port Royal Road, Springfield Va. 22151

DISCLAIMERS

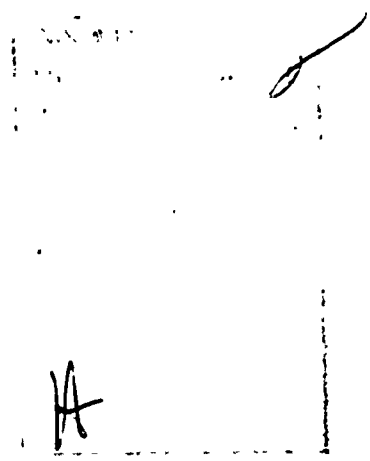
The findings in this report are not to be construed as an official Department of the Army position unless so designated by other authorized documents.

When Government drawings, specifications, or other data are used for any purpose other than in connection with a definitely related Government procurement operation, the United States Government thereby incurs no responsibility nor any obligation whatsoever; and the fact that the Government may have formulated, furnished, or in any way supplied the said drawings, specifications, or other data is not to be regarded by implication or otherwise as in any manner licensing the holder or any other person or corporation, or conveying any rights or permission, to manufacture, use, or sell any patented invention that may in any way be related thereto.

Trade names cited in this report do not constitute an official endorsement or approval of the use of such commercial hardware or software.

DISPOSITION INSTRUCTIONS

Destroy this report when no longer needed. Do not return it to the originator.

A handwritten signature is visible in the lower-left quadrant of the page, consisting of a stylized 'A' and some illegible scribbles. There are also some faint, scattered marks and lines in the upper-left area of the page.

UNCLASSIFIED

Security Classification

AD 773025

DOCUMENT CONTROL DATA - R & D		
(Security classification of title, body of abstract and indexing annotation must be entered when the overall report is classified)		
1. ORIGINATING ACTIVITY (Corporate author)		2a. REPORT SECURITY CLASSIFICATION
Boeing Vertol Company P.O. Box 16858 Philadelphia, Pennsylvania		Unclassified
		2b. GROUP
3. REPORT TITLE		
DESIGN, FABRICATION, AND FLIGHT TEST OF THE ACTIVE ARM EXTERNAL LOAD STABILIZATION SYSTEM FOR CARGO HANDLING HELICOPTERS		
4. DESCRIPTIVE NOTES (Type of report and inclusive dates)		
Final Technical Report		
5. AUTHOR(S) (First name, middle initial, last name)		
J. H. Smith G. M. Allen D. Vensel		
6. REPORT DATE	7a. TOTAL NO. OF PAGES	7b. NO. OF REFS
September 1973	168/170	5
8a. CONTRACT OR GRANT NO.	9a. ORIGINATOR'S REPORT NUMBER(S)	
DAAJ02-72-C-0046	USAAMRDL Technical Report 73-73	
b. PROJECT NO.		
Task 1F163209DB3303		
c.	9b. OTHER REPORT NO(S) (Any other numbers that may be assigned this report)	
d.	D210-10638-1	
10. DISTRIBUTION STATEMENT		
Approved for public release; distribution unlimited.		
11. SUPPLEMENTARY NOTES		12. SPONSORING MILITARY ACTIVITY
		Eustis Directorate, U. S. Army Air Mobility R&D Laboratory Fort Eustis, Virginia
13. ABSTRACT		
<p>This report discusses the analysis, design, fabrication, and flight test of an experimental Active Arm External Load Stabilization System (AAELSS). The purpose of this effort was to achieve the load damping required for helicopter instrument flight rules (IFR) operations (load modal damping ratio greater than 0.25) without imposing excessive power requirements on the helicopter subsystems or unsafe conditions on the helicopter. Flight test of the system on the Boeing Model 347 helicopter demonstrated adequate load dynamic stability characteristics and elimination of pilot-induced oscillation throughout the test flight envelope. Specifically, the AAELSS increased the load pendular damping ζ from a value of 0.05 (system off) to 0.3, which is three times the minimum required by MIL-H-8501A for IFR operation. Also, as part of this effort, a number of system design improvements were identified for eventual incorporation in a production system to be used on a variety of cargo handling helicopters.</p>		
<p>NATIONAL TECHNICAL INFORMATION SERVICE 11 Springfield, VA 22151</p>		

DD FORM 1473

NOV 68

ia

UNCLASSIFIED

Security Classification

UNCLASSIFIED
Security Classification

14. KEY WORDS	LINK A		LINK B		LINK C	
	ROLE	WT	ROLE	WT	ROLE	WT
active arm external load stabilization cargo handling helicopter cargo helicopter IFR flight load stabilization IFR cargo handling						

UNCLASSIFIED
Security Classification

10457-73



DEPARTMENT OF THE ARMY
U. S. ARMY AIR MOBILITY RESEARCH & DEVELOPMENT LABORATORY
EUSTIS DIRECTORATE
FORT EUSTIS, VIRGINIA 23604

This report was prepared by the Boeing Company, Vertol Division under the terms of Contract DAAJ02-72-C-0046. It documents a program of design, fabrication, and flight test of an experimental Active Arm External Load Stabilization System (AAELSS).

The objective of this program was to evaluate the AAELSS concept as a viable method of eliminating pilot-induced oscillation and thus enable unimpaired IFR operation of helicopters with external cargo loads. The system was also evaluated with respect to external load damping in all helicopter flight modes.

The conclusions and recommendations contained herein are concurred in by this Directorate.

The technical monitors for this contract were Thomas B. Allardice of the Systems Support Division and Richard E. Lane of the Military Operations Technology Division.

ie/

Task 1F163209DB3303
Contract DAAJ02-72-C-0046
USAAMRDL Technical Report 73-73
September 1973

DESIGN, FABRICATION, AND FLIGHT TEST OF THE
ACTIVE ARM EXTERNAL LOAD STABILIZATION
SYSTEM FOR CARGO HANDLING HELICOPTERS

Final Report

D210-10638-1

By

J. H. Smith
E. M. Allen
D. Vensel

Prepared by

Boeing Vertol Company
(A Division of The Boeing Company)
Philadelphia, Pennsylvania

for

EUSTIS DIRECTORATE
U.S. ARMY AIR MOBILITY RESEARCH AND DEVELOPMENT LABORATORY
FORT EUSTIS, VIRGINIA

Approved for public release;
distribution unlimited.

SUMMARY

This report discusses the analysis, design, fabrication, and flight test of an experimental Active Arm External Load Stabilization System (AAELSS). The purpose of this effort was to achieve the load damping required for helicopter instrument flight rules (IFR) operations (load modal damping ratio greater than 0.25) without imposing excessive power requirements on the helicopter subsystems or unsafe conditions on the helicopter. Flight test of the system on the Boeing Model 347 helicopter demonstrated adequate load dynamic stability characteristics and elimination of pilot-induced oscillation throughout the test flight envelope. Specifically, the AAELSS increased the load pendular damping ζ from a value of 0.05 (system off) to 0.3, which is three times the minimum required by MIL-H-8501A for IFR operation. Also, as part of this effort, a number of system design improvements were identified for eventual incorporation in a production system to be used on a variety of cargo handling helicopters.

FOREWORD

The results of the work reported herein conclusively establish the technical and operational feasibility of the Active Arm External Load Stabilization System (AAELSS) for cargo handling helicopters.

This work was performed by the Boeing Vertol Company, Philadelphia, Pa., for the U. S. Army Air Mobility Research and Development Laboratory, Eustis Directorate, Fort Eustis, Va., under Contract DAAJ02-72-C-0046, Task 1F163209DB3303, during the period 14 April 1972 through 11 December 1972.

The Army technical representatives were Mr. T. Allardice and Mr. R. Lane. The contributions of Army personnel to this effort are gratefully acknowledged.

The following Boeing Vertol personnel contributed to this program:

Mr. B. B. Blake and Mr. W. W. Walls	Program Managers
Mr. E. M. Allen	Project Manager
Mr. J. H. Smith	Project Engineer
Mr. R. M. Richmond	Flight Test Project Engineer
Mr. A. J. Hutto	HLH Project Pilot
Mr. D. McGettigen	Test Engineering
Mr. H. Gantz	Systems Engineer
Mr. D. Vensel	Flying Qualities Engineer

The work accomplished by the ground crew, manufacturing personnel, and others in support of the flight operations must be mentioned because without their spirit of getting the job done the test goal could not have been accomplished.

TABLE OF CONTENTS

	<u>Page</u>
SUMMARY	iii
FOREWORD.	v
LIST OF ILLUSTRATIONS	ix
LIST OF TABLES.	xiii
LIST OF SYMBOLS	xiv
INTRODUCTION	1
TECHNICAL APPROACH	4
Objective	4
Concept	4
Development Program	6
Problem Definition	7
SYSTEM DESCRIPTION	12
Design	12
Servo Control System	15
Sling Configuration	18
Hardware Description	18
THEORETICAL ANALYSIS	24
Control Laws Studies Using Simplified Model	24
Hardware Sizing	30
Hybrid Math Model	34
Simulation	54
FLIGHT TEST PROGRAM PREPARATION	73
Aircraft Configuration.	73
Flight Test Plan.	75
Safety-of-Flight Review	75
Laboratory and Preliminary Helicopter Tests	78
Instrumentation and Recorded Data	81
FLIGHT TEST RESULTS	84
Scope of Tests and Data Format.	86
AAELSS Damping Characteristics.	88
AAELSS Failure Testing.	111
Longitudinal Pilot-Induced Oscillation.	114

	<u>Page</u>
Command Augmentation	118
Experimental AAELSS Weight	118
Hydraulic Power Requirements	121
Prototype AAELSS Limitations	121
CONCLUSIONS	125
RECOMMENDATIONS	127
LITERATURE CITED	129
APPENDIXES	
I. Flight Test Log	130
II. Pilot Comments from Active External Load Stabilization Flight Test Program	138
III. Load Stabilization System Problems.	147
DISTRIBUTION	151

LIST OF ILLUSTRATIONS

<u>Figure</u>		<u>Page</u>
1	Active Arm External Load Stabilization System on Boeing Model 347	3
2	Load Stabilization System	5
3	Dual Hook External Load VFR Flight Limits	8
4	External Load Dynamics	11
5	AAELSS Installation	13
6	Arm Details	14
7	General Control Block Diagram	16
8	Typical Actuator Controls	17
9	Basic Sling Configuration	19
10	Beam Installation	20
11	Beam Restraints	23
12	Simple Pendulum Model	25
13	First Control Law	26
14	Sling Load Stability of First Control System, Fixed Airframe	27
15	Controller Selected for Study	28
16	Load Stabilization System Dynamic Stability, Fixed Airframe, Hover, Time-Constant Sensitivity	29
17	Load Stabilization System Dynamic Stability, Fixed Airframe, Hover, Gain Sensitivity	31
18	Load Stabilization System Dynamic Stability, Fixed Airframe, Hover, 50-Foot Riser	32
19	Limits of Linear Operation	33
20	Side View of External Load Free-Body Diagram (Longitudinal Axis)	35
21	Rear View of External Load Free-Body Diagram (Lateral Axis)	36

<u>Figure</u>		<u>Page</u>
22	Directional Moments on Load (Top View)	37
23	Side View of Suspension	38
24	Spreader Bar Forces	40
25	Airframe and Arm Forces	41
26	Lateral Suspension Geometry	42
27	Directional Displacement Diagram	43
28	Riser/Arm Directional Displacement Diagram.	44
29	Normalized Wind Axis Data Lift and Side Force (f_1) on 8x8x20-Foot Smooth Container	47
30	Normalized Wind Axis Data Drag Force (f_2) on 8x8x20-Foot Smooth Container	47
31	Normalized Wind Axis Data Pitching and Yawing Moment (f_3) on 8x8x20-Foot Smooth Container	48
32	Axis for Application of Aerodynamic Forces and Moments to Sling Load	49
33	Longitudinal Arm Controller	53
34	Lateral-Directional Arm Controller	55
35	Longitudinal Arm Control System Hardovers	57
36	Lateral Arm Control System Hardovers	59
37	Right Failure of Forward Lateral Arm at 60 Knots	60
38	Longitudinal Response to 0.1 Foot Displacement in Hover	62
39	External Load Response to Yaw Moment	63
40	Helicopter Response for Various Gains	64
41	Computed Response to Airframe Step Displacement	69

<u>Figure</u>	<u>Page</u>
42 Higher-Order Controller	70
43 AAELSS Mounted on Laboratory Test Stand	79
44 Summary of Load Damping Characteristics	85
45 Angles Describing Load Motion	87
46 Longitudinal Damping With AAELSS Off, Empty MILVAN	89
47 Yaw Damping With AAELSS Off, Empty MILVAN	90
48 Roll Damping With AAELSS On, Empty MILVAN	91
49 Longitudinal Damping With AAELSS On, Empty MILVAN	92
50 Lateral-Directional Damping With AAELSS On, Empty MILVAN	94
51 Yaw Damping With AAELSS Off, Loaded MILVAN.	95
52 Longitudinal Damping With AAELSS On, Loaded MILVAN	96
53 Longitudinal Damping With Large Lag Time Constant	98
54 Longitudinal Damping With 58-Foot Riser, AAELSS Off	100
55 Lateral Damping With 58-Foot Riser, AAELSS Off	101
56 Longitudinal Damping With 58-Foot Riser, AAELSS on Low Gain	102
57 Longitudinal Damping With 58-Foot Riser, AAELSS on High Gain	103
58 Lateral Damping With 58-Foot Riser, AAELSS On	104
59 Lateral Stability at 60 Knots With AAELSS Off, Empty MILVAN	106
60 Yaw Oscillation With AAELSS Off	107
61 Longitudinal Pilot-Induced Oscillation, Loaded MILVAN	109

<u>Figure</u>		<u>Page</u>
62	AAELSS Stops Sustained Oscillations of Loaded MILVAN	110
63	Lateral Oscillation With AAELSS On, Empty MILVAN. .	112
64	Single-Arm Oscillation, Loaded MILVAN	113
65	Yaw Actuator Failure at 80 Knots, Empty MILVAN . .	115
66	Longitudinal Damping With AAELSS On, Loaded MILVAN.	116
67	Yaw Actuator Failure, Loaded MILVAN	117
68	Normal Control Augmentation Gain	119
69	Roll Command Augmentation With 58-Foot Riser . . .	120
70	AAELSS-On Oscillation	122
71	Nonlinear Damping	123

LIST OF TABLES

<u>Table</u>		<u>Page</u>
I	Angular Travel Limits	23
II	Fixed Parameters for Hybrid Model	56
III	Hardware Sizing Requirements	71
IV	Model 347 Active Load Stabilization Program, Basic Aircraft Configuration	74
V	Test Configurations	76
VI	Simulated AAELSS Failures	77
VII	AAELSS Flight Test Data Acquisition	83
VIII	Damping/Time Constant Trends, Longitudinal Axis	97
IX	Model 347 Flight Configuration Log	131
X	Test Conditions for Flight 660	132
XI	Test Conditions for Flight 660A	133
XII	Test Conditions for Flights 661, 661A, and 661B .	134
XIII	Test Conditions for Flight 662	135
XIV	Test Conditions for Flight 663	136
XV	Test Conditions for Flight 664	137

LIST OF SYMBOLS

A	angle between front leg and load top, rad
B	angle between rear leg and load top, rad
d_B	distance from spreader bar to load cg, ft
d_p	distance from aircraft cg to arms, ft
Drag	rearward aerodynamic force on load, lb
e	chord of directionally displaced sling load, rad
f_1	lift and side force data from charts
f_2	drag data from charts
f_3	pitch and yaw moment data from charts
F_{BZ_F}	vertical force on front of spreader bar, lb
F_{BZ_R}	vertical force on rear of spreader bar, lb
F_{XA}	longitudinal aircraft body-axis force due to sling load, lb
F_{YA}	lateral aircraft body-axis force due to sling load, lb
F_{ZA}	vertical aircraft body-axis force due to sling load, lb
F_{XL}	total longitudinal force on load in earth axis, lb
F_{YL}	total lateral force on load in earth axis, lb
F_{ZL}	total vertical force on load in earth axis, lb
F_{ZLF}	vertical tension on front riser assuming no roll, lb
F_{ZLR}	vertical tension on rear riser assuming no roll, lb
g	acceleration of gravity, ft/sec ²
h	height of load, ft
I	longitudinal riser angle relative to aircraft, rad
I_x	longitudinal pitching inertia of load, lb
I_y	longitudinal rolling inertia of load, lb

I_z	longitudinal yawing inertia of load, lb
J	longitudinal arm angle relative to aircraft, rad
K	average lateral arm angle relative to aircraft, rad
K_i	$i = 1, 2, 3$ gains defined on block diagrams (dimensionless)
K_F	angle of front lateral arm relative to aircraft, rad
K_R	angle of rear lateral arm relative to aircraft, rad
K_G	longitudinal controller gain (dimensionless)
K_{IF}	lateral front controller gain (dimensionless)
K_{IR}	lateral rear controller gain (dimensionless)
$K\Delta_S$	gain from pilot's lateral stick to lateral arm motion, rad/in.
$K\Delta_R$	gain from pilot's directional stick to lateral arm motion, rad/in.
L_{CG}	aircraft body-axis rolling due to sling load, lb
Lift	load upward aerodynamic force, lb
L_{IM}	longitudinal angle between riser and arms which causes hydraulic bypass, rad
L_P	total rolling moment at arm attachment point, ft-lb
L_{PF}	rolling moment at front arm attachment point, ft-lb
L_{PR}	rolling moment at arm attachment point, ft-lb
L_{ZF}	lateral angle between riser and front arm which causes hydraulic bypass, rad
L_{ZR}	lateral angle between riser and rear arm which causes hydraulic bypass, rad
l_B	length of spreader bar, ft
l_{CF}	length of front leg, ft
l_{CR}	length of rear leg, ft
l_L	effective pendulum length, ft

L_{PL}	arm torque lateral limit, ft-lb
l_P	length of arms, ft
l_F	length of load, ft
M	mass of load, $\frac{\text{ft-sec}^2}{\text{lb}}$
M_{PL}	sum of torque limits of longitudinal arms, ft-lb
l_S	length of riser, ft
N_A	load yaw-right aerodynamic moment, ft-lb
N_{PL}	cable torque on load, ft-lb
P	longitudinal (I-J) relative cable angle, rad
Q	torque applied to arm by actuator, ft-lb
q	load dynamic pressure, lb/ft ²
R	lateral (U-K) relative cable angle, rad
Side Force	load rightward aerodynamic force, lb
T_F	front leg tension, lb
Torque	load pitch-up aerodynamic moment, ft-lb
T_R	rear leg tension, lb
u	helicopter longitudinal velocity, ft/sec
U	average lateral riser angle relative to aircraft, rad
U_F	front lateral riser angle relative to aircraft, rad
U_R	rear lateral riser angle relative to aircraft, rad
u_L	load body-axis longitudinal velocity, ft/sec
v_L	load body-axis lateral velocity, ft/sec
w_L	load body-axis vertical velocity, ft/sec
v	helicopter lateral velocity, ft/sec
V	total air velocity, ft/sec
w	helicopter vertical velocity, ft/sec

X_B	longitudinal earth-axis position of aircraft, ft
Y_B	lateral earth-axis position of aircraft, ft
Z_B	vertical earth-axis position of aircraft, ft
X_L	load earth-axis longitudinal displacement, ft
Y_L	load earth-axis lateral displacement, ft
Z_L	load earth-axis vertical displacement, ft
X_R	longitudinal position of load in aircraft body-axis, ft
Y_R	lateral position of load in aircraft body-axis, ft
Z_R	vertical position of load in aircraft body-axis, ft
X_{RE}	relative longitudinal earth-axis position of load to aircraft, ft
Y_{RE}	relative lateral earth-axis position of load to aircraft, ft
Z_{RE}	relative vertical earth-axis position of load to aircraft, ft
\bar{Z}	radius of gyration of load about its vertical axis, ft
α	angle of imaginary screw thread analogy, rad
α_L	load angle of attach, rad
β_L	load sideslip angle, rad
γ	lateral riser angle, rad
δ_B	longitudinal control stick displacement, in.
δ_S	lateral control stick displacement, in.
δ_R	directional pedal displacement, in.
θ	aircraft pitch euler attitude, rad
θ_L	load pitch euler attitude (relative to aircraft), rad
τ_i	$i = 1, 2, 3$ time-constants defined in block diagram
τ_G	longitudinal controller lag time constant, sec
τ_{WG}	longitudinal controller washout time constant, sec

τ_{Lag}	lag-time time constant (general), sec
$\tau_{\delta R}$	lag time constant in directional stick to arm controller, sec
τ_{IF}	lateral front controller lag time constant, sec
τ_{WIF}	lateral front controller washout time constant, sec
τ_{IR}	lateral rear controller lag time constant, sec
τ_{WIR}	lateral rear controller washout time constant, sec
τ_{WO}	washout time constant (general), sec
ϕ	aircraft roll euler attitude, rad
ϕ_L	load roll euler attitude, rad
ψ	aircraft yaw euler attitude, rad
ψ_L	load yaw euler attitude, rad
ψ_P	load yaw angle due to arm motion, rad
ψ_X	yaw angle of sling load relative to aircraft, rad

INTRODUCTION

In the history of helicopters carrying cargo externally, a need has been established for an effective load stabilization system to allow instrument flight rules (IFR) operations, to improve load placement capability, and to increase aircraft productivity and safety.

Most of the commonly transported external loads exhibit poor dynamic stability, which arises from an aerodynamic static instability of the load or from low damping of the load-suspension system. These dynamic instabilities are manifested during flight operations and are known to cause one or more of the following cargo handling operational limitations:

- Restriction of the maximum airspeed to a value below the power-limited airspeed due to the promotion of large-amplitude load displacements
- Excessive time requirements for accurate positioning or placement of the load due to poor system damping (precision hovering)
- Degradation of operations by introducing disorienting or false motion cues to the pilot that create the environment for persistent pilot-induced oscillation (PIO) and inferior handling qualities

Thus, the overall result of load instability is a usable operational capability which is less than the inherent performance potential of the helicopter system.

A variety of load stabilization schemes have been considered in the past in order to reduce or eliminate the undesirable dynamic instabilities of externally slung loads. Among these are the addition of load stabilizing appendages such as drogues and fins, special load suspension rigging arrangements, and the automatic control of the helicopter itself. Each of these schemes is, in some measure, limited to a particular load geometry or a particular helicopter and as such is not well suited for general application. That is, most appendage additions are generally tailored for specific external loads, most suspension arrangements are designed for selected vehicles and loads, and automatic load control by means of the helicopter itself generally involves a control subsystem designed for application to one specific air vehicle.

A solution to these limitations was sought that would not only improve external load modal damping, provide the pilot command control augmentation of the load, and minimize PIO tendencies, but would also be universally adaptable to a wide variety of helicopters.

This system, known as the Active Arm External Load Stabilization System (AAELSS), basically consists of actuator-driven rigid pendants or arms attached to an auxiliary beam mounted in the helicopter, suitable pendant and cable position sensors and the associated electronics, and electrohydraulic control systems. In a disturbed mode, the arm and cable angular positions are sensed by synchro sensors, and a corrective control signal is sent electronically to the actuators which damp the load motion by moving the rigid pendants that attach the flexible riser and the load. The overall arrangement of the AAELSS as mounted on the Boeing Model 347 helicopter is presented in Figure 1.

This report presents the technical approach used in the development of this system, a detailed description of the system, a theoretical analysis, the flight test program, and a discussion of the test data. Conclusions from this study and recommendations for future improvements are also included.

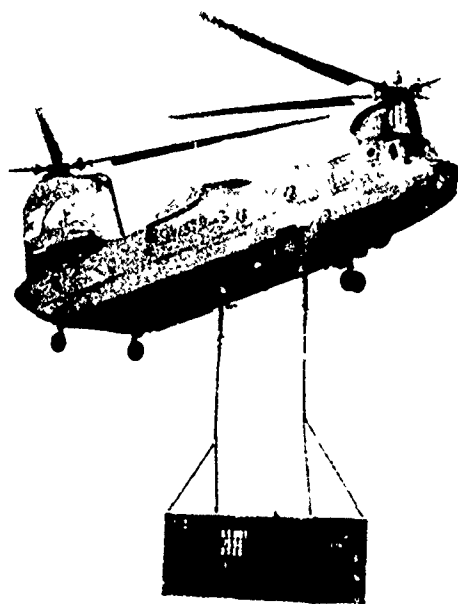


Figure 1. Active Arm External Load Stabilization System on Boeing Model 347.

TECHNICAL APPROACH

OBJECTIVE

This development was undertaken in order to prove that the damping afforded by the AAELSS was the solution to the problems associated with external load operations. The objective was to achieve the load damping required for helicopter IFR flight operations without imposing excessive power requirements on the helicopter subsystem or unsafe conditions. A 0.25 damping ratio was chosen as a design target.

CONCEPT

Additional details of the concept chosen for demonstrating the AAELSS are illustrated in Figure 2. It is a further development of the dual-tandem-hook suspension, which had improved load stability over a single-point suspension by adding yaw restraint.

The external load used in the analysis and test was an 8x8x20-foot MILVAN container suspended on conventional nylon slings that were in turn attached to the two cargo hooks. To apply damping action to the load, an automatic control was developed which detected sling motion from the riser and arm angle sensors, processed these signals, and forced the load by moving the arm (rigid pendants) via the actuators indicated. Both the arms and the cargo hook at the ends of the arms were mounted on universal joints that were fixed in yaw but had longitudinal and lateral freedom.

External load modes of motion are conveniently described as being longitudinal, lateral, and directional. Longitudinal motion is defined as the fore and aft swinging of the load and arms, lateral motion by the sideward swinging of the load and arms, and directional motion by a yawing of the load or a differential sideward displacement of the arms. The kinematics of the design were selected to prohibit any inter-axis mechanical cross-coupling between the longitudinal and lateral actuator motions.

With the exception of power supplies, there are four separate control subsystems, one for each actuator. The two longitudinal subsystems are duplicate and parallel in their action. The control law for each of the control subsystems is the same. It functions to detect the load position by the riser (hook or cable) angle and commands the arm to exert a force on the load, and thereby provides load damping. The front and rear lateral actuator controls are independent, but by virtue

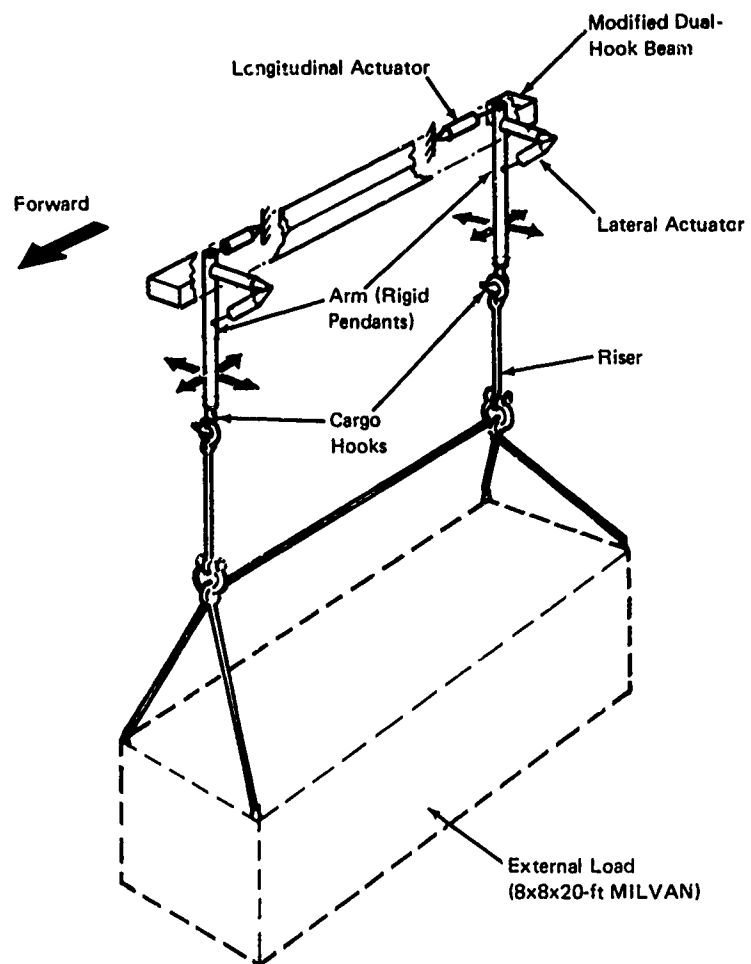


Figure 2. Load Stabilization System.

of the mechanical restraint of the slings, their control systems act to damp both the lateral and directional motions of the load. A large part of this development program dealt with configuring the control system to provide design damping levels while prohibiting any possibility of instability.

DEVELOPMENT PROGRAM

This program was constructed to provide a flight test demonstration of the AAELSS using the Boeing Model 347 helicopter as the test vehicle. The activities of this program logically fall into five categories: analysis, design, fabrication, laboratory testing, and flight testing.

Equations were derived to define load motions, and analytical models of the AAELSS were developed and used to determine the system control laws. Analytical effort then concentrated on assessing AAELSS performance characteristics, sensitivity to load mass, arm length, sling length, actuator size and servo-valve size. Results from this parametric study were used to establish safety criteria and safety limits. Finally, analyses were performed to compare AAELSS performance with other load stabilization concepts.

The AAELSS design utilized an existing dual-tandem-hook load beam mounted on the Model 347 helicopter by the standard CH-47C cargo hook. Quick-disconnect fittings were installed in the electrical and hydraulic lines running between the helicopter and load beam. All the emergency jettison features of the CH-47C cargo hook system were retained to permit positive emergency jettisoning of the AAELSS components external to the fuselage. The existing load beam was modified for the AAELSS installation to permit proof of AAELSS feasibility without extensive component development.

Laboratory tests of the complete AAELSS, less the aircraft power supplies, were conducted to adjust and calibrate the electronic and hydraulic units. These tests also served to check out the total system and verify its proper functioning prior to flight.

Flight test preparations consisted of formulating and documenting a plan for the flight test phase of activity, and the conduct of a formal safety-of-flight review. Subsequently, flight testing of the AAELSS was conducted with the Model 347 helicopter over the speed range from hover to the maximum safe forward-flight airspeed. Data recorded included pilot commentary, ground and airborne motion pictures, and oscillograph time histories of the system dynamics. The flying was done with two container weights and two sling lengths, and included simulated failures and parametric

variations of system gains and time constants at each test configuration.

PROBLEM DEFINITION

There has been an evolution in helicopter external cargo handling that will eventually lead to operations with external loads at power-limit airspeeds and in IFR conditions. Initially, helicopter cargo delivery was accomplished using a single-point cargo hook system. The CH-47 is a typical example. This system allows VFR flight to power-limit speeds with high-density loads such as ammunition stacks, artillery pieces, or petroleum products. Low-density loads, such as the empty MILVAN, encounter aerodynamic instability which causes large and uncontrolled motions of the load. On single-point sling rigging, an empty 8x8x20-foot MILVAN limits helicopter airspeed to approximately 40 knots, since beyond that, large load motions interfere with control of the helicopter.¹ The poor cargo handling economics resulting from this speed restriction focused attention on improving productivity and aircraft utilization by increasing external load stability to permit operations at higher cruising speeds.

One step in this direction was the dual tandem cargo hook system, which has been extensively tested. Even with its tremendous potential, the dual hook system still imposes certain limitations on maximum acceptable airspeed (see Figure 3). For example, the level-rigged 5000-pound MILVAN load sustained yaw oscillations even with 24-foot separation of the risers. It was subsequently established that a nosedown rigging of the load using the sling leg arrangement shown in the figure provided considerably better load stability and allowed satisfactory operation to 120 knots for the 7.5-foot riser. The nosedown attitude rigging was used in all other data presented in Figure 3. Although a speed of 120 knots was obtained with a 12-foot riser separation on the CH-47, the Model 347 was limited to about 75 knots due to a lateral pilot-induced oscillation (PIO) tendency. This PIO tendency suggests a problem stemming from a lateral stick pickoff in the SAS in which riser length has a pronounced effect on load stability. Any increase in riser length reduces the system yaw stiffness and hence its stability. This effect is exemplified in Figure 3, where 50 knots was the limit for the uncontrolled 50-foot riser sling load. Certain AAELSS program results are noted in Figure 3 to illustrate that testing did not exceed the sling failure limit line. Flight at airspeeds above this limit line risk load-airframe collision in the event of a riser or sling leg failure. The limit shown was established from wind tunnel test experience cited in Reference 2. Sling failures are worse with light weights, where the gravity force is less influential in counteracting the aerodynamic disturbing forces. The results

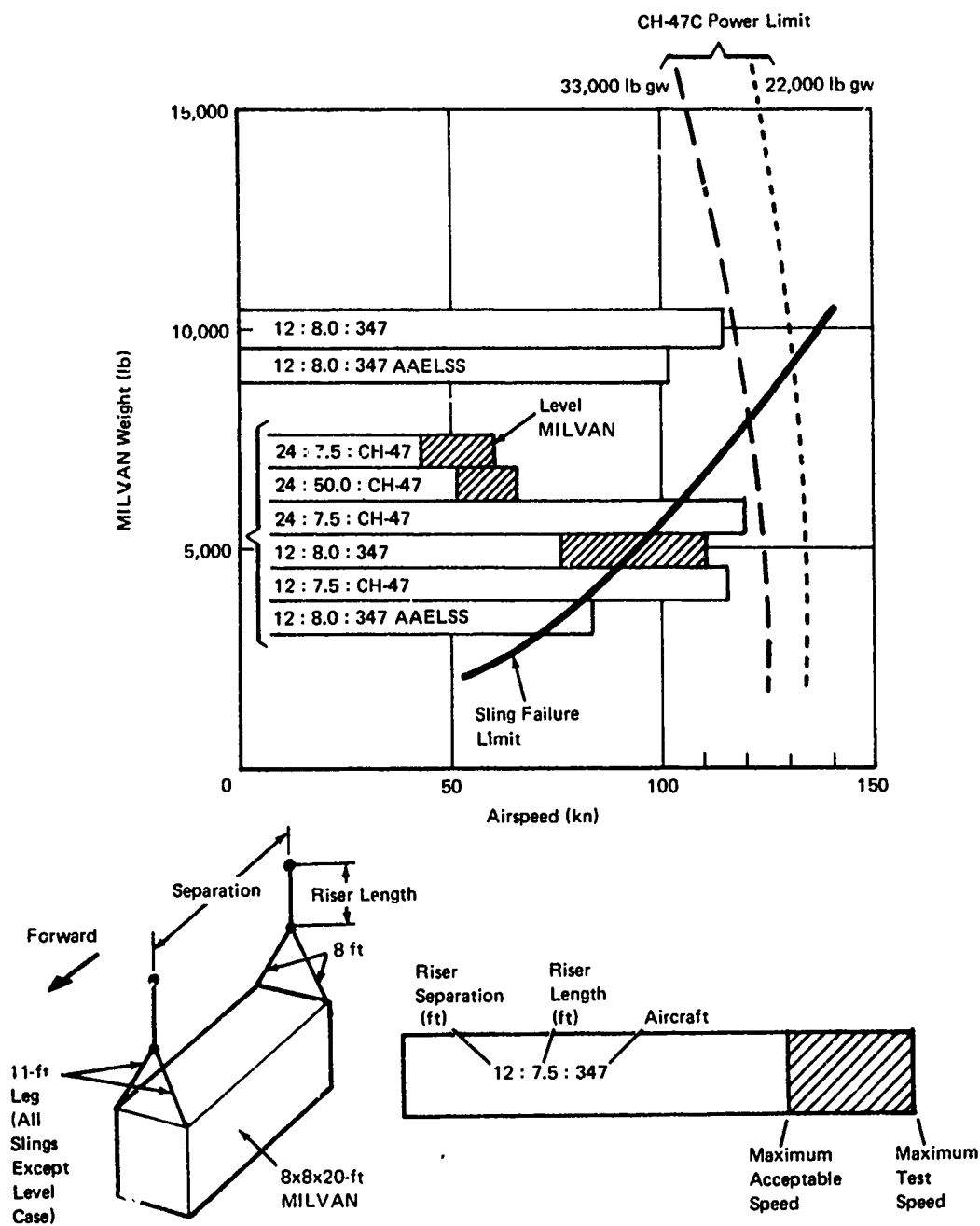


Figure 3. Dual Hook External Load VFR Flight Limits.

given in Figure 3 do not show any limitations due to longitudinal PIO problems; they impose limitations only under IFR conditions.

The boundaries of Figure 3 were established by pilot comment and generally resulted from a condition of sustained oscillation or neutral stability. The first real quantitative look at stability data occurred on the Model 347 as reported in Reference 3 and plotted in Figure 4. Characteristic frequency and damping ratio are shown for the external loads without load stabilization. The data apply largely to the longitudinal axis, although similar data are available for the lateral axis. Lines indicated by the bold letters IFR and VFR are the MIL-H-8501A flying qualities specification for dynamic stability requirements. Specification compliance requires that the data points in Figure 4 fall to the left of the respective requirements lines.

Figure 4 shows that the VFR requirements are met in hover and forward flight. IFR compliance, however, does not exist except at the highest airspeed with the heavy load. Even though the VFR flying qualities specification is satisfied, it is important to recognize that inefficient operations may still exist. For example, in a precision hover task with a 50-foot riser (having a 0.035 damping ratio), 30 seconds is required for a disturbance to decay to half amplitude. This test data also points out that the load weight has little influence on stability for either the 8-foot or the 50-foot riser. Further, no matter what changes were made in rigging riser lengths, the damping ratio remained about 0.05 and increased only when aerodynamic damping became significant at high airspeeds.

In summary, it appears that there are three categories of existing external load operational problems which could benefit from the use of an active arm external load stabilization system. These improvements, which are needed even with the additional benefits offered by a dual tandem hook, are:

- Precision hover
- External sling load instabilities in forward flight resulting from aerodynamic causes even with controls fixed
- Inability to operate IFR or at high speeds due to longitudinal and lateral pilot-induced oscillations that do not exist stick-fixed

The precision hover tasks without load stabilization are complicated by the light damping and by the ease with which the pilot causes undesirable motions of the load. Typical missions in which this would occur are: loading MILVANS into and

out of container ships, bridge placement, stacking of MILVANS, and erection of elements for construction.

Forward-flight instabilities, which are usually evidenced as roll or roll-yaw oscillations, develop to various degrees depending on load attitude and general rigging arrangement. They are especially critical for empty MILVAN containers. They force a significant reduction in airspeed and therefore lower the operational productivity of the helicopter.

In the past, the PIO problem has been dominantly a longitudinal one and was a serious problem only when going into IFR conditions. There has been a minor lateral PIO problem with the Model 347-type flight control system seemingly attributable to the stick pickoff/bank angle hold circuitry peculiar to that aircraft.

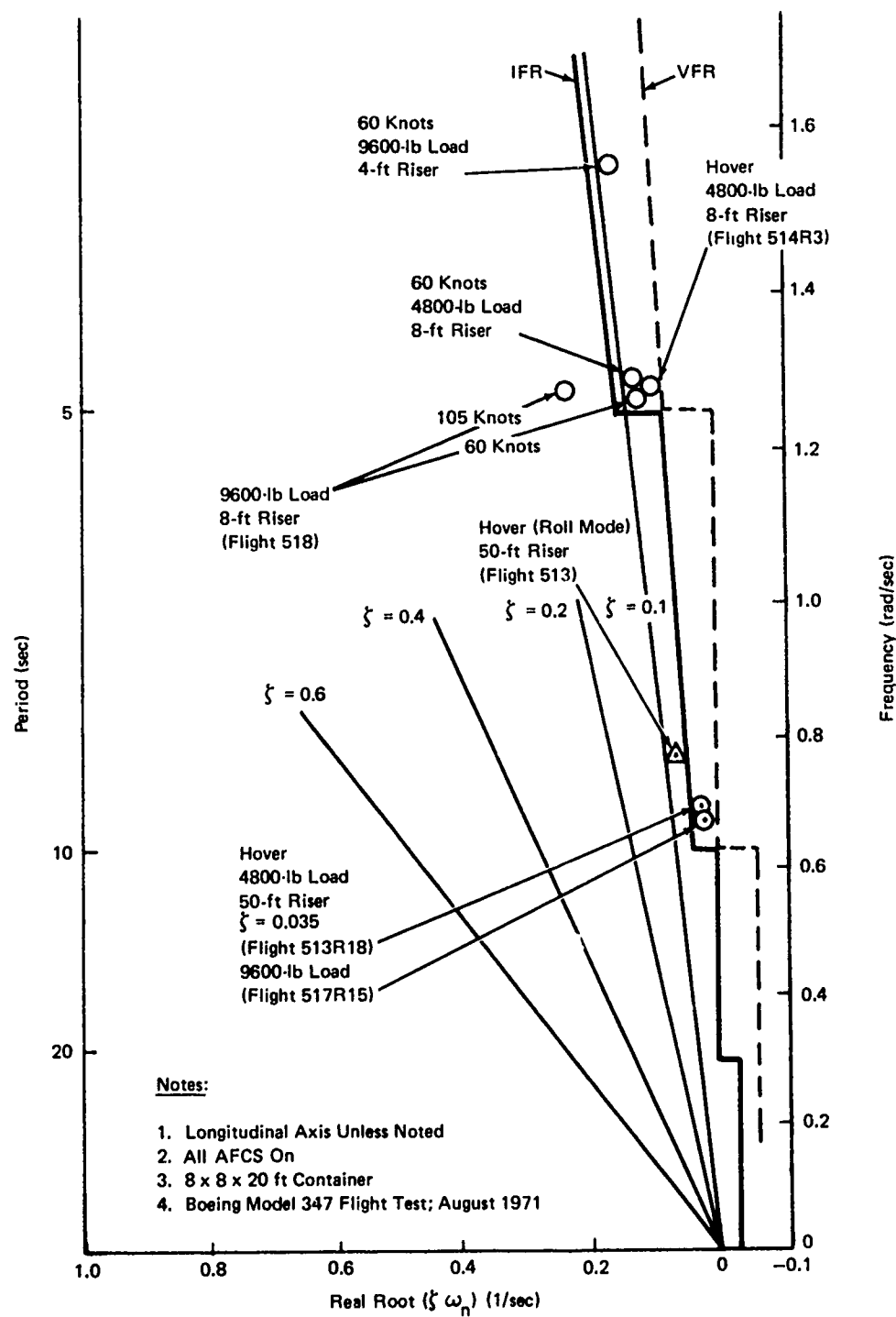


Figure 4. External Load Dynamics.

SYSTEM DESCRIPTION

Detailed descriptions of the AAELSS design, servo control, sling rigging, and hardware components are presented in this section.

DESIGN

The arrangement of the AAELSS on the Model 347 is shown in Figure 5, with the arms in the retracted position. The test article consists of the modified dual-hook load beam which contains most of the AAELSS hardware and provides a single pin and cargo hook attachment to the helicopter. Mounted at the extremities of the beam are two rigid pendants (arms), nominally 4 feet long and 6 inches square in cross section. These arms are attached to the beam by means of pillow-block type universal joints with coincident pitch and roll axes.

The single-point attachment using the existing CH-47 type cargo hook allows the use of the standard production hook release system to jettison the external load in the event of an emergency such as a sling failure. The release of the cargo hook frees the pin and beam so that they can fall free. The airframe beam end restraints are boxes that contain the beam ends in a manner such that all loads are carried into the airframe without interfering with the emergency release capability.

The hydraulic lines connecting the AAELSS to the helicopter utility hydraulic supply are shown in Figure 5. The manifolds mounted on the beam aft of the hook contain the servo and other valves.

Figure 6 shows the general arrangement of an arm in its normal operating position; the arm pivot joints are clearly illustrated. The longitudinal actuator housed within the beam drives the arm about a pivot in the pillow-block on the bottom of the beam. The lateral actuator, which is predominate in the photo, drives the arm about a pivot at the upper end of the arm. Since the lateral actuator rotates on the longitudinal axis, it stays in plane with this pivot; therefore, there is no interaxis coupling (that is, no longitudinal motion with lateral actuator stroking). Likewise, there is no lateral coupling with longitudinal actuator motion. At the arm's lower end, the cylinder shaped covers contain the synchro signal transmitters which are in line with the two cargo hook pivots. Two other synchros are mounted on the arm pivots, but only the longitudinal one is visible in the photograph. At the hook, the upper pivot provides longitudinal freedom and also has a cam attached to hold the hook up when the arm is retracted.

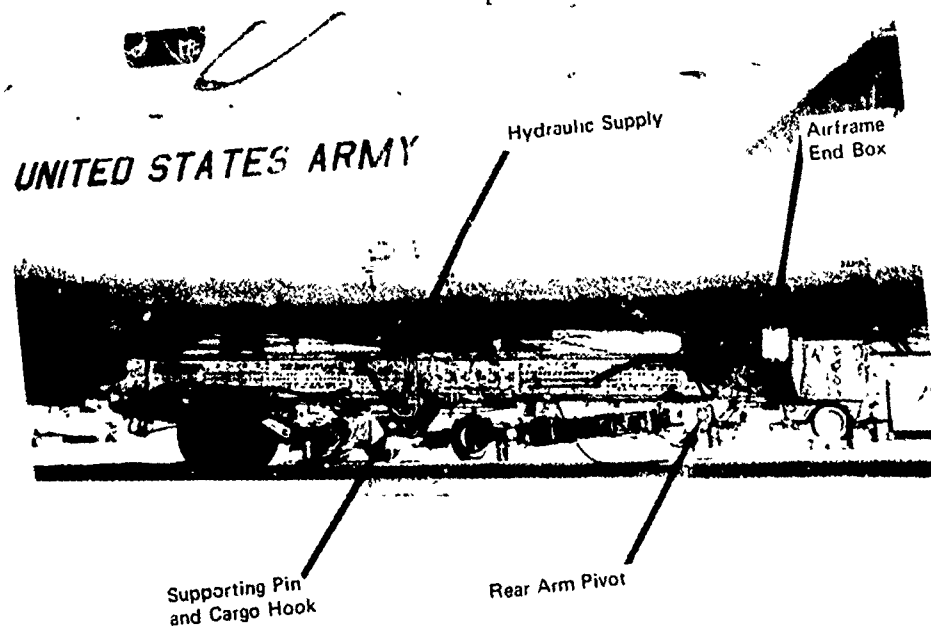


Figure 5. AAELSS Installation.

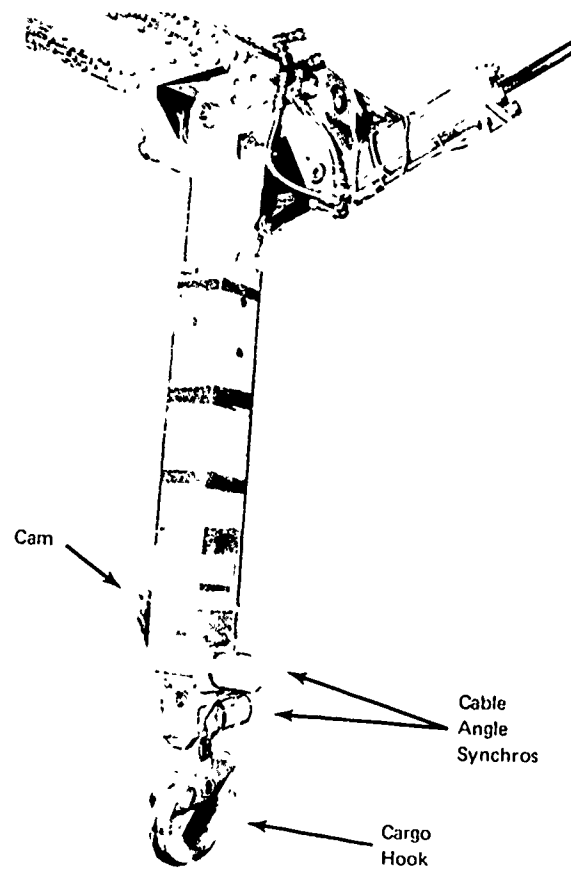


Figure 6. Arm Deta'ls.

SERVO CONTROL SYSTEM

Figure 7 is a block diagram which outlines the key elements of the AAELSS. It describes only one independent actuator and is an oversimplification of the overall system dynamics, but it provides the format for an initial understanding of the system.

The prime signal used in the control system is the angle of the riser with respect to the helicopter airframe (noted here as point (1)). This signal is formed by summing the arm position (2) and angle of the riser relative to the arm (3). The control laws (4) provide processing or shaping of the signal to obtain the desired damping, and this signal in turn commands the actuator servo (5). The actuator servo, which converts the electrical signal to an arm position, is a conventional position control loop that also includes the arm synchro signal for its feedback. The external load dynamics (6) and helicopter dynamics (7) are influenced by the arm motion, with one of the resultant outputs being the cable (riser) angle. The pilot commands (8) influence the helicopter and sling load via the conventional controls, but in addition, a command augmentation function (9) is provided to improve load placement efficiency by forcing the load to follow the helicopter's motion. For this test program, the load command function was mechanized only for the lateral and directional modes. In the lateral axis, it used the pilot lateral cyclic stick position (roll) to command both arms laterally. For the directional mode, the system used pedal position through shaping to command differential lateral arm motion. For the command augmentation, the desired overall effect is to keep the load closely following the helicopter and also to minimize excitation of the load natural modes of motion.

The functions of AAELSS are further detailed in Figure 8 for a single-arm degree of freedom. The arm with its lower cargo hook pivot and upper airframe pivot and their appropriate synchro transmitters is at the center of the diagram. In addition to the synchro signals being summed and fed into the control law, the arm position synchro signal is also used to form the feedback of the actuator position servo. Other elements of this position servo are the amplifier, electrohydraulic valve, and actuator ram (piston-cylinder) which drives the arm. The bypass valve acts to connect the two cylinder ports of the electrohydraulic valve with the ram when hydraulic pressure is present at point C as provided by the solenoid upon system engagement. Loss of either electrical or hydraulic power results in venting pressure at C and the bypass moving right, thus allowing the ram and arm freedom by passing the fluid through the bypass. This means that, should failure occur in either power source, the arm will become free. The relief valves shown are used to avoid overpressurization of the

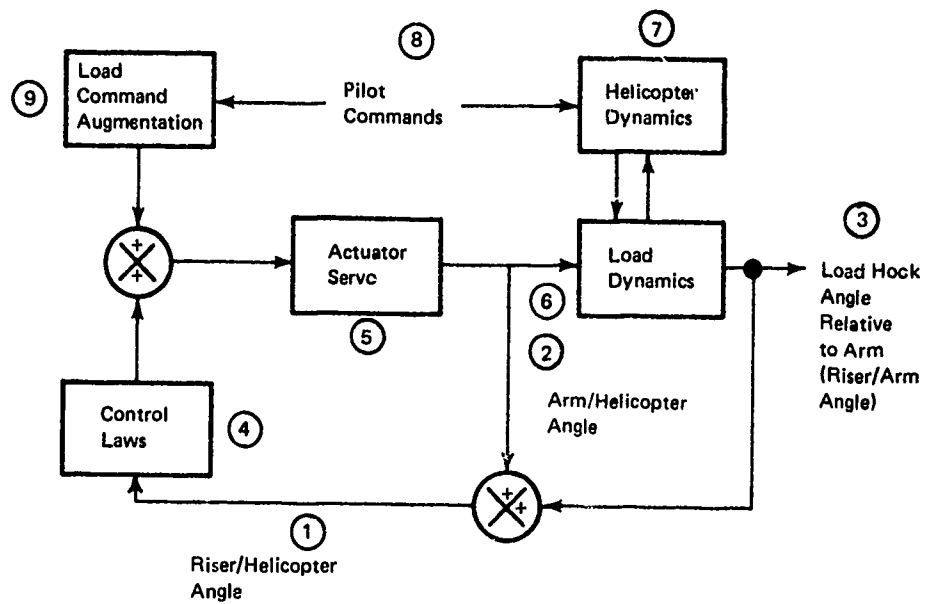


Figure 7. General Control Block Diagram.

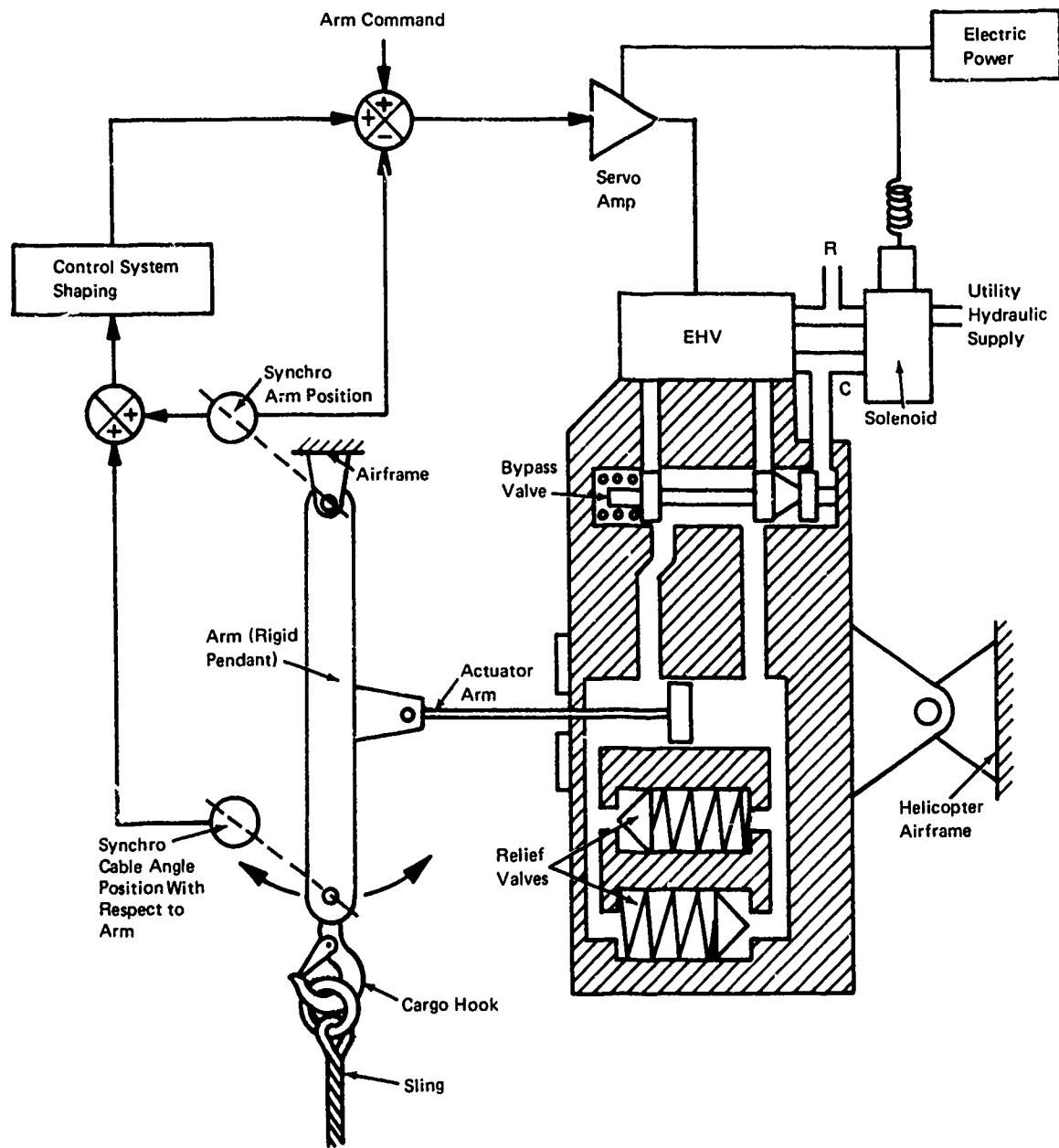


Figure 8. Typical Actuator Controls.

cylinder in the event that the applied moment exceeds the stall moment with the electrohydraulic valve closed.

The arm was retracted by inducing saturating signals into the servo amplifiers in the required direction.

SLING CONFIGURATION

The sling rigging depicted in Figure 9 was used throughout the program. The only exceptions were a hover flight with a pair of 50-foot steel cables added to the 8-foot riser and some in-field flights with 8-foot risers but without the paralleling cable. The load was the standard 8x8x20-foot MILVAN rigged with dual-element nylon slings as shown in Figure 9. The longer legs attached to the corners of the front end of the MILVAN provide a nosedown attitude which was previously shown to contribute stability in forward flight. Dual elements were used to minimize the possibility of nylon sling failure. The paralleling cable would not normally be needed, but it was incorporated in this AAELSS prototype to reduce the arm aft travel and conserve longitudinal actuator travel. This sling arrangement has significantly less yaw stiffness than the 8-foot riser sling flown in previous testing due to its longer riser length (effectively 12 feet) and the reduced separation at the sling legs due to the paralleling cable. In the analysis section which follows, the yaw stiffness is shown to be directly proportional to the square of the riser separation distance and inversely proportional to the sling riser length. The drawing of the sling also indicates the beam pin and cargo hook that provide the single-point beam retention.

HARDWARE DESCRIPTION

The existing dual-tandem-hook load beam was chosen to mount the arms for the prototype AAELSS for the convenience of the test program. It is not necessarily the most weight efficient or desirable arrangement for a production system. For prototype purposes, the beam allowed the maximum use of existing helicopter equipment, minimum modification to the helicopter, and use of a beam already fabricated for a similar test, all of which lend themselves to better design understanding and a minimum of peripheral development. Figure 10, a right-hand view of the beam installation, gives more detail of the pin and hook retention. The cross beam that mounts the cargo hook is seen above the beam in the hatch. In the right of the photo is the structural modification made to the bottom of the airframe to provide the modified beam end restraint boxes. Details of the forward lateral actuator and hydraulic lines from the manifold containing the electrohydraulic valves and relief valves are also evident in the picture.

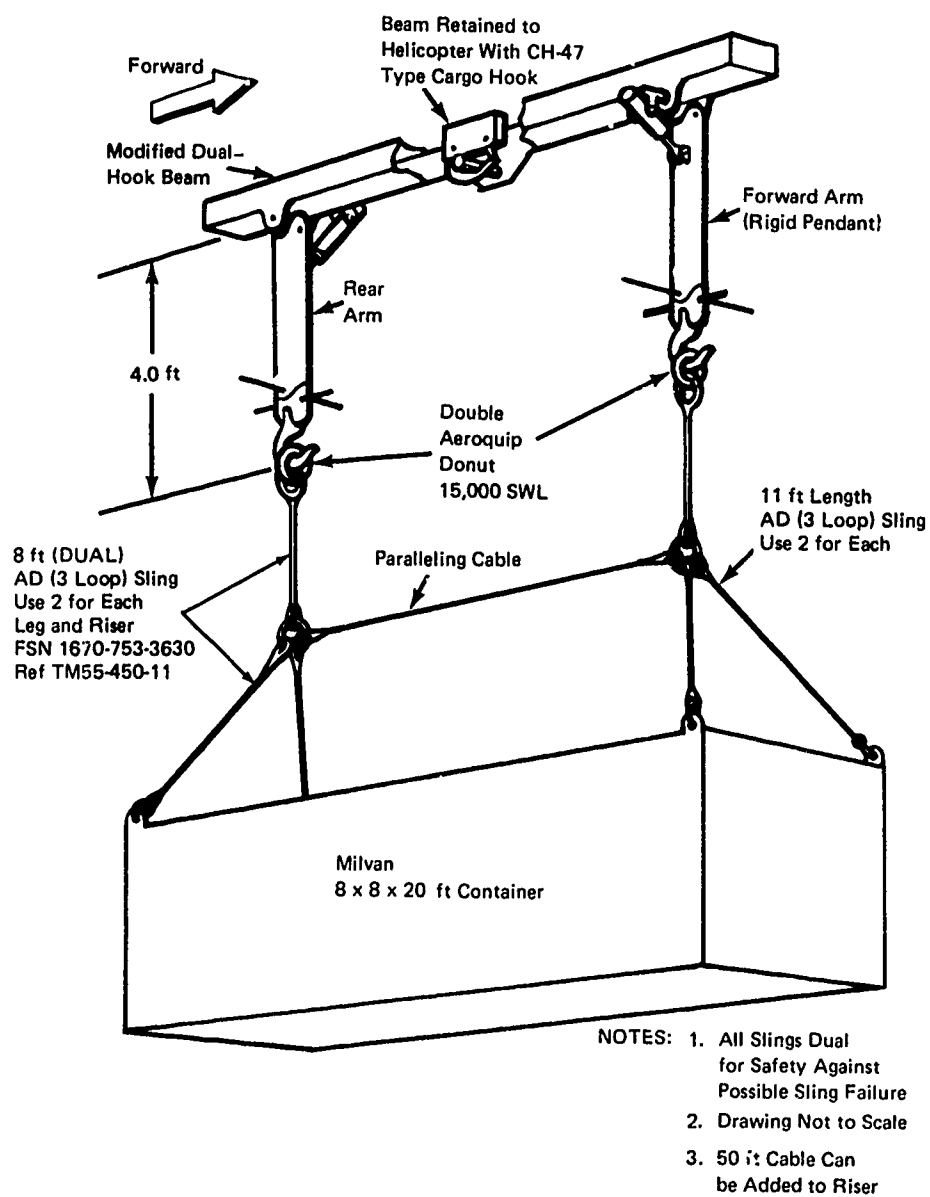


Figure 9. Basic Sling Configuration.

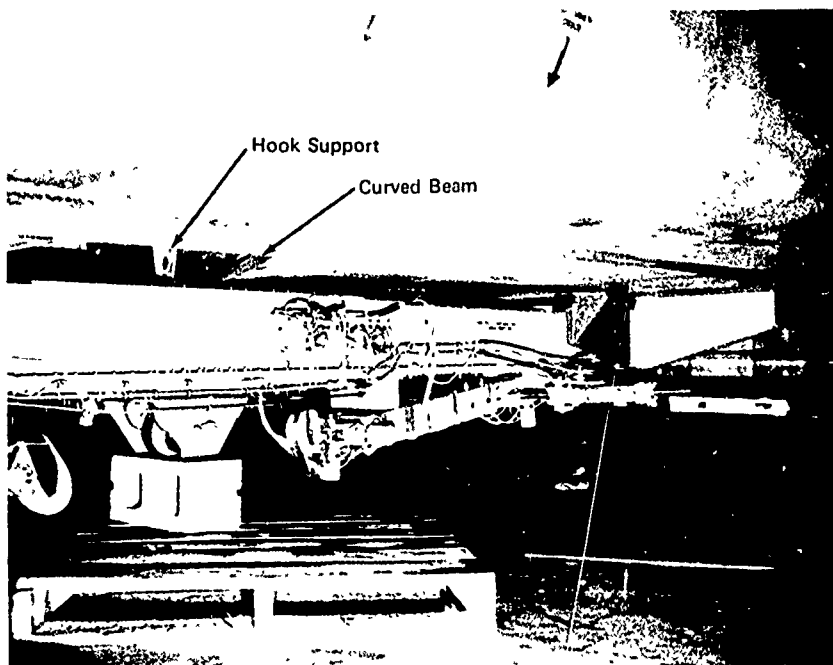


Figure 10. Beam Installation.

When carrying a load, the beam does deflect somewhat at its ends, and this results in some motion of the beam within the end restraints. This situation was accommodated by rubber pads between the beam and both the end restraints and the fuselage.

Figure 11 shows the side and front pads. These pads showed evidence of wear during the program, and the motion causing this should be eliminated in future designs, possibly by the use of preloading.

Figure 11 also shows the tubing and lubricators used to pressure feed the arm pivot journal bearings with grease. This installation was made on all longitudinal pivots early in the test program following a seizure of the forward pivot shaft in the journal bearing. This forward bearing is subject to loads of nearly 70 percent of the total external load and is subject to rapid (small but frequent) angular motions of the arm. This final design which incorporated generous clearance in the arm pivot bearings (to tolerate assembly misalignments) and grease pressure lubrication, worked satisfactorily.

Table I lists the arm travels provided in the design. Other overall guidelines such as component sizing, travel, and general criteria are given at the end of the analysis section of this report. Computations showed that at 120 knots airspeed, a load trail angle of 30 degrees was to be expected with a 5,000-pound external load. This left a 15-degree motion for load disturbances, which is less than previous AAELSS-off experience had indicated, so it was monitored during flight testing.

Although the monitoring indicated that this 15-degree motion margin was sufficient for the restricted flight envelope of the prototype AAELSS test program, more aft trail angle capability is desirable for a production AAELSS.

Table I shows the arm and hook pivot angular travel limits used in the prototype AAELSS design.

Since the AAELSS detects the load force line of action by sensing the hook angle, any hook pivot friction causes hysteresis of this signal. Such hysteresis is undesirable in the system and was minimized by using the smallest possible bearing size. These joints are seen in Figure 6 near the cargo hook. Future designs may circumvent this with better sensor concepts. The sensor itself is accurate, but the friction causes the hook to misalign with the force line of action. However, the hook pivot design used did allow the hook to align well enough that there was no motion of the donut or chance of its being forced out of the hook with the resulting loss of the sling load.

The hydraulic fluid for the AAELSS is supplied through the existing helicopter utility system, which is a 3000-psi system with a 200-cubic-inch accumulator and 13.5-gpm pump capacity. The only modification to the aircraft hydraulic system was the addition of pressure and return lines, each with breakaway fittings and manual cutoff valves. The breakaway fittings accommodated emergency jettisoning of the beam, and the manual cutoff valves permitted cutoff of beam hydraulics in the event of a leak to conserve the aircraft's hydraulic fluid supply.

The hydraulic circuits used in the arm servo actuator are shown in Figure 8. Only one solenoid was used for both lateral actuators and only one for both longitudinal actuators. Physically, the electrohydraulic valve and relief valves were mounted on the manifold some 6 to 8 feet away from the actuator, but this separation did not cause any control loop stability problems during either bench or flight test for the 10-radian corner frequency set for the servo.

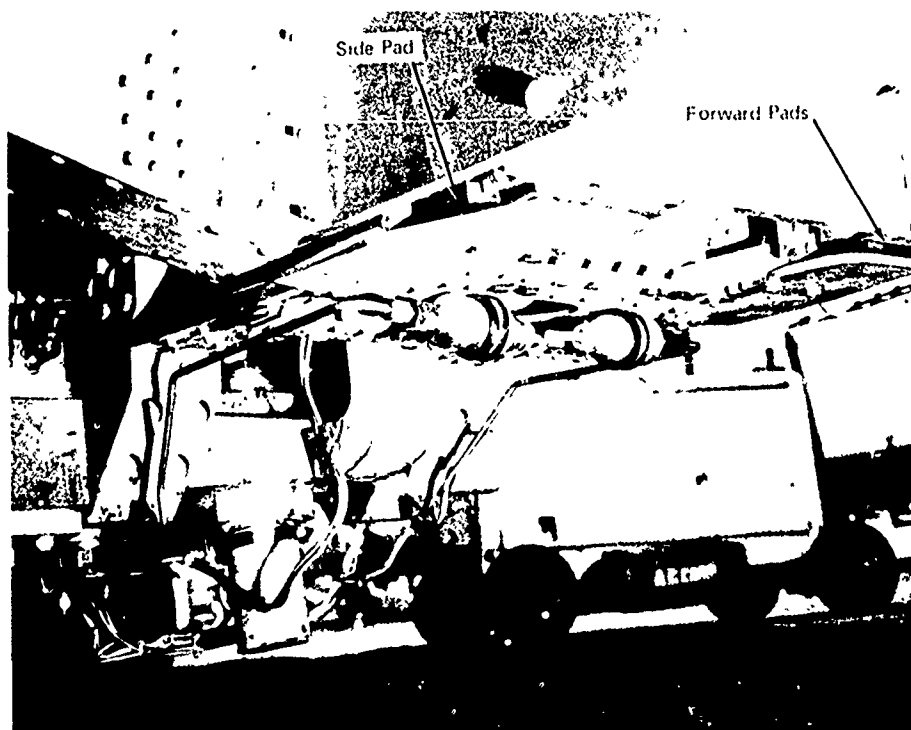


Figure 11. Beam Restraints.

TABLE I. ANGULAR TRAVEL LIMITS			
	Lateral (deg)	Forward Direction (deg)	Aft Direction (deg)
Cargo Hook	<u>+30</u>	30	30
Front Arm	<u>+30</u>	45	90
Rear Arm	<u>+30</u>	90	45

THEORETICAL ANALYSIS

This section presents the studies conducted and the hardware design criteria selected for development of the AAELSS. Both a simplified pendulum model and an extensive (hybrid) model were used in the development of the system. The simplified model provides a rapid overall understanding of the system when used with typical control system root locus techniques. The hybrid model includes sling geometry effects; detail description of the controls; aerodynamic forces and moments about the pitch, roll, and yaw axes; and sufficient detail to describe all significant modes, either airframe coupled or fixed. The hybrid model was used for transient response studies by solving it either as a separate digital subroutine with fixed airframe or as a digital real-time subroutine to a hybrid simulation including pilot-in-the-loop.

CONTROL LAWS STUDIES USING SIMPLIFIED MODEL

Two basic types of control laws were studied using the simplified pendulum model as shown in Figure 12. This model is applicable to either the longitudinal or the lateral roll mode. Here l_p is the length of the arm driven by the controls, and the external load is considered a point mass with an effective length below the arm equal to l_L .

Figure 13 is a block diagram of the first control law studied. The figure also gives the equation matrix for the complete system using the simple pendulum and fixed airframe. The equations are expressed in Laplace operator notation, as it is convenient for computer solutions. Initially, the system was patterned to behave as an equivalent damper between the external load and the support. This required only the two gains (K_1 and K_2) and the lag (τ_1) set to about 100 seconds with all other time constants zero. Review of this system's dynamic stability on a root plot shows a structure identical to the lower one in Figure 14. This structure appeared to be nearly ideal because one could set any damping value from that of the basic sling to beyond critical, and the only compromise was a slight loss in the undamped natural frequency. However, this system proved to be impractical because any small phase error (such as that caused by the actuator time constant) creates a second root path that can go unstable. This was discovered on the hybrid model, where even the small computation-cycle delay caused instability. Figure 14 illustrates one of the better attempts to compensate for this problem. The plot shows that a lead $\tau_3 = 0.3$ and gain of $K_1 = 45$ nets a damping of 0.30.

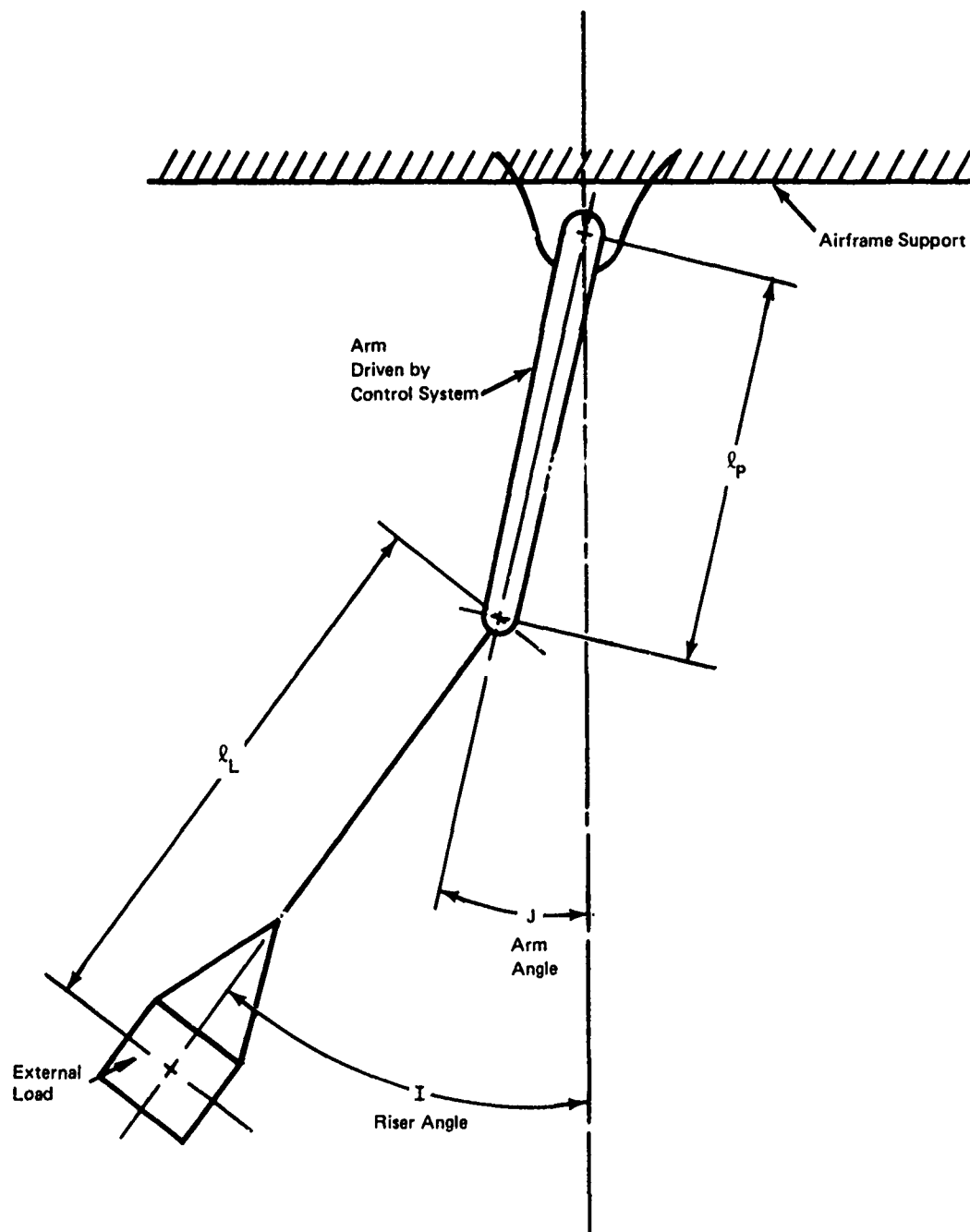
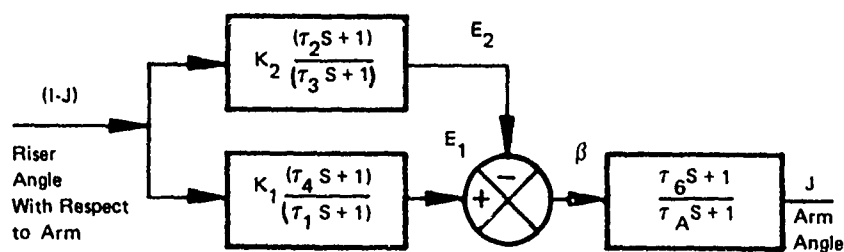


Figure 12. Simple Pendulum Model.



Fixed Airframe Matrix

$$\begin{pmatrix} \ell_L s^2 + g & (\ell_L + \ell_p) s^2 + g & 0 & 0 & 0 \\ 0 & \tau_A s + 1 & -\tau_6 s - 1 & 0 & 0 \\ 0 & 0 & +1 & +1 & -1 \\ K_1 \tau_4 s + K_1 & 0 & 0 & 0 & -\tau_1 s - 1 \\ K_2 \tau_2 s + K_2 & 0 & 0 & -\tau_3 s - 1 & 0 \end{pmatrix} \begin{pmatrix} (1-J) \\ J \\ \beta \\ E_2 \\ E_1 \end{pmatrix} = 0$$

Figure 13. First Control Law.

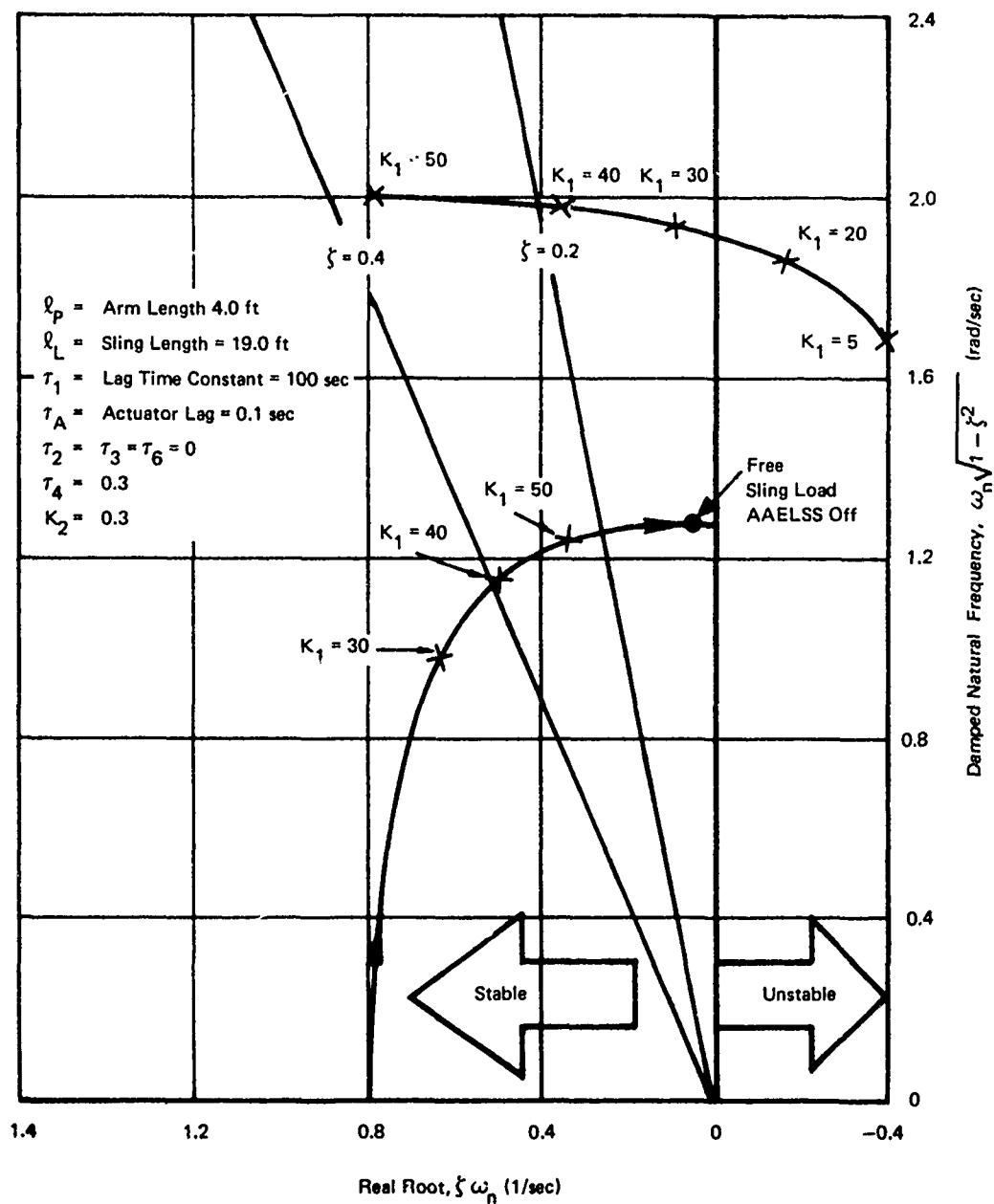


Figure 14. Sling Load Stability of First Control System, Fixed Airframe.

This was about the best that could be obtained. Because the system was so critical to parameter settings and because, as the plot shows, the system goes unstable with loss of gain K_1 , this control law was judged to be unacceptable.

Further studies of candidate control laws resulted in the selection of the controller indicated in Figure 15.

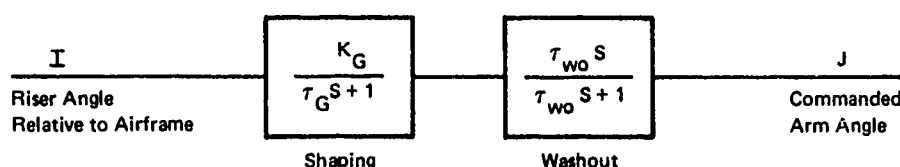


Figure 15. Controller Selected for Study.

This controller uses a single signal channel which takes angle I, the load force line of action, through a gain K_G and a lag-time constant to command the arm angle J. The washout serves only to realign the arm to a zero position over a long period of time. The basic action of the AAELSS in response to a disturbance is to detect the change in angle I and, within the condition of the gain and lag, to command the arm to move over the load. Note that this system uses the riser angle with respect to the airframe; the first control laws used the relative angle between arm and riser and had two parallel commands: K_1 and the negative feedback K_2 .

Two equations describe the adopted system. One is based on the block diagram, and the other is that of the simple pendulum. The following equation is derived from the first row of the matrix by eliminating the difference coordinate (I-J) and expressing terms directly.

$$(\ell_L S^2 + g) I + \ell_p S^2 J = 0 \quad (1)$$

Figure 16 presents dynamics using this law along with a comparison of this system with that of a passive system using a damper on the arm. This is a characteristic root-plot equation. The ordinate is the damped natural frequency, and the abscissa is the real part of the characteristic root with stability increasing toward the left. In this figure, radials of constant damping ratio are designated, and they can be easily related to step transient response. The curve with the specific values of the lag time constant, τ_1 , is for the AAELSS

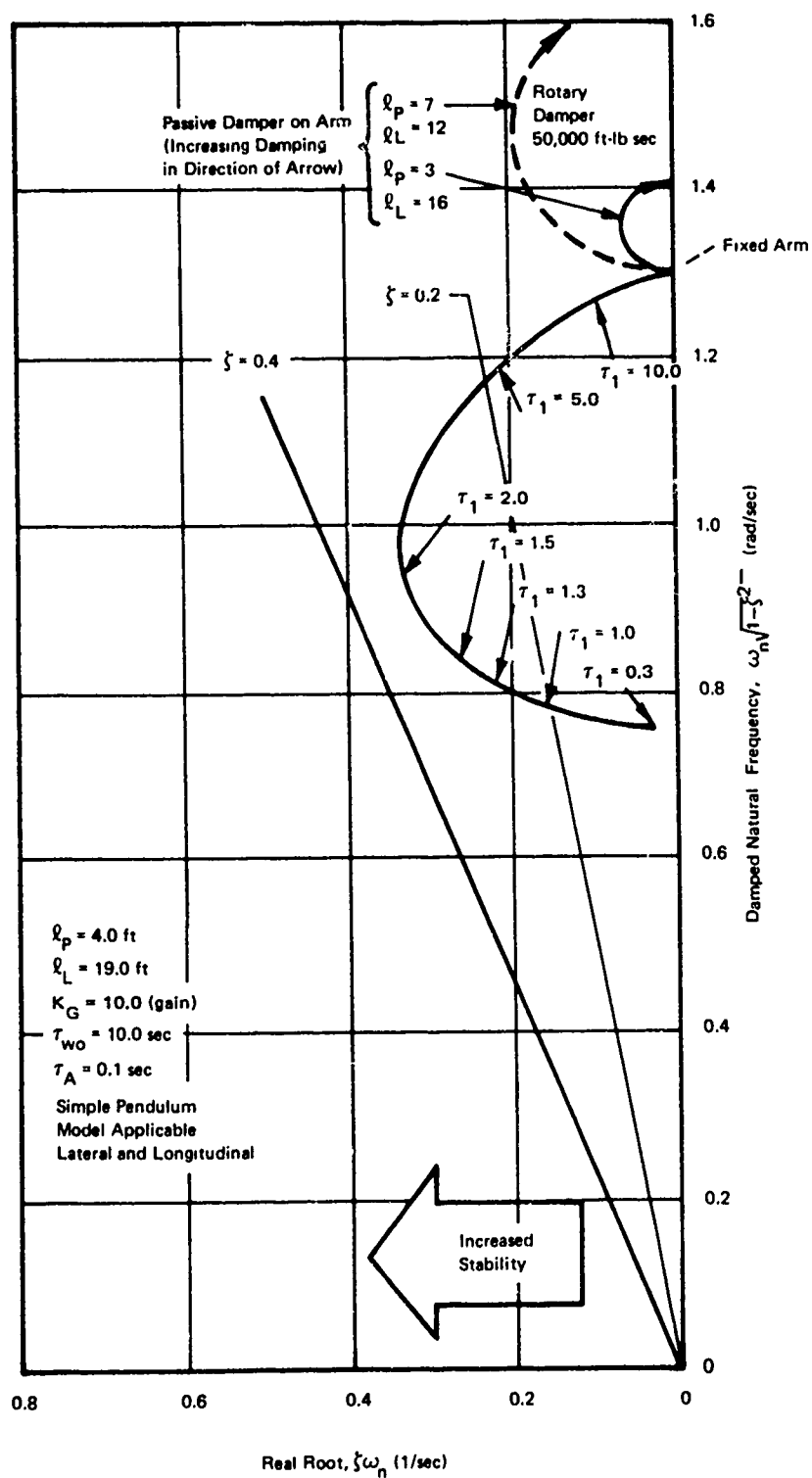


Figure 16. Load Stabilization System Dynamic Stability, Fixed Airframe, Hover, Time-Constant Sensitivity.

at a gain of 10. This curve indicates that, if the time constant is very large, the controls tend to hold the arm fixed; and the overall response is that of a free pendulum at the end of the fixed arm. As the lag is decreased, damping can improve to 0.35; however, very short time constants result in the arm moving just to increase the effective sling length (and therefore to decrease the frequency) but with minimum damping benefit.

The influence of gain on the AAELSS is shown in Figure 17. Increasing gain nets increased damping with only a minor change in the undamped natural frequency (proportional to the radius vector length). In other words, increasing the gain improves the AAELSS with no loss in the speed at which disturbances are reduced. The lag time constant that maximizes damping ratio is increased slightly with the increased gain. Best lag is 2 seconds with the gain set at 10 and 3 seconds with the gain set at 20. A washout set at 10 seconds was used in this study, but other information showed that its presence netted a damping ratio loss of only 0.03 or 0.04.

This controller has none of the critical aspects of the first one, and as the root plot indicates, gains and lag-time constants can go to their limits without producing any instabilities. For this reason alone, the selected concept has a distinct advantage, but it can also provide a high damping ratio (0.7), if needed.

The powered servo control in the AAELSS is superior to a passive rotary damper connected to the arm. The passive damper was evaluated using two arm lengths (3 and 7 feet) with the total arm and sling length equal to 19 feet (comparable to the AAELSS fixed arm). It was effective only with long arms and even then required a proper setting of the rotary damper value. If the rotary damping was set too high, the effect was poor overall system damping since the arm became more rigid and resulted in increased frequency. The obvious advantage of the active load stabilization system is its ability to obtain very high damping ratios, if needed, while using only a moderate arm length.

Figure 18 shows characteristics of the AAELSS operating with a long pendulum length, in this case 61 feet. Of the two gains shown, it is obvious that the larger gain (20) is necessary to even approach the design target damping ratio of 0.25. The best lag time constant for the 20 gain is about 3.0 seconds.

HARDWARE SIZING

The hardware sizing was based on the first control law and the initial condition set by position offset of the load. Figure 19

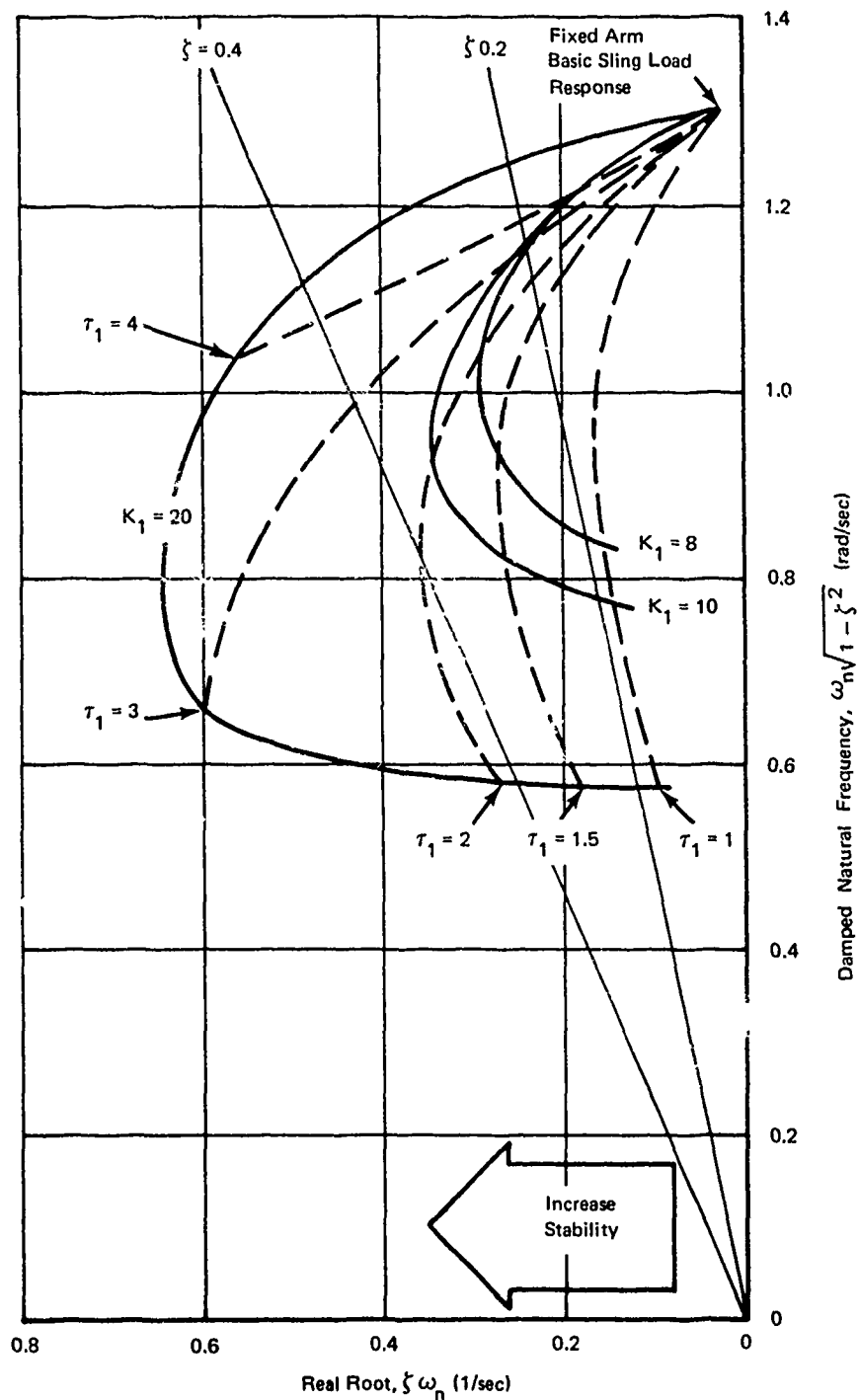


Figure 17. Load Stabilization System Dynamic Stability, Fixed Airframe, Hover, Gain Sensitivity.

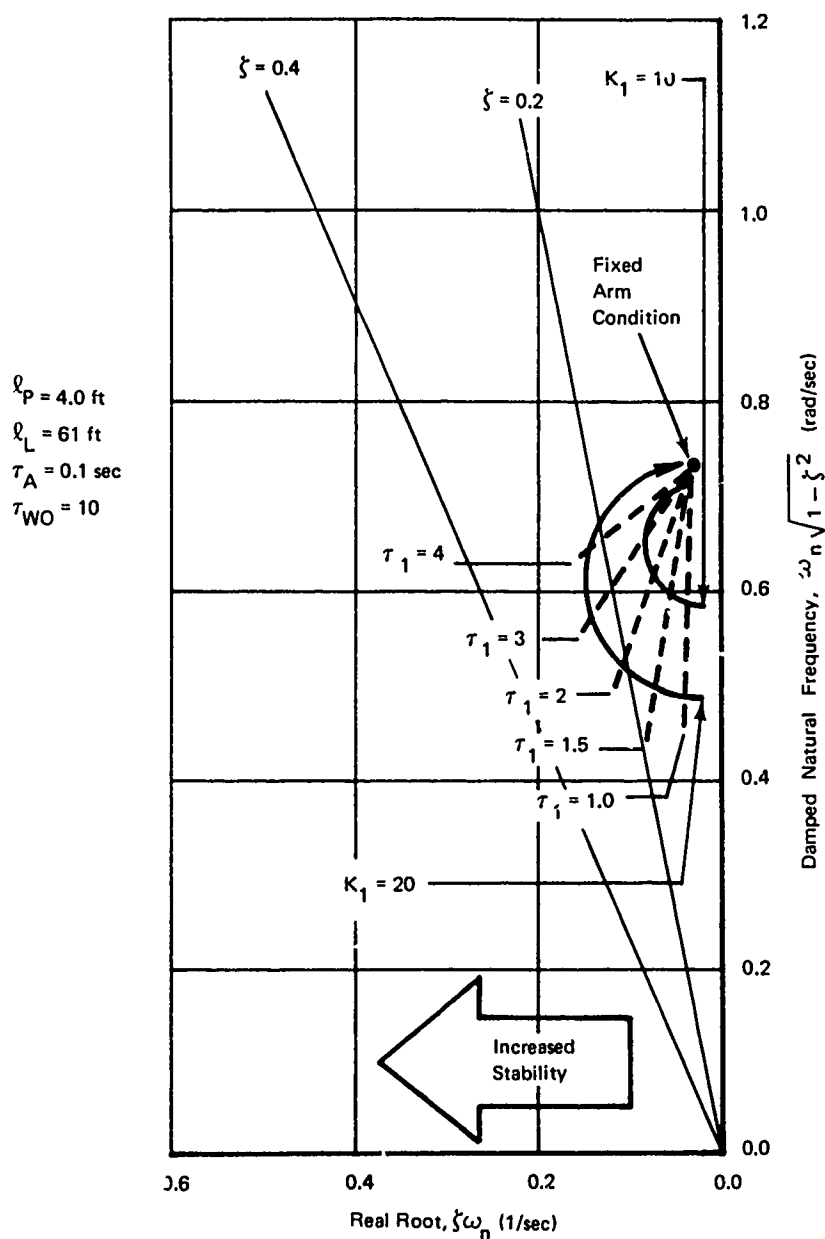


Figure 18. Load Stabilization System Dynamic Stability, Fixed Airframe, Hover, 50-Foot Riser.

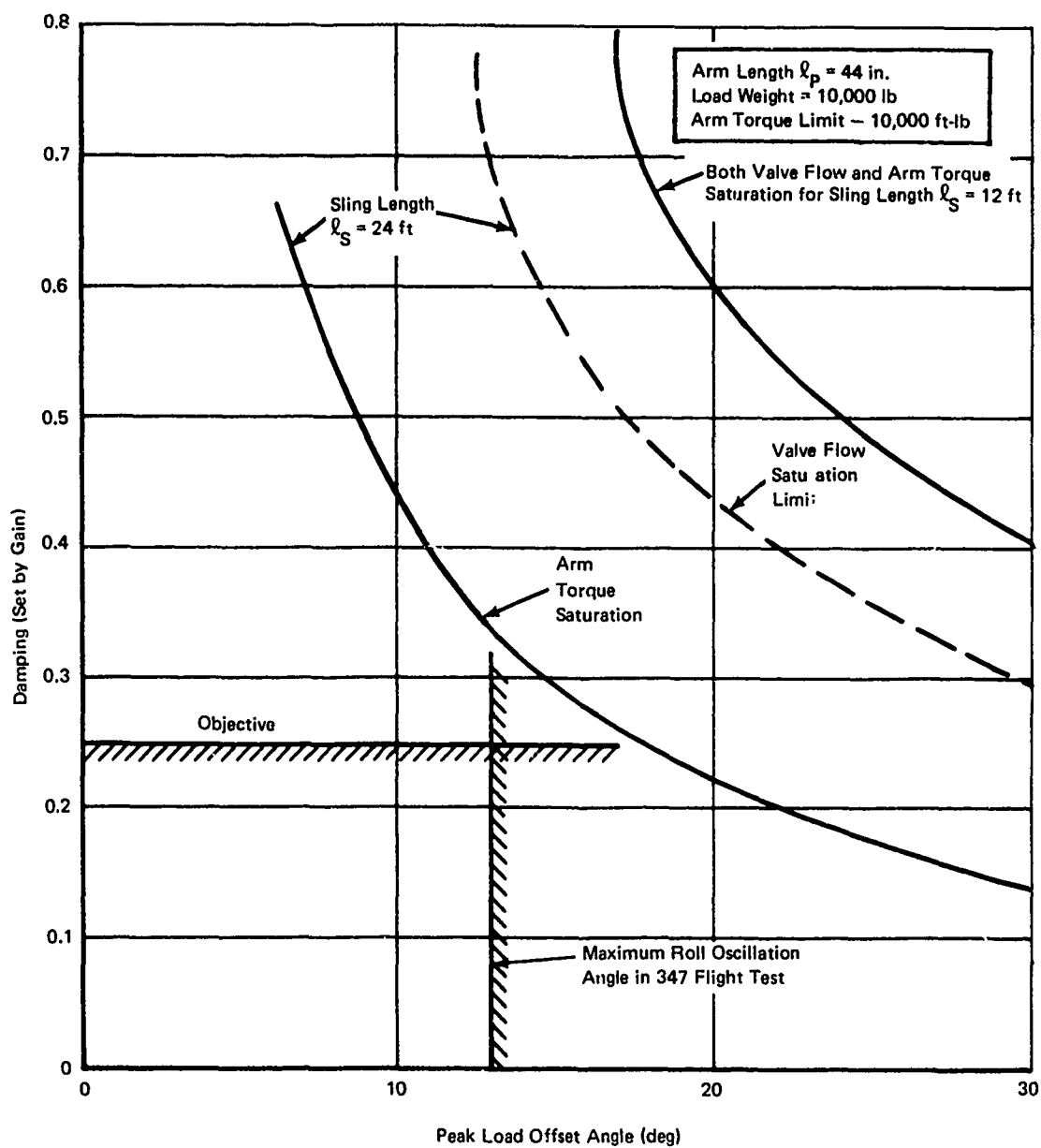


Figure 19. Limits of Linear Operation.

illustrates the linear operational range capability of the active external load stabilization system in terms of achievable damping ratio at various peak (i.e., maximum) load disturbance angles. Both 12-foot and 24-foot slings are considered, and the limits of linear system operation are shown in terms of control torque and servovalve flow-rate saturations. As shown, both the torque and flow-rate limits occur simultaneously for the short (12-foot) sling and permit very high load damping ($\zeta > 0.7$) even at the largest load disturbances previously reached in flight test. With the 24-foot sling, torque limiting occurs first, but still permits linear operation to a damping ratio of 0.34 at the largest load disturbance previously recorded. Damping ratios greater than 0.34 can be achieved once the amplitudes reduce below the torque saturation line, since operation above the torque and below flow rate saturation is not destabilizing. This sizing curve suggests that, in cases where torque saturation (stalling) occurs, a reduction of gain as a function of amplitude might be employed. This is particularly apparent with very long slings.

The sizing study established that the arm should be as long as practical (or as long as needed for structural weight efficiency) because, for any given external disturbance, it reduces the valve flow requirements with only a minor increase in torque. The equipment for this flight test program was designed with the arms as long as the space and operating travel limits allowed.

HYBRID MATH MODEL

A math model was derived for the load stabilization system which included the external load, the sling suspension system, and the active arms with their sensors and controller. The model is designed to be used for real-time piloted-flight simulation when coupled with a small-perturbation airframe model. The model given here accepts the aircraft motion parameters, uses these in the computation of external load motions, which in turn are coupled back to the aircraft.

The math model discussed here allows investigation of system failures, controller gain and time constant sensitivities, and suspension size and configuration changes. It may be used in an uncoupled mode (with large airframe-to-load inertia ratio) or coupled to investigate interacting airframe/load dynamics.

The discussion of the math model is separated into five segments:

- Equations of load motion
- Suspension system geometry

- Load aerodynamic forces and moments
- Axis system transformations
- Arm controller model

Equations of Load Motion

The equations of motion of the load consist of second-order differential equations which represent rigid-body motion in three orthogonal translations and three orthogonal rotations (parallel to earth axis but aligned with the helicopter heading). Gravity and the sling geometry produce the restoring force coefficient, while the damping coefficient provided by wind is adjusted to match flight-test data.

Although some parts of this model are limited to small-perturbation transients, the model does permit large trim excursions in the equations of motion and in the suspension system geometry, as discussed in the following sections.

Figure 20 presents the free-body diagram from which the equations of motion are derived.

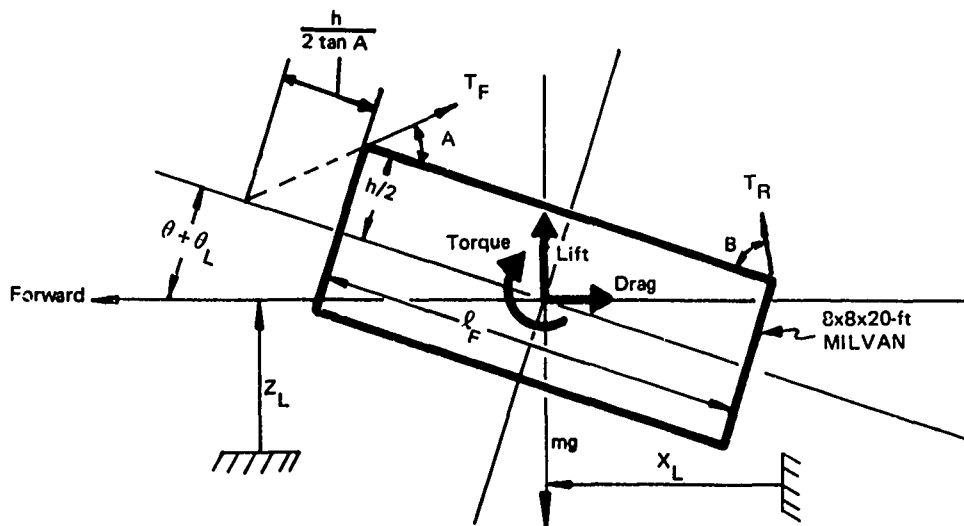


Figure 20. Side View of External Load Free-Body Diagram (Longitudinal Axis).

The following three equations specify the conditions required to solve for the longitudinal motion of the external load in space. These account for all aerodynamic forces including resolving the side force component (wind axis) into the longitudinal axis. T_F and T_R are the sling forces.

$$F_{XL} - m\ddot{X}_L = 0 \quad (1)$$

where

$$F_{XL} = \left[T_R \cos (B + \theta + \theta_L) - T_F \cos (A - \theta - \theta_L) - \text{drag} \right] \cos \psi$$

$$- \left[F_{ZL} \tan (\phi + U) + \text{side force} \right] \sin \psi$$

$$\Sigma M_{Y_L} = - T_R \left(\frac{l_F}{2} + \frac{h}{2 \tan B} \right) \sin B + T_F \left(\frac{l_F}{2} + \frac{h}{2 \tan A} \right) \sin A$$

$$+ \text{torque} - I_Y (\ddot{\theta} + \ddot{\theta}_L) = 0 \quad (2)$$

$$\Sigma F_{ZL} = - T_R \sin (B + \theta + \theta_L) + T_F \sin (A - \theta - \theta_L) + \text{Lift} - mg$$

$$- m\ddot{Z}_L = 0 \quad (3)$$

Equations 4 and 5 are developed to solve for the lateral roll motion by summing forces along the y axis and moments about the x axis. Figure 21 indicates the applicable terms.

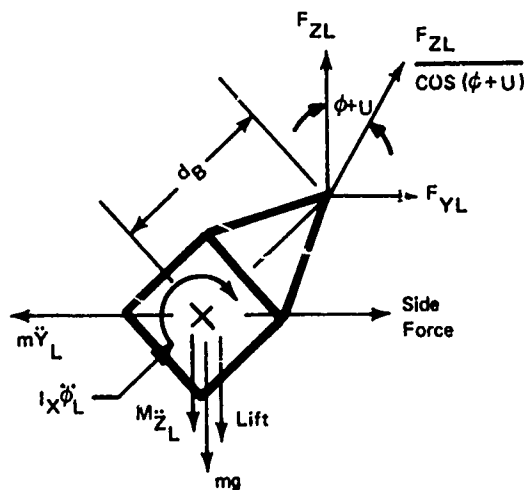


Figure 21. Rear View of External Load Free-Body Diagram (Lateral Axis).

$$F_{YL} - m \ddot{Y}_L = 0 \quad (4)$$

where

$$F_{YL} = \left[T_R \cos (B+\theta+\theta_L) - T_F \cos (A-\theta-\theta_L) - \text{drag} \right] \sin \psi \\ + \left[F_{ZL} \tan (\phi+U) + \text{side force} \right] \cos \psi$$

$$\Sigma M_{XL} = F_{ZL} \tan (\phi+U) d_B \cos (\phi_L) - F_{ZL} d_B \sin (\phi_L) + \text{moment} \\ - I_X (\ddot{\phi}_L) = 0 \quad (5)$$

Figure 22 and Equation 6 illustrate the directional equation of motion. N_{PL} is the torque exerted by the sling forces and external load geometry.

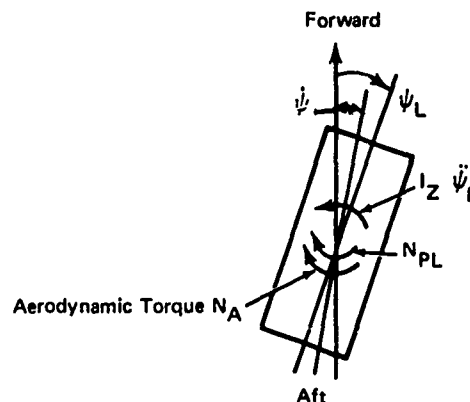


Figure 22. Directional Moments on Load (Top View).

$$\Sigma M_{ZL} = 0 \quad N_A + N_{PL} - I_Z \ddot{\psi}_L = 0 \quad (6)$$

Suspension System Geometry

Most of the difficulties in deriving a simulation model of the sling load arise from the relative complexity of the suspension system geometry. Not only must the exact position of each suspension member be determined, but the forces in each member must be determined, also. The model described here employs

simplifications that restrict sling transients to small perturbations, but large independent longitudinal, lateral, or directional excursions are permissible.

The longitudinal position of the load in terms of X_R and Z_R in the helicopter axis system is found from the geometry of the sling as shown in Figure 23.

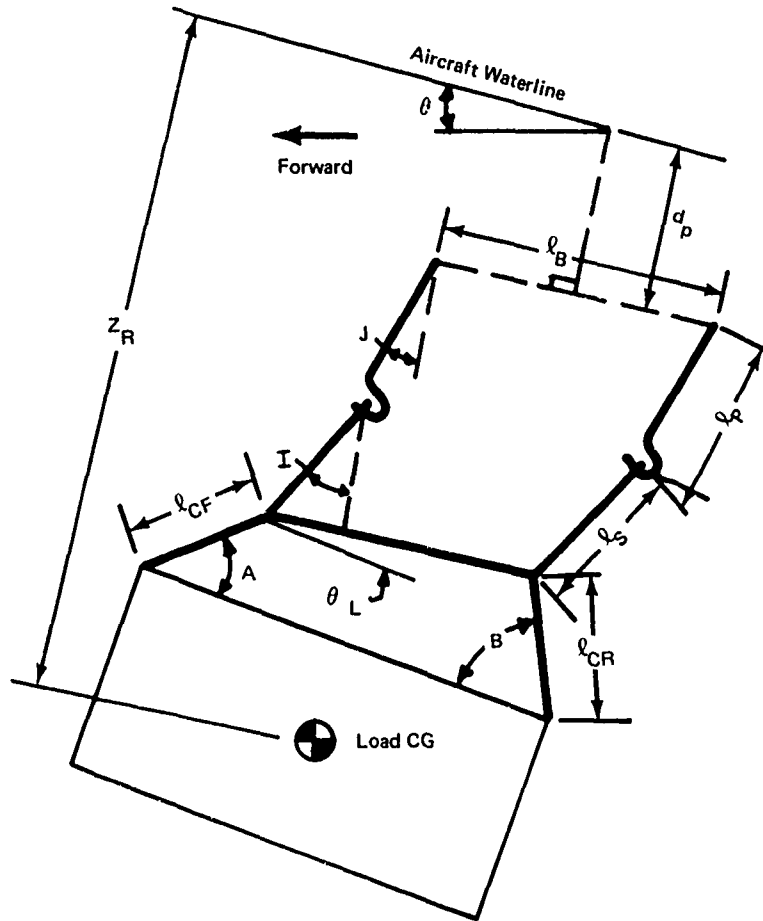


Figure 23. Side View of Suspension.

The X_R equation is rearranged and solved for the angle I in the final computation.

$$X_R = \frac{l_F}{2} + l_P \sin J + l_S \sin I + a \sin \theta_L + a' \cos \theta_L - \frac{l_F}{2} \cos \theta_L + \frac{h}{2} \sin \theta_L + (d_p + l_P + l_S + d_B) \tan \theta \quad (7)$$

$$\begin{aligned}
Z_R = & -d_p - l_p \cos J - l_s \cos I - a \cos \theta_L + a' \sin \theta_L \\
& - \frac{l_F}{2} \sin \theta_L - \frac{h}{2} \cos \theta_L
\end{aligned} \tag{8}$$

where

$$a = l_{CF} \sin A$$

$$a' = l_{CF} \cos A$$

The angles A and B formed by the sling legs and load are required for the solution of Equation (8). They are found from the following set:

$$\begin{aligned}
B = \sin^{-1} & \left(\frac{l_F^2 + l_B^2 + l_{CR}^2 - l_{CF}^2 - 2 l_F l_B \cos \theta_L}{2 l_{CR} \sqrt{l_F^2 + l_B^2 - 2 l_F l_B \cos \theta_L}} \right) \\
& - \tan^{-1} \left(\frac{l_F - l_B \cos \theta_L}{l_B \sin \theta_L} \right)
\end{aligned} \tag{9}$$

$$\begin{aligned}
A = \sin^{-1} & \left(\frac{l_F^2 + l_B^2 + l_{CF}^2 - l_{CR}^2 - 2 l_F l_B \cos \theta_L}{2 l_{CF} \sqrt{l_F^2 + l_B^2 - 2 l_F l_B \cos \theta_L}} \right) \\
& - \tan^{-1} \left(\frac{l_F - l_B \cos \theta_L}{l_B \sin \theta_L} \right)
\end{aligned} \tag{10}$$

Five equations representing forces at the spreader bar (or paralleling cable as the case may be) and the vertical sling stiffness (see Figure 24) are used to solve for the five parameters P, P_F, P_R, T_F, and T_R. These are given in Equations 11 through 15.

$$P_F + P_R = P \tag{11}$$

$$\Sigma F_X = -P \sin I + T_F \cos (A - \theta_L) - T_R \cos (B + \theta_L) = 0 \tag{12}$$

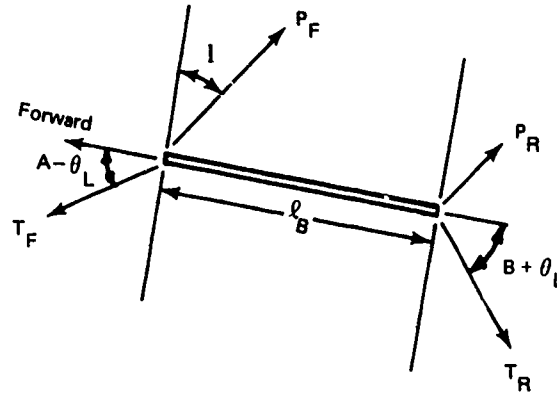


Figure 24. Spreader Bar Forces.

$$\Sigma F_Z = -P \cos I + T_F \sin (A - \theta_L) + T_R \sin (B + \theta_L) = 0 \quad (13)$$

$$\Sigma M_O = P_F \cos I - P_R \cos I - T_F \sin (A - \theta_L) + T_R \sin (B + \theta_L) = 0 \quad (14)$$

$$T_R \sin (B + \theta_L) = 0$$

Equation 15 is an expression for the sum total of riser tension forces.

$$P = K (\ell_s - \ell_{s0}) + P_o \quad (15)$$

where ℓ_{s0} and P_o are initial trim conditions.

Equations 16 through 19 sum the forces of the two arms into a single item.

$$F_{ZF} + F_{ZR} = F_{ZA} \quad (16)$$

$$F_{XF} + F_{XR} = F_{XA} \quad (17)$$

$$M_F + M_R = M_P \quad (18)$$

$$F_{ZL} = P \cos (\theta + I) \quad (19)$$

Equations 20 through 22 further relate the forces and moments acting on the helicopter by using a single angle for each riser and arm.

$$\Sigma M_{FR} = -M_P + P \ell_P \sin (I - J) = 0 \quad (20)$$

$$\Sigma F_X = -F_{XA} + P \sin I = 0 \quad (21)$$

$$\Sigma F_Z = -F_{ZA} + P \cos I = 0 \quad (22)$$

Equation 23 then describes the moments acting on the helicopter (see Figure 25).

$$\Sigma M_{CG} = M_{CG} - M_P - F_{XA} d_p + (P_F - P_R) (\cos I) \frac{\ell_S}{2} = 0 \quad (23)$$

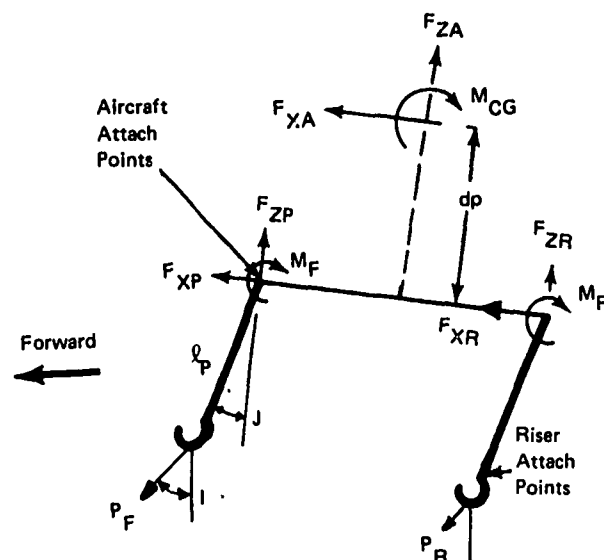


Figure 25. Airframe and Arm Forces.

Figure 26 and the following equations are presented to show the lateral displacements and how they were obtained.

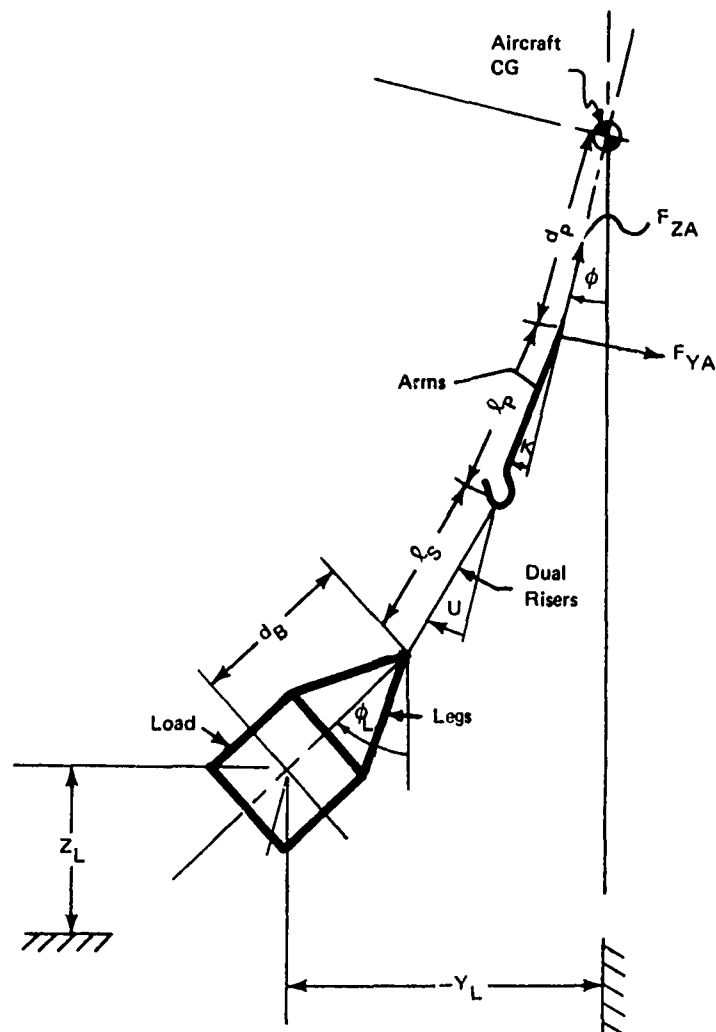


Figure 26. Lateral Suspension Geometry.

The equations in the math model are actually solved for angle U , since Y_R is found from the basic equation of motion.

$$Y_R = -\ell_P \sin K - \ell_S \sin U - d_B \sin (\phi_L - \phi) - (d_P + \ell_P + \ell_S + d_B) \tan \phi \quad (24)$$

where

$$U = - \frac{1}{2} (U_F + U_R)$$

$$K = - \frac{1}{2} (K_F - K_R)$$

The formula describing the restoring torque due to load yaw is developed with the aid of Figure 27.

The load follows the spreader bar in directional heading with no error, so the restoring torque in yaw is

$$N_{PL} = F_{ZL} \frac{\ell_B}{2} \tan \alpha \quad (25)$$

where F_{ZL} is the sum total of vertical force in the risers and ℓ_B is the spreader bar length. Equations 28 and 29 are derived from geometry indicated in Figure 27.

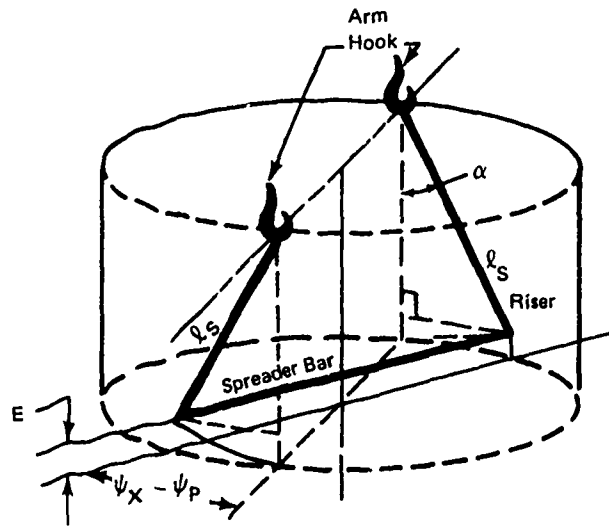


Figure 27. Directional Displacement Diagram.

$$\tan \quad = 2E/\ell_B (\psi_x - \psi_p) \quad (26)$$

where

$$E = \frac{\ell_B^2}{4\ell_S} \left[1 - \cos(\psi_x - \psi_p) \right] = \frac{\ell_L^2}{2\ell} \left[\sin^2 \frac{1}{2}(\psi_x - \psi_p) \right]$$

The effects of the arm displacement . . . spreader bar yaw motion are illustrated in Figure 28 and the following equations.

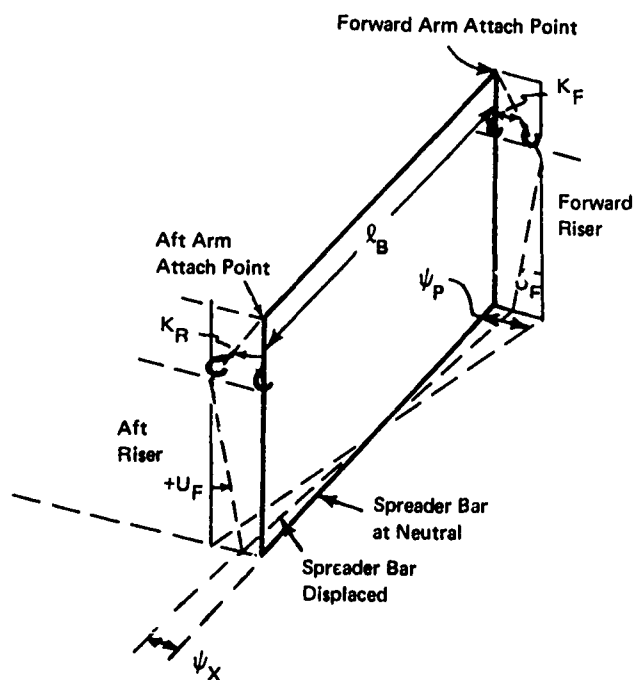


Figure 28. Riser/Arm Directional Displacement Diagram.

$$\psi_P = \frac{\ell_P}{\ell_B} (\sin K_F - \sin K_R) \quad (27)$$

$$\psi_X - \psi_P = \frac{\ell_S}{\ell_B} (\sin U_R - \sin U_F) \quad (28)$$

Equation 32 results from combining equations 27, 28, 29, and 31.

$$N_{PL} = \text{cable torque on the load} = F_{ZL} \frac{\ell_B^2}{4 \ell_S} \left[\frac{1 - \cos (\psi_X - \psi_P)}{\psi_X - \psi_P} \right] \quad (29)$$

The moments about the front and rear arm pivots are

$$L_{PF} = \frac{F_{ZLF}}{\cos (\phi - U_F)} \ell_P \sin (U_F - K_F) \quad (30)$$

$$L_{PR} = \frac{F_{ZLR}}{\cos (\phi - U_R)} \ell_P \sin (U_R - K_R) \quad (31)$$

where

$$F_{ZLF} = T_F \sin (A - \theta - \theta_L) \quad (32)$$

$$F_{ZLR} = T_R \sin (B + \theta + \theta_L) \quad (33)$$

The total moment and lateral forces at the arm pivot are

$$L_P = \frac{F_{ZL}}{\cos (\theta + U)} \ell_P \sin (U - K) \quad (34)$$

$$F_{YA} = \frac{-F_{ZL}}{\cos (\phi + U)} \sin U \quad (35)$$

The roll moment on the helicopter can be found from the following equation:

$$L_{CG} - L_P + F_{YA} d_P = 0 \quad (36)$$

Large trim displacements in the longitudinal or lateral directions are possible; they reflect sling nonlinearities such as those in Equations 7 and 24. The equations of motion have been written as if the displacements of the load are independent and additive. Under small-perturbation conditions, linearity is preserved; therefore, the motions of the load may be superimposed to find the resultant position of the load.

It is evident that displacements of the load in the longitudinal, lateral, and directional dimensions cause a change in the distance between the load and the aircraft. The suspension geometry has therefore been described by equations that accurately represent load position for large excursions in longitudinal vertical-planar motion. This may be seen in the sling geometry equations (7, 8, 9 and 10). These equations allow an accurate definition of load position and attitude at high airspeeds (where the load will trail and pitch due to aerodynamic loads and aircraft attitude). A minor restriction is applied to simplify the geometry; the risers are required to remain parallel, thus giving identical descriptions of both arm controllers.

The legs are assumed to remain in tension at all times; therefore, the suspension (consisting of the legs relative to the spreader bar) has only a longitudinal degree of freedom. From the rear view, the load top surface and the front or rear legs to the spreader bar form a rigid triangular structure. For purposes of directional displacements, then, the rotation is considered to be from the spreader bar to the arm hooks, when the arms are being controlled, or to the arm attachment points, when the arms are in the bypass mode.

Load Aerodynamic Forces and Moments

Wind tunnel test results of an 8x8x20-foot container were used to model aerodynamic forces and moments acting on the load. The data used are shown in Figures 29, 30, and 31. The data permit determination of lift, side force, drag, and pitching and yawing moments acting on the load; rolling moment was considered negligible. Because the load width and height are the same, an interchange of α_L and β_L is permissible in Figures 30 and 31, but lift is determined using α_L for the abscissa and the applicable β_L curve. Likewise, side force is found by using β_L for the abscissa and the correct α_L curve.

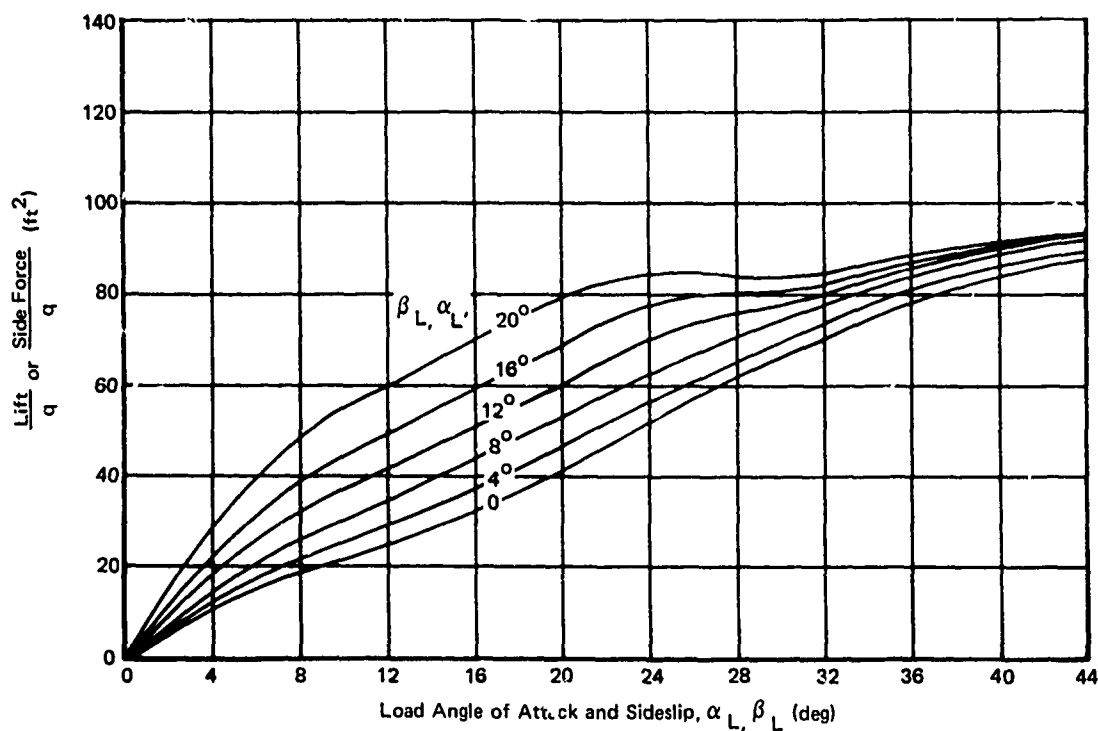


Figure 29. Normalized Wind Axis Data Lift and Side Force (f_1) on 8x8x20-Foot Smooth Container.

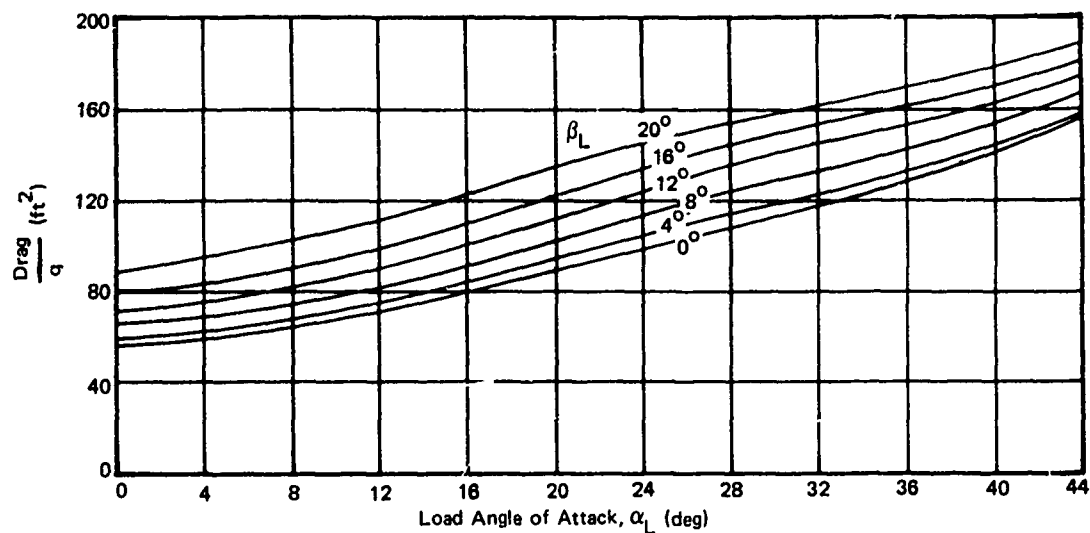


Figure 30. Normalized Wind Axis Data Drag Force (f_2) on 8x8x20-Foot Smooth Container.

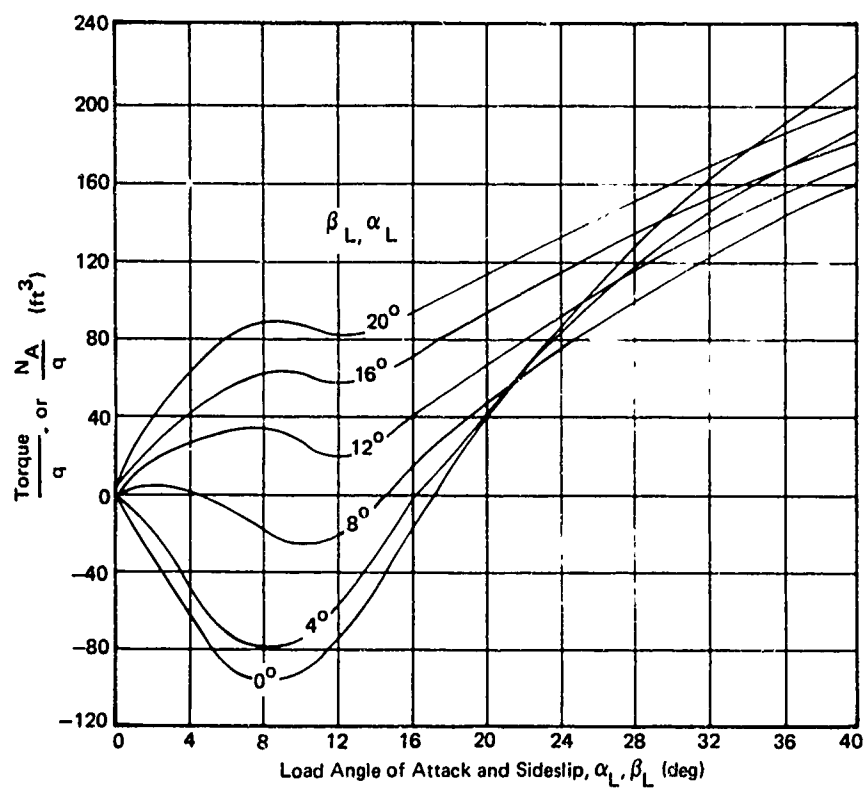


Figure 31. Normalized Wind Axis Data Pitching and Yawing Moment (f_3) on 8x8x20-Foot Smooth Container.

The forces and moments are based on the definitions of wind angles and dynamic pressures given in Figure 32 and Equations 37 through 41. Rotor downwash and interference are neglected, and no aerodynamic forces are applied to the suspension cables.

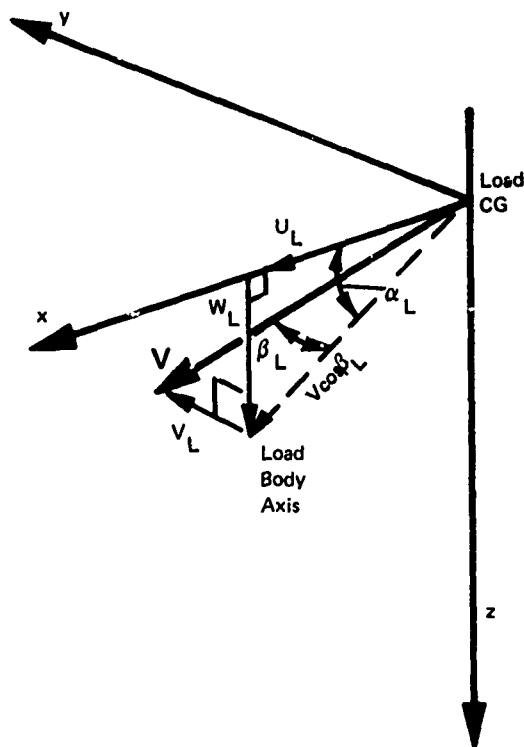


Figure 32. Axis for Application of Aerodynamic Forces and Moments to Sling Load.

The following equations define the velocity and angles required to define the aerodynamic characteristics of the load.

$$V \equiv \sqrt{u_L^2 + v_L^2 + w_L^2} \quad (37)$$

$$\beta_L \equiv \sin^{-1} \frac{v_L}{V} \quad (38)$$

$$\alpha_L \equiv \tan^{-1} \frac{w_L}{u_L} \quad (39)$$

$$q \equiv \frac{1}{2} \rho V^2 \quad (40)$$

where

V = total air velocity, ft/sec

β_L = load sideslip, rad

α_L = load angle of attack, rad

q = load dynamic pressure, lb/ft²

Equation 41 indicates the aerodynamic forces with the applicable f_1 , f_2 , and f_3 functions found in the previous plots.

$$\begin{aligned} \text{lift} &= f_1 (\alpha_L, \beta_L) \bullet q \\ \text{side force} &= f_1 (\beta_L, \alpha_L) \bullet q \\ \text{drag} &= f_2 (\alpha_L, \beta_L) \bullet q \\ \text{pitch moment} &= f_3 (\alpha_L, \beta_L) \bullet q \\ \text{yaw moment} &= f_3 (\beta_L, \alpha_L) \bullet q \end{aligned} \quad (41)$$

Axis System Transformations

The equations of motion for the load are derived in the earth axis system, and forces due to the load are applied to the aircraft in body axes, as discussed previously.

The equations of motion written in earth axes exhibit the following advantages:

- Sling-load position relative to the earth is important in loading, hovering, and unloading;
- Wind tunnel data are referenced to wind which is parallel to earth, so it can be applied directly;
- Sling-load motion can be readily compared to well-known simple pendulum motion; and
- In this axis system, the equations of motion are in their simplest form.

The suspension-system equations written in an aircraft body-axis system exhibit the following advantages:

- The sling is attached to the aircraft, and position of the risers is measured relative to the aircraft;
- The controller positions the arms relative to the aircraft;
- Forces are generated in the suspension that are applied in the aircraft body-axis equations of motion; and
- In this axis system, the sling geometry equations are in their simplest form.

Because two different axis systems are used, the transformations between earth and aircraft-body axis must be applied in the solution of the equations.

The first transformation is used to convert load earth-axis velocities into helicopter-body-axis velocities.

$$\begin{bmatrix} u_L \\ v_L \\ w_L \end{bmatrix} = \begin{bmatrix} \cos(\theta+\theta_L) \cos(\psi_L) & \cos(\theta+\theta_L) \sin(\psi_L) & -\sin(\theta+\theta_L) \\ \cos(\psi_L) \sin(\phi_L) \sin(\theta+\theta_L) & \sin(\phi_L) \sin(\theta+\theta_L) \sin(\psi_L) & \sin(\phi_L) \cos(\theta+\theta_L) \\ -\sin(\psi_L) \cos(\phi_L) & +\cos(\phi_L) \cos(\psi_L) & \\ \cos(\phi_L) \sin(\theta+\theta_L) \cos(\psi_L) & \cos(\phi_L) \sin(\theta+\theta_L) \sin(\psi_L) & \cos(\phi_L) \cos(\theta+\theta_L) \\ +\sin(\phi_L) \sin(\psi_L) & -\sin(\phi_L) \cos(\psi_L) & \end{bmatrix} \begin{bmatrix} \dot{x}_L \\ \dot{y}_L \\ \dot{z}_L \end{bmatrix}$$

(42)

The position of the load relative to the helicopter in earth-axis system is

$$\begin{aligned} X_{RE} &= X_L - X_B \\ Y_{RE} &= Y_L - Y_B \\ Z_{RE} &= Z_L + Z_B \end{aligned} \quad (43)$$

The load position in helicopter-body axes are found from the following transformation:

$$\begin{bmatrix} X_R \\ Y_R \\ Z_R \end{bmatrix} = \begin{bmatrix} \cos(\theta)\cos(\psi) & \cos(\theta)\sin(\psi) & -\sin(\theta) \\ \cos(\psi)\sin(\phi)\sin(\theta) & \sin(\phi)\sin(\theta)\sin(\psi) & \sin(\phi)\cos(\theta) \\ -\sin(\psi)\cos(\phi) & +\cos(\phi)\cos(\psi) & \\ \cos(\phi)\sin(\theta)\cos(\psi) & \cos(\phi)\sin(\theta)\sin(\psi) & \cos(\phi)\cos(\theta) \\ +\sin(\phi)\sin(\psi) & -\sin(\phi)\cos(\psi) & \end{bmatrix} \begin{bmatrix} X_{RE} \\ Y_{RE} \\ Z_{RE} \end{bmatrix} \quad (44)$$

Arm Controller Model

To simplify the math model of the load suspension system, it is assumed that, in longitudinal-vertical suspension displacement, both arms receive the same information from their lower pivot arm sensors (at the hook) and command the same arm displacement. This permits simplification of the riser geometry and replaces two arms and their controllers with equivalent single-arm equations. These are given in Equations 20, 21, 22, and 23.

Figure 33 presents the block diagram of the longitudinal controller. As shown, any displacement of the riser is lagged and washed out as a command to the arm-positioning servo. This figure also shows the simulation modeling of the hydraulic-bypass characteristics of the servo and the input point for saturation of the servo (indicated by the limit LIM).

Because of the load dynamics, it is beneficial to employ compensation to the arm-position commands to achieve the best possible damping of the load oscillations consistent with the sling geometry. The lag function (τ_G) provides the damping of the load oscillations, while the washout (τ_{WG}) permits a steady-state alignment of the arm with the riser. The $1/K_G$ branch allows the steady-state alignment of the arm and riser to have the same control authority from quiescence to overtorque, or bypass operation from any flight condition.

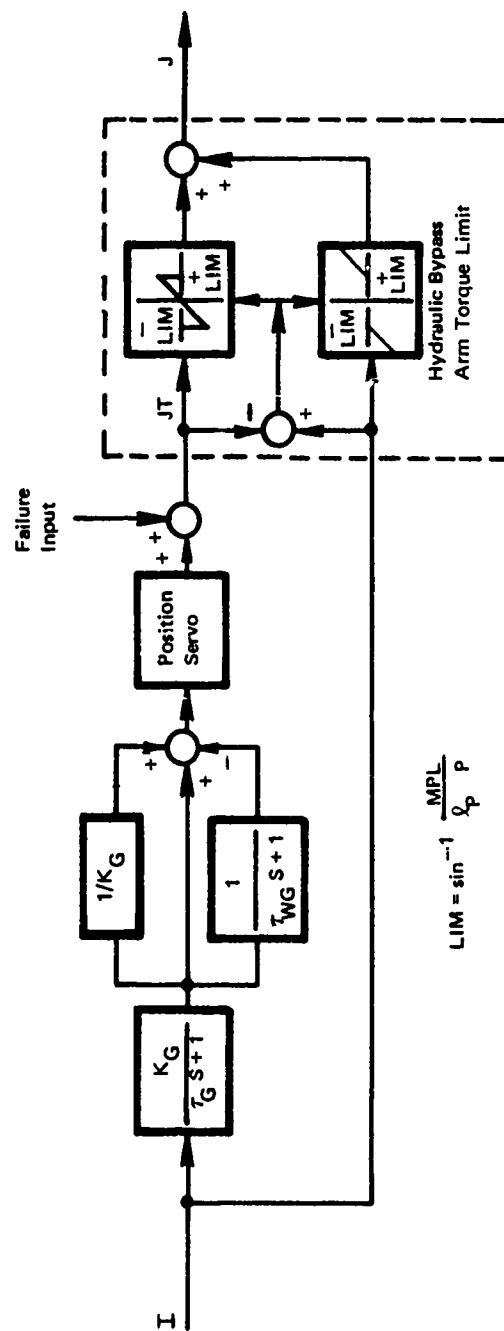


Figure 33. Longitudinal Arm Controller.

The arms are permitted to move independently in lateral and directional motion, and each is positioned by its own controller (similar in form to the longitudinal controller). The lateral-directional controller is shown in Figure 34.

An additional feature of the lateral-directional controller is the command-augmentation circuit, which gives the ability to reposition the load in anticipation of aircraft motion (thus minimizing yawing and lateral oscillations of the load). The pilot's lateral and directional commands (which precede any aircraft motion) are used to position the load in the commanded direction before the aircraft motion is felt at the riser lower-pivot-arm sensor.

SIMULATION

Part of the stated objective of this program is to obtain load stabilization without excessive power requirements or any unsafe conditions on the helicopter. The hybrid model failure analysis was used to accomplish the objective and determine safety requirements. This analysis was accomplished with fixed airframe in order to obtain data promptly, as the coupled-sling-load airframe program interface was not yet operational.

The parameter values of the results discussed in this section are given in Table II. In all cases, the sling geometry in the model accurately represents the arrangement used in the flight test. The only differences between the two are in weight and in the radius of gyration for the MILVAN, which was calculated assuming uniform weight per surface area of the empty MILVAN.

The failure studies simulated hardover failures of the actuators, a condition possible due to a loss of feedback. The model describes these as a large saturated signal that forces and holds the actuator to the torque limit. Under this condition, the model accounts for all inertia, weight, and aerodynamic forces on the MILVAN and computes the load motion and forces on the airframe.

Data on the simultaneous failure of both longitudinal actuators is given in Figure 35 together with curves showing the steady trim moment and arm trail angle. These data consider that the airframe is at zero pitch attitude and that controls accurately place the arm in line with the riser. This longitudinal failure only adds a 15-degree motion above the existing trail angle, and the peak moment change requires the equivalent of a 3/16-inch stick movement to offset it. Since the aircraft's control sensitivity is strong (80,000 ft-lb/inch), only small corrective control inputs are needed.

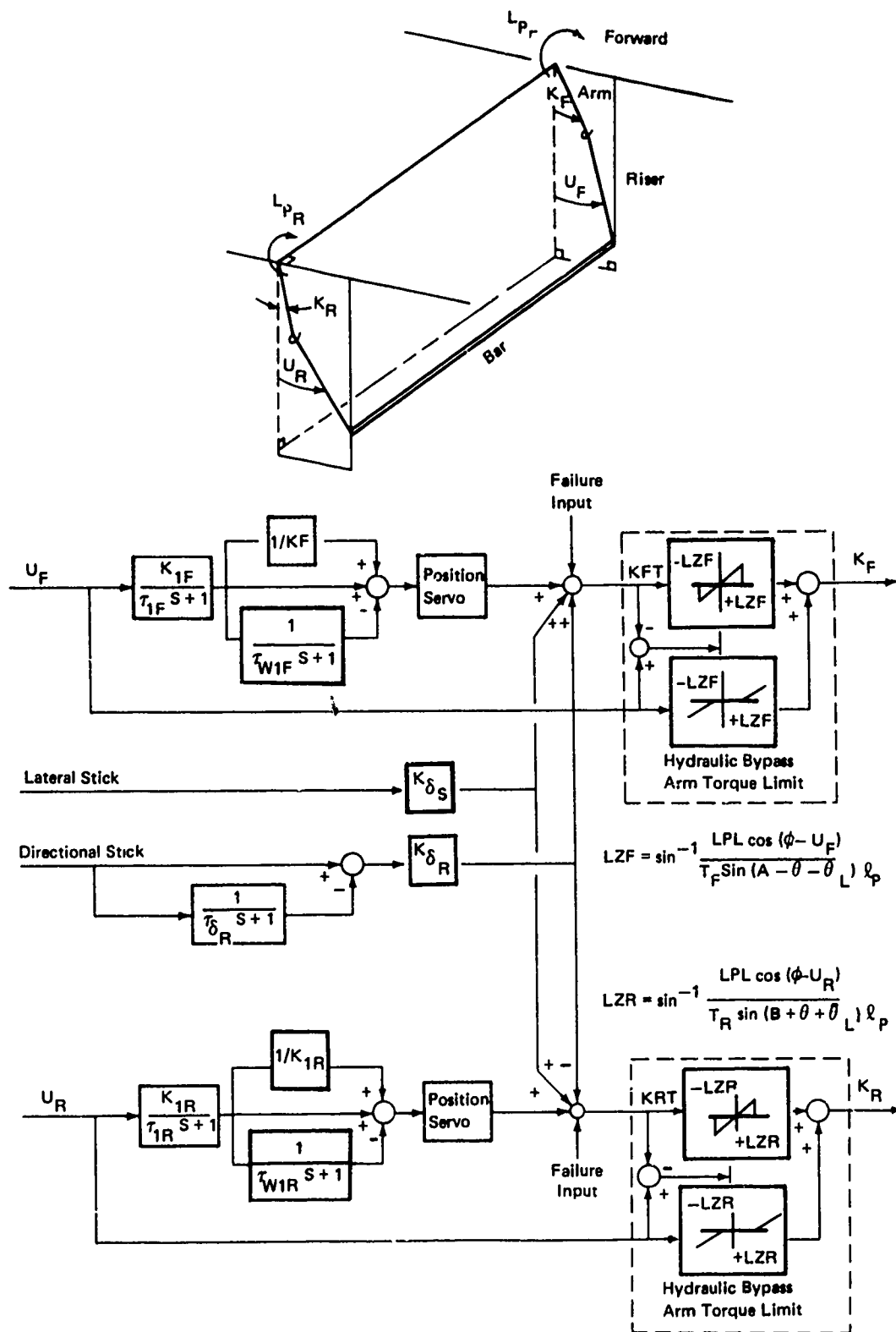


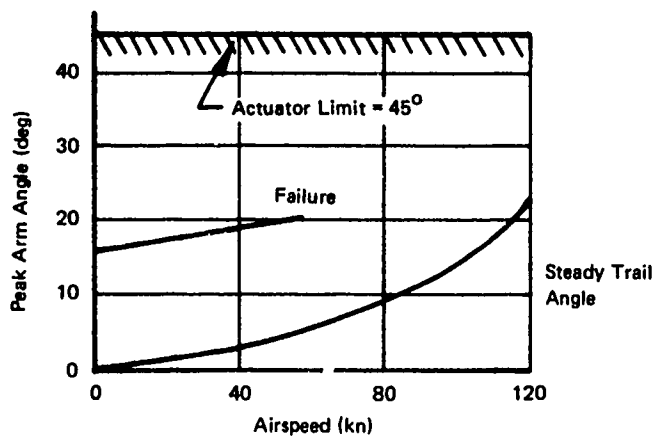
Figure 34. Lateral-Directional Arm Controller.

TABLE II. FIXED PARAMETERS FOR HYBRID MODEL

d_B	= 12 ft
d_P	= 8 ft
h	= 8 ft
I_X	= 6,000 lb-ft-sec ²
I_Y	= 16,800 lb-ft-sec ²
K_{IF}	= 10 (or noted)
K_{IR}	= 10
K_G	= 10
l_B	= 12.0 ft
l_{CF}	= 10.3 ft
l_{CR}	= 7.0 ft
l_F	= 20.0 ft
l_P	= 4.0 ft
l_S	= 8.0 ft
L_{IM}	= 5,000 ft-lb
m	= $\frac{10,000 \text{ lb}}{32.2 \text{ ft/sec}^2}$
M_{PL}	= 10,000 ft-lb
τ_G	= 2 sec (or noted)
τ_{WG}	= 10 sec (or noted)
τ_{IF}	= 2 sec (or noted)
τ_{WIF}	= 10 sec (or noted)
τ_{IR}	= 2 sec (or noted)
τ_{WIR}	= 10 sec (or noted)

Note:

Aerodynamic forces are found from Figures 29, 30, and 31.



Notes:

1. 8x8x20-ft Container
2. 10,000 lb Weight
3. Basic Sling Configuration [8 ft Riser (23 ft Length from CG to Top of Arm)]
4. Both Long Failure Aft - 5000 ft-lb Moment Limit for Each Actuator Fixed Airframe

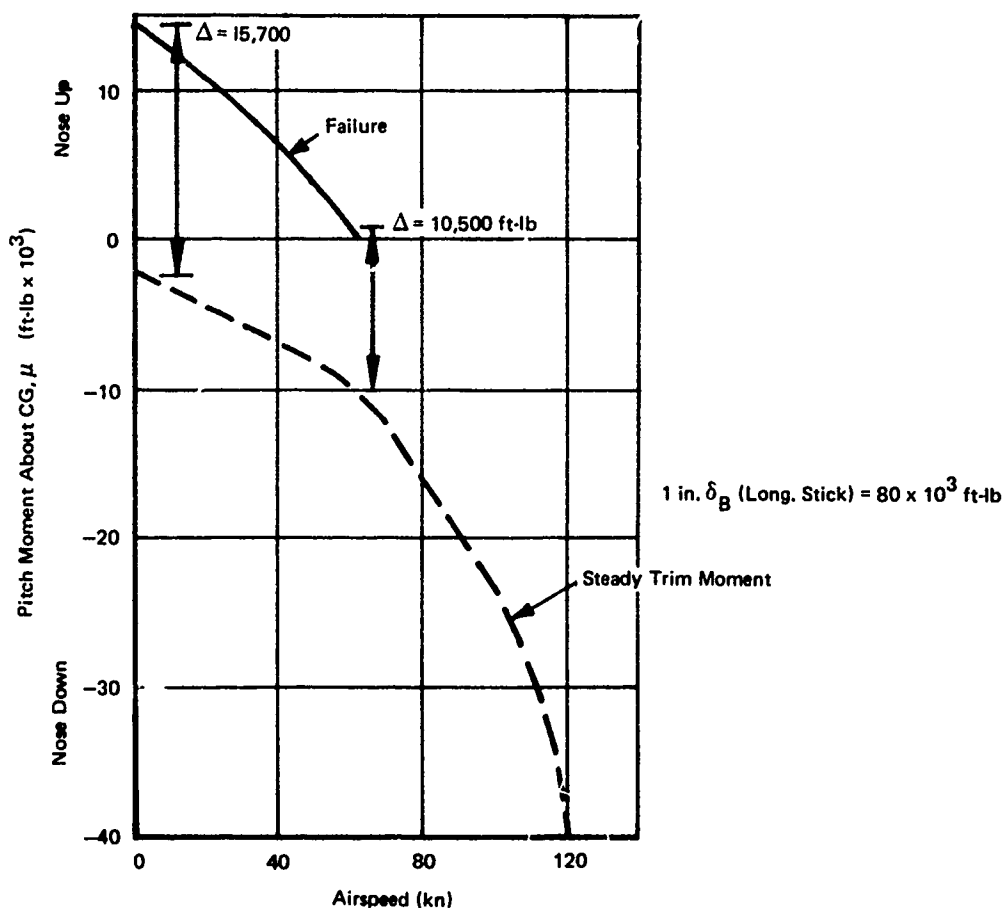
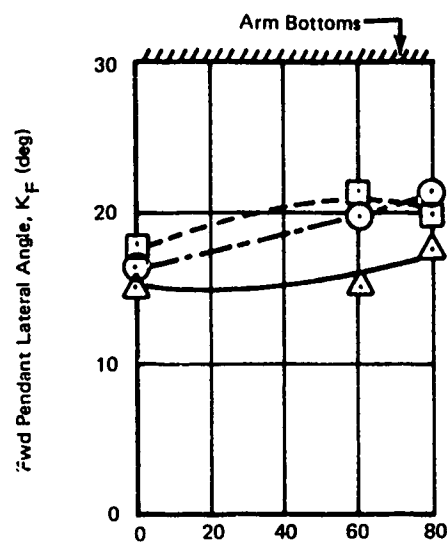


Figure 35. Longitudinal Arm Control System Hardovers.

The lateral failure effects are shown in Figure 36 as a function of airspeed and the three possible failure modes. There appears to be no danger of bottoming the actuator for these conditions, and only moderate control travel is required to offset these failures. The transient dynamics of the load yaw angle and forward arm angle which occur during a simulated yaw failure at 60 knots are presented in Figure 37. Here, the response following failure resembles that of an uncontrolled system because the hardover negates any lateral damping action or normal function of the stabilization system.

The complete hybrid model of the sling was used to compute the longitudinal response to a step helicopter longitudinal displacement shown in Figure 38. This overshoot converts to a 0.34 damping ratio in hover, which is the same as that indicated by the simple model. For the same analytical model, the influence of a yaw moment on the sling load at hover is given in Figure 39, which shows a damped response with the AAELSS-on for 15 seconds. This time history illustrates one unfavorable aspect of the system control law: the system damps yaw by moving the arm in the direction of motion, thereby reducing the yaw spring stiffness. The static yaw spring rate for this 5,000-pound load is 15,000 ft-lb/radian; for the 10 ft-lb torque, it should exhibit only a 0.00067-radian offset, yet it exhibits a peak almost ten times greater. A gain of 10 was used in this case. Reduction of the gain could minimize the problem.

Time histories of the longitudinal response are given in Figure 40. They were solved using the coupled hybrid computer simulation, complete with a linear perturbation model and the sling load digital subroutine. Again, the condition applicable to this solution is given in Table II. Part (a) of the time history is for the system-off; it clearly indicates a 0.05 damping, typical of the system-off hover. In all the cases, the input was large; it caused a 30-degree riser angle, and in the case of AAELSS-on, forced the actuator into stall, as seen by the truncated arm angles. The 3.0 gain in part (c) resulted in some improved damping, but not nearly as much as in the last oscillation of part (b), where the gain was 12. Also obvious in the time history with a gain of 12 is the poor damping in the first few cycles where actuator stall is occurring; this improves once the actuator unstalls. For this load weight, actuator stall occurs when the relative riser angle (I-J) exceeds 16 degrees. This behavior, where the motion slowly decays due to actuator stall and then almost jumps to a stop, was subsequently observed in flight test and requires a solution such as reducing gain at large amplitudes. The value of this solution is indicated by the more rapid initial decay with the lower gains than with high gain in the data presented.



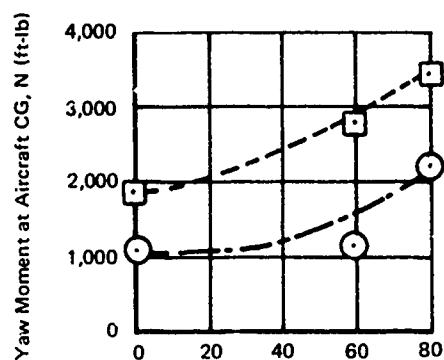
Notes:

1. Type of Failure Input

- Fwd Lateral Actuator
- △—△ Both Lateral Actuators
- Diff Lateral Actuator

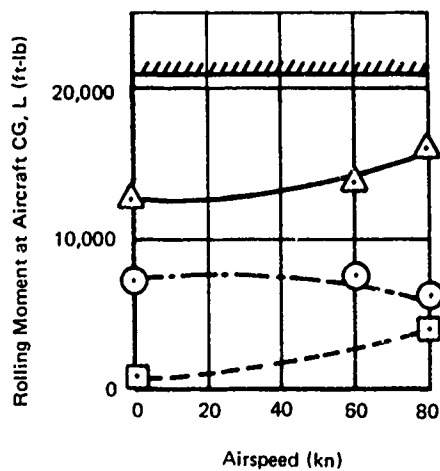
2. Basic Sling Configuration, 8-ft Riser

3. Data Computer Generated



1 in. δ_R (Pedal) = 65,000 ft-lb

Maximum Available Moment = - 150,000 ft-lb



1 in. δ_S (Lateral Stick) = 21,000 ft-lb

Maximum Available Moment = \pm 85,000 ft-lb

Figure 36. Lateral Arm Control System Hardovers.

		MINIMUM		Forward Arm Angle	MAXIMUM
		-6.5356E-02		KF VFRSUS TIME	
TIME	KF	I (-37°)		(rad)	3.3465E-01 I (19°)
2.0400E C1	-6.2549E-02	+			
2.0800E C1	-6.3853E-02	+			
2.1200E C1	-6.4555E-02	+			
2.1600E C1	-6.5149E-02	+			
2.2000F C1	-6.5343E-02	+			
2.2400E O1	-6.5255E-02	+			
2.2800F C1	-6.4786E-02	+			
2.3200F C1	-6.4012E-02	+			
2.3600E C1	-6.2758E-02	+			
2.4000E C1	-6.1362E-02	+			
2.4400E C1	-5.9375E-02	+			
2.4800F C1	-5.7328E-02	--+			
2.5200F C1	1.1592E-01	-----+			
2.5600E O1	1.8444E-01	-----+			
2.6000E C1	1.8722E-01	-----+			
2.6400F C1	2.1913E-01	-----+			
2.6800E C1	2.5195E-01	-----+			
2.7200E O1	2.7875E-01	-----+			
2.7600E C1	3.0893E-01	-----+			
2.8000E O1	3.2476E-01	-----+			
2.8400E C1	3.3450E-01	-----+			
2.8800E C1	3.3033E-01	-----+			
2.9200E C1	3.1686E-01	-----+			
2.9600E O1	2.9482E-01	-----+			
3.0000E C1	2.6821E-01	-----+			
3.0400E O1	2.3951E-01	-----+			
3.0800E C1	2.1382E-01	-----+			
3.1200E C1	1.9241E-01	-----+			
3.1600E C1	1.7895E-01	-----+			
3.2000E C1	1.7445E-01	-----+			
3.2400E O1	1.8003E-01	-----+			
3.2800E O1	1.9454E-01	-----+			
3.3200E O1	2.1617E-01	-----+			
3.3600E C1	2.4266E-01	-----+			
3.4000E C1	2.6978E-01	-----+			
3.4400E C1	2.9446E-01	-----+			
3.4800E C1	3.1352E-01	-----+			
3.5200E O1	3.2394E-01	-----+			
3.5600E C1	3.2497E-01	-----+			
3.6000E O1	3.1639E-01	-----+			
3.6400E C1	3.0053E-01	-----+			
3.6800E O1	2.7877E-01	-----+			
3.7200E C1	2.5521E-01	-----+			
3.7600E C1	2.3177E-01	-----+			
3.8000E O1	2.1208E-01	-----+			
3.8400E O1	1.9856E-01	-----+			
3.8800E C1	1.9222E-01	-----+			
3.9200E C1	1.9413E-01	-----+			
3.9600E O1	2.0390E-01	-----+			
4.0000E O1	2.2022E-01	-----+			

Conditions: As in Table II

Figure 37. Right Failure of Forward Lateral Arm at 60 Knots.

ψ_X Load Yaw Angle (rad)
PSL VERSUS TIME

 MAXIMUM
1.3831E-01
1(7.9°)

TIME	PSL	MINIMUM -2.1082E-02 1(-1.2°)
2.0400E C1	-2.0358E-02	+
2.0800E C1	-2.0681E-02	+
2.1200E C1	-2.0906E-02	+
2.1600E C1	-2.1039E-02	+
2.2000E C1	-2.1082E-02	+
2.2400E C1	-2.1043E-02	+
2.2800E C1	-2.0922E-02	+
2.3200E C1	-2.0723E-02	+
2.3600E C1	-2.0445E-02	+
2.4000E C1	-2.0085E-02	+
2.4400E C1	-1.9646E-02	+
2.4800E C1	-1.9126E-02	+
2.5200E C1	-1.8109E-02	+
2.5600E C1	-8.6093E-03	---+
2.6000E C1	1.1550E-02	-----+
2.6400E C1	3.7613E-02	-----+
2.6800E C1	6.6854E-02	-----+
2.7200E C1	9.5047E-02	-----+
2.7600E C1	1.1818E-01	-----+
2.8000E C1	1.3304E-01	-----+
2.8400E C1	1.3743E-01	-----+
2.8800E C1	1.3081E-01	-----+
2.9200E C1	1.1418E-01	-----+
2.9600E C1	9.0088E-02	-----+
3.0000E C1	6.1950E-02	-----+
3.0400E C1	3.3717E-02	-----+
3.0800E C1	9.1409E-03	-----+
3.1200E C1	-8.8120E-03	---+
3.1600E C1	-1.8272E-02	+
3.2000E C1	-1.8333E-02	+
3.2400E C1	-9.0598E-03	---+
3.2800E C1	8.5111E-03	-----+
3.3200E C1	3.2462E-02	-----+
3.3600E C1	6.0015E-02	-----+
3.4000E C1	8.7707E-02	-----+
3.4400E C1	1.1183E-01	-----+
3.4800E C1	1.2923E-01	-----+
3.5200E C1	1.3770E-01	-----+
3.5600E C1	1.3629E-01	-----+
3.6000E C1	1.2548E-01	-----+
3.6400E C1	1.0708E-01	-----+
3.6800E C1	8.3871E-02	-----+
3.7200E C1	5.9107E-02	-----+
3.7600E C1	3.6221E-02	-----+
3.8000E C1	1.8135E-02	-----+
3.8400E C1	6.9944E-03	-----+
3.8800E C1	3.9486E-03	-----+
3.9200E C1	9.1614E-03	-----+
3.9600E C1	2.1569E-02	-----+
4.0000E C1	4.0861E-02	-----+

Conditions: As in Table II

Figure 37. Continued.

TIME	XL	MINIMUM 9.5000E-02	XL (Load Position)	VERSUS TIME	MAXIMUM 2.2954E-01
0.0	9.5000E-02	+			1
4.0000E-01	9.5647E-02	+			
8.0000E-01	9.5281E-02	+			
1.2000E 00	9.5555E-02	+			
1.6000E 00	9.5474E-02	+			
2.0000E 00	9.5376E-02	+			
2.4000E 00	9.7634E-02	+			
2.8000E 00	1.0696E-01	-----+			
3.2000E 00	1.2760E-01	-----+-----+			
3.6000E 00	1.5387E-01	-----+-----+-----+			
4.0000E 00	1.8077E-01	-----+-----+-----+-----+			
4.4000E 00	2.0245E-01	-----+-----+-----+-----+-----+			
4.8000E 00	2.1780E-01	-----+-----+-----+-----+-----+-----+			
5.2000E 00	2.2660E-01	-----+-----+-----+-----+-----+-----+-----+			
5.6000E 00	2.2954E-01	-----+-----+-----+-----+-----+-----+-----+-----+			
6.0000E 00	2.2818E-01	-----+-----+-----+-----+-----+-----+-----+-----+			
6.4000E 00	2.2378E-01	-----+-----+-----+-----+-----+-----+-----+-----+			
6.8000E 00	2.1789E-01	-----+-----+-----+-----+-----+-----+-----+-----+			
7.2000E 00	2.1155E-01	-----+-----+-----+-----+-----+-----+-----+-----+			
7.6000E 00	2.0562E-01	-----+-----+-----+-----+-----+-----+-----+-----+			
8.0000E 00	2.0070E-01	-----+-----+-----+-----+-----+-----+-----+-----+			
8.4000E 00	1.9683E-01	-----+-----+-----+-----+-----+-----+-----+-----+			
8.8000E 00	1.9420E-01	-----+-----+-----+-----+-----+-----+-----+-----+			
9.2000E 00	1.9262E-01	-----+-----+-----+-----+-----+-----+-----+-----+			
9.6000E 00	1.9188E-01	-----+-----+-----+-----+-----+-----+-----+-----+			
1.0000E 01	1.9182E-01	-----+-----+-----+-----+-----+-----+-----+-----+			
1.0400E 01	1.9212E-01	-----+-----+-----+-----+-----+-----+-----+-----+			
1.0800E 01	1.9269E-01	-----+-----+-----+-----+-----+-----+-----+-----+			
1.1200E 01	1.9332E-01	-----+-----+-----+-----+-----+-----+-----+-----+			
1.1600E 01	1.9393E-01	-----+-----+-----+-----+-----+-----+-----+-----+			
1.2000E 01	1.9448E-01	-----+-----+-----+-----+-----+-----+-----+-----+			
1.2400E 01	1.9490E-01	-----+-----+-----+-----+-----+-----+-----+-----+			
1.2800E 01	1.9521E-01	-----+-----+-----+-----+-----+-----+-----+-----+			
1.3200E 01	1.9541E-01	-----+-----+-----+-----+-----+-----+-----+-----+			
1.3600E 01	1.9551E-01	-----+-----+-----+-----+-----+-----+-----+-----+			
1.4000E 01	1.9554E-01	-----+-----+-----+-----+-----+-----+-----+-----+			
1.4400E 01	1.9551E-01	-----+-----+-----+-----+-----+-----+-----+-----+			
1.4800E 01	1.9545E-01	-----+-----+-----+-----+-----+-----+-----+-----+			

Conditions: As in Table II

Figure 38. Longitudinal Response to 1-Foot Displacement in Hover.

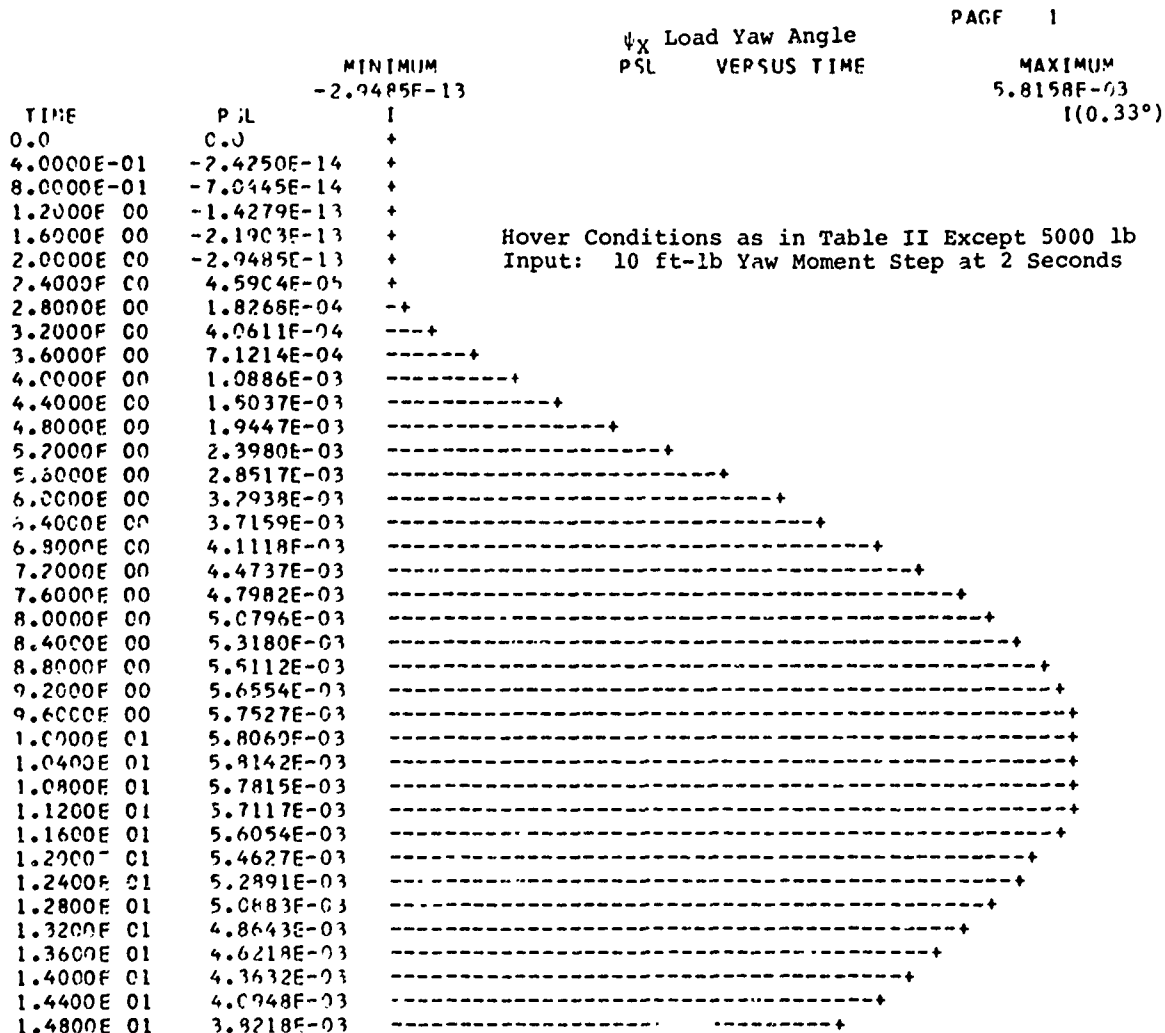


Figure 39. External Load Response to Yaw Moment.

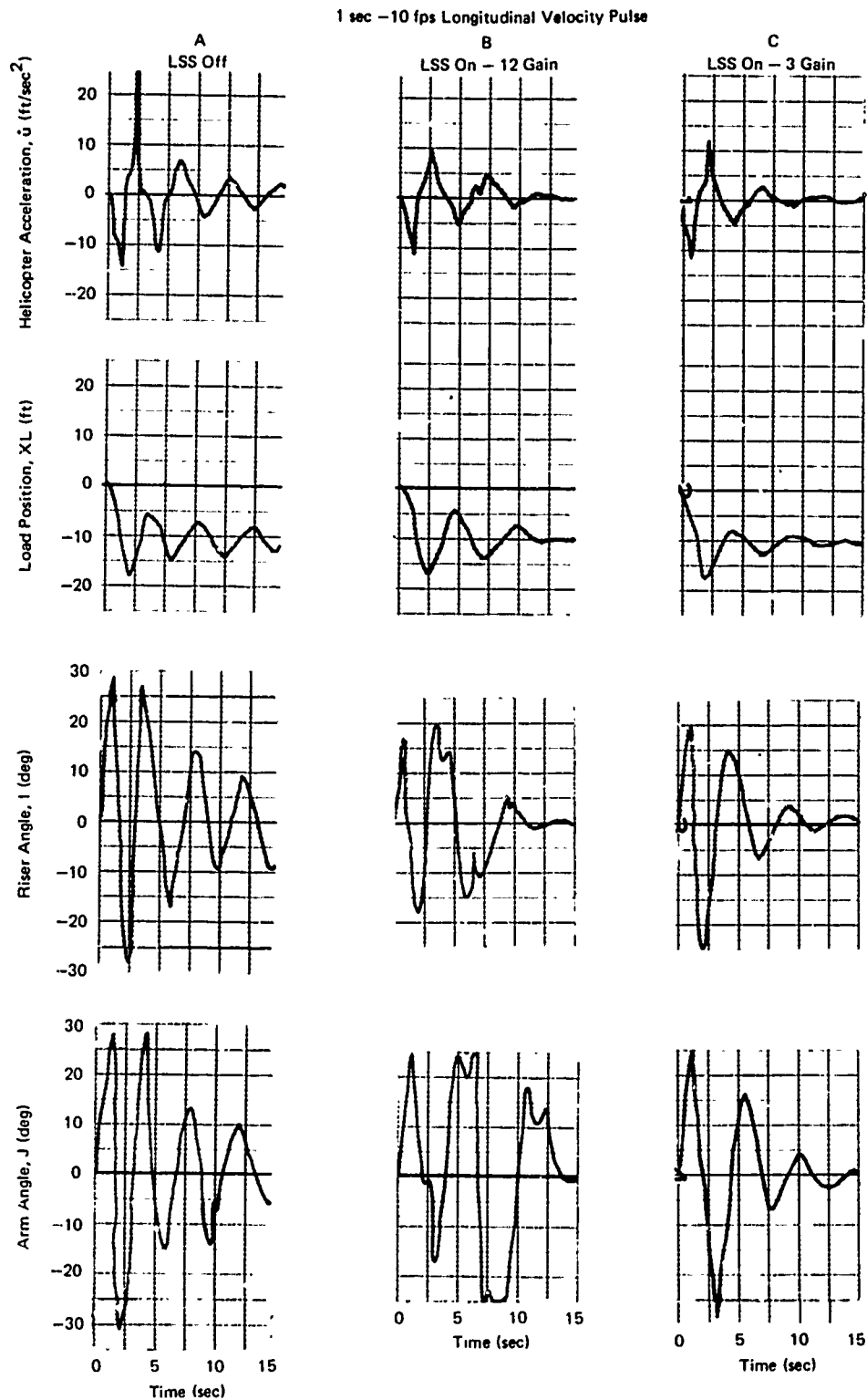


Figure 40. Helicopter Response for Various Gains.

Pilot-in-the-loop studies were conducted using the hybrid computer and Boeing Vertol moving-base flight simulator with a computer-generated heads-up three-dimensional visual display. In addition, a horizontal situation display on a cathode ray tube was used to present the helicopter position with respect to the ground. An experiment representative of a precision hover task was set up wherein the pilot made translations and a turn from one location to another. This was accomplished with a conventional Model 347 control system (no linear velocity loops) with and without the 10,000-pound external load attached. In this task, the pilot positioned the helicopter based on the display, using the cockpit instruments or visual outside-world display for attitude, direction, and velocity information. He was influenced by the load only through the acceleration or the velocity coupling into the aircraft; he had no direct indication of the load position.

Several piloted simulator flights were conducted both with and without the AAELSS operating. These evaluation flights did prove that there were no characteristics of the AAELSS, within the intended scope of the planned flight test program, which were in any way conducive to any airframe or load instability for the fully coupled (i.e., AAELSS-helicopter) system. Results pertinent to pilot control activity as a function of automatic load stabilization were, however, inconclusive. There was no significant difference in results with various degrees of load stability, and the pilot control activity appeared to be predominately a function of pilot technique.

Upon review of the AAELSS flight simulator results, two general conclusions were drawn with respect to simulator-task compatibility.

1. The pilot visual cueing was inadequate for precision load placement tasks. In the real world the helicopter pilot or load controlling crewman has either accurate visual knowledge of load position with respect to the load placement point or zone, or visual and/or aural cueing instructions from a ground observer. The AAELSS evaluation pilots had neither and could therefore operate only on disturbances of the helicopter position with respect to the ground. Since the Model 347 helicopter is a very stable one, the benefits of load stability augmentation could not be accurately assessed. For example, the AAELSS benefit to load pendulum damping which drastically reduces the time required to place a load could not be successfully evaluated in the AAELSS flight simulation investigations.
2. The pilot motion cueing was inadequate for moderate load disturbances. In precision load placement tasks,

unless the sling is very short, the load displacements tend to be fairly small and of low frequency. This results in motion cues (i.e., acceleration cues) to the pilot which are below his threshold for detection. In the real world this requires the pilot to operate solely with visual cues, requiring the accurate visual/aural cueing mentioned in the preceding conclusion. For moderate and large load disturbances, such as those generally employed to evaluate a system's performance, the real-world accelerations become most significant in a pilot's assessment of flying qualities. This case is also true in cruising flight with externally slung loads, becoming the basis for PIO problems. The AAELSS simulation involved a moderately long sling and a simulator cockpit having rather limited travel. This resulted in cockpit acceleration cues which were generally below pilot perception thresholds even with moderate load displacements. The poor fidelity of cockpit motion cues deprived the AAELSS simulator pilot of correct motion cues and forced him to rely on his inadequate visual information. This, for example, prohibited an accurate assessment of PIO.

The proper representation of the motion cues, where both amplitude and phase of the acceleration are within reason, indicated that for the long sling used in this program and a 1.0 radian system natural frequency, a 1.6-foot travel is required of the moving-base simulator cockpit to obtain a 0.05g pilot perception level. In general, the washout used on the motion base must be set to a corner frequency lower than the sling frequency so that the phase will be a reasonable representation. Since this motion base was limited to 1/3 foot of travel, only a very short sling could be studied with accuracy.

Any future simulator studies of external load dynamics should carefully consider the requirement for motion-base travel along the applicable helicopter axis. Also, the simulator, when used in precision hover tasks, should have an overall visual presentation that is representative of the real-world task. This may include a load-controlling crew station view or the pilot's view of the external load position with respect to the aircraft and background.

Command Augmentation

This part of the system uses pedal and lateral cyclic stick pickoffs driving the arm to force the load to follow the lateral and heading motion commanded by the pilot. This is accomplished in the AAELSS by taking signals proportional to the directional pedal and using them to command a lateral differential motion of the arms, and therefore to apply a yaw torque to the external load. Likewise, the roll stick signal is used

to command lateral arm motion and a lateral accelerating force to the load. In this way, as the pilot translates laterally or changes heading, the load is accelerated and decelerated along with the helicopter. This diminishes the excitation of the load natural modes of motion.

The roll and yaw circuit mechanizations are shown in Figure 34.

To make the load acceleration equal to the helicopter acceleration for this sling load arrangement, the arm angle should move six times the angle of lateral cyclic input. This is equivalent to a gain of 18 degrees of arm movement per inch of roll stick movement. For yaw, the gain parameter is given in Equation 45.

$$K_{\delta_R} = \frac{2\ell_s \bar{z}^2}{\ell_B \ell_P g} N_{\delta_R} \quad (45)$$

where N_{δ_R} is the yaw control sensitivity in radians/second-inch.

For this program, K_{δ_R} computed to be 0.1 radian/inch. The gain parameter is based on that needed to obtain equal load and helicopter accelerations. It is used with a pedal position signal washout set equal to the helicopter's time constant so that dynamic responses are matched.

Comparative Performance

Numerous schemes for stabilizing an external sling load exist. Some presently under consideration for use on helicopters are:

- The active-arm type as in this report
- A passive damper on the arm
- A control system using helicopter motion
- Aerodynamic devices on the external load

All of these systems can stabilize a load about any of the three axes of response (longitudinal, lateral, and directional) in forward flight. However for precision hover, only the first three are usable, and among those the passive damper is limited because it cannot provide the command augmentation function.

The clear superiority of the active arm system over the passive device is shown in Figure 16. A 0.3 damping ratio is obtained for a 4-foot arm with the active system, and only a marginal 0.1 damping ratio is obtained with the passive device using a

7-foot arm. The passive device is attractive because of its simplicity (no power supply needed, less maintenance), but in order to be effective, the arm must be a significant part of the pendulum length (i.e., long). The passive device is therefore useless in a winch application, where the effective sling length may be 50 or 100 feet. The active arm system, however, is still effective with only a 4-foot arm; the 50-foot riser data previously presented proves this.

Preliminary root studies of a load stabilizer system, using helicopter motion, have shown the ability to obtain a 0.2 damping ratio for all modes. This system uses cable angle, position, and rate information which, with proper control laws, commands the helicopter to move to damp the load motion. Some control augmentation is also possible by commanding special response shaping to the helicopter motion. This technique is used by overhead crane operators. The crane is stopped ahead of the desired point; the load is allowed to swing to a stop, and then the crane is brought over the load. During stabilization, this method will require significant helicopter movements that may be annoying to the pilot either in hover or in forward flight. The approximate magnitude of this motion can be assessed from the studies on the active arm since the motion at the top of the sling and cargo hook must be the same for both systems. It appears that 16 degrees is a typical peak motion of the arm. This is equivalent to a 1-foot offset and, if required by direct airframe motion, would occur with a 0.03g acceleration. Since the cockpit is four times farther from the cg than the load attachment point, the cockpit will undergo four times the acceleration. If the motion to be stabilized by the airframe is in yaw, then the acceleration at the cockpit will be 0.12g laterally (well into the objectionable level).

An example of precision hover performance in maintaining load position with respect to the ground for different types of control systems is given in Figure 41. Here a disturbance of the helicopter results in a damped response for the AAELSS control scheme, but with a steady offset that must be corrected by the pilot. However, the AAELSS response avoids the lengthy decay that exists without the controller. The higher-order control system is designed to hold position error to zero; while the others only damp the motion, and position error becomes that of the helicopter. During the step disturbance, the higher-order control holds the transient error to 1/10 that of the presently configured AAELSS system. Figure 42 is the block diagram applicable to the higher-order system. Only the longitudinal axis is shown therein, but a similar diagram is applicable to each lateral arm.

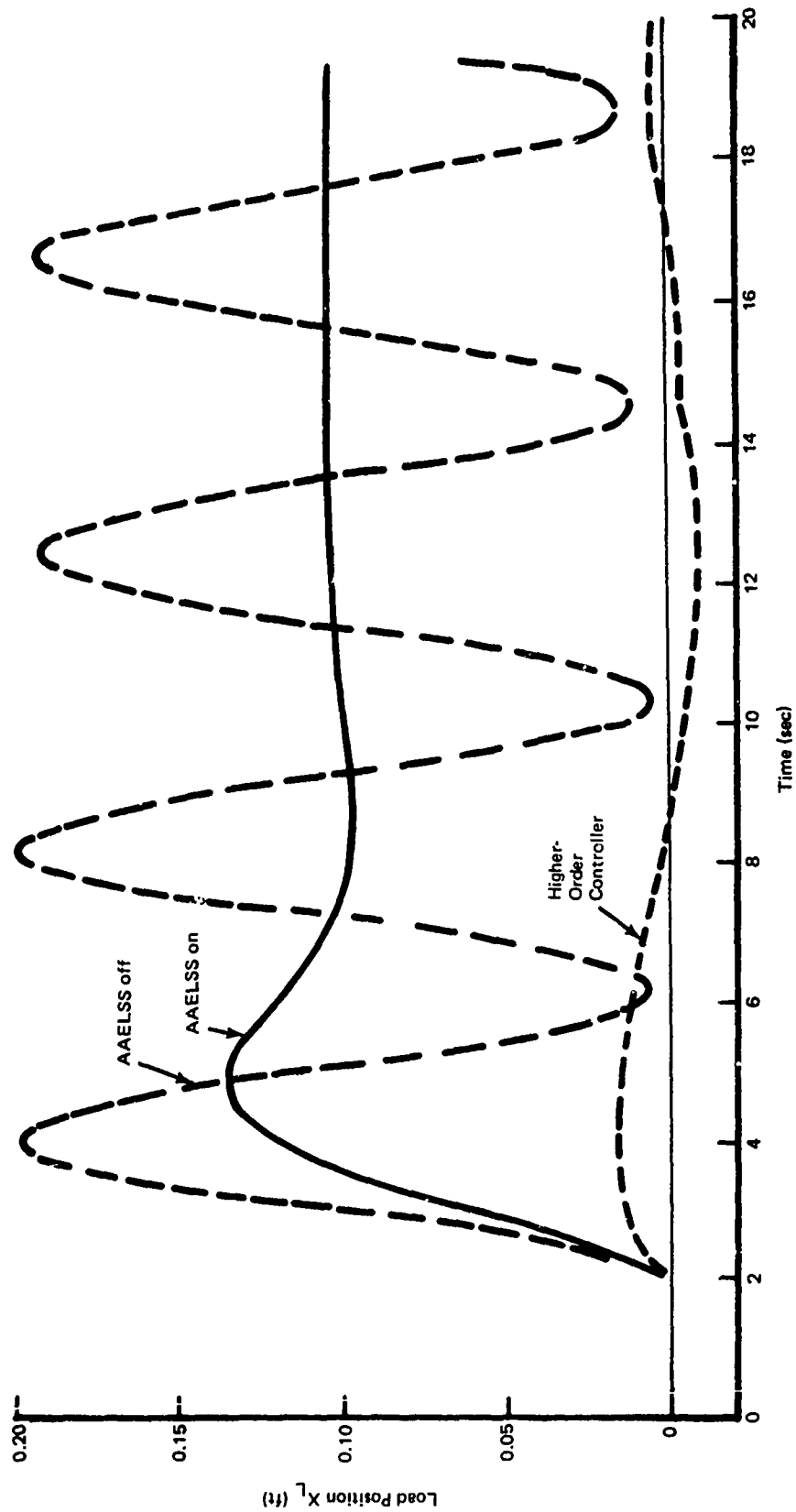


Figure 41. Computed Response to Airframe Step Displacement.

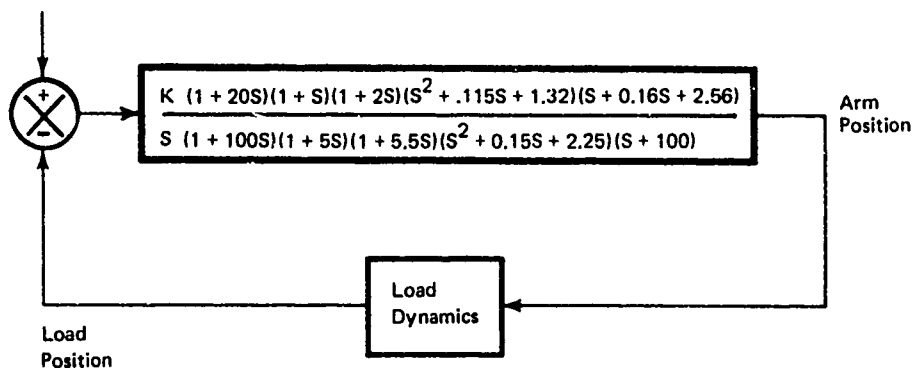


Figure 42. Higher-Order Controller.

The higher-order system is different from the AAELSS in two ways. First, it uses a true ground position of the load (X_L) for feedback. Second, it has shaping that allows a strong negative feedback, while the AAELSS controller does not. This negative feedback has the advantage of adding position restraint and reducing load position errors.

The AAELSS controller tends to reduce the inherent sling restraint (as shown for yaw response in Figure 39). The higher-order controller was not selected for flight test because it required more components, it was derived late in the program, and the selected AAELSS controller offers excellent simplicity for demonstrating the concept in flight test.

Summary of Hardware Design Requirements

The analytical study resulted in the design requirements given in Table III. The range of gains and time constants necessary for control parameter variations during flight test is also given in Table III.

The time period of the Model 347 helicopter's availability as an AAELSS test bed required that hardware design and procurement be initiated prior to the completion of the analytical phase of the program effort. Thus, it became necessary to prescribe the AAELSS hardware design requirements at a very early point in the program. The selections shown in the Table I requirements were based on preliminary sizing analyses using simplified conservative math models. Rationale for the selections of Table I was the provision of hardware components whose capability would be adequate for a meaningful flight test evaluation of the AAELSS for any foreseeable

TABLE III. HARDWARE SIZING REQUIREMENTS					
Item	Value				
Arm Length	41.0 in. Longitudinal 45.5 in. Lateral				
Arm Control Torque	5,000 ft-lb Each (Max)				
Arm Actuator Arm	9.5 in.				
Servovalve Flow Rate - Nominal	5.0 gpm				
- Required at Stall	2.0 gpm				
Aircraft Utility Hydraulic System Capacity	13.5 gpm				
Maximum Demonstration External Load	10,000 lb				
Servo Control Setting	Gain	Lag Time Constant (sec)	Washout Time Constant (sec)	Gain Parallel To Washout	Servo Position Loop Time Constant (sec)
Front Arm Longitudinal	0 to 20	0.1 to 5.0	0 to 20	0 - 2	0.1
Rear Arm Longitudinal	0 to 20	0.1 to 5.0	0 to 20	0 - 2	0.1
Front Arm Lateral	0 to 20	0.1 to 5.0	0 to 20	-	0.1
Rear Arm Lateral	0 to 20	0.1 to 5.0	0 to 20	-	0.1
Lateral Stick Pickoff	0 to 24°/in.	0	-	-	-
Directional Pedal Pickoff	0 to 9°/in.	0	0 to 3	-	-

revision to the servo control system, or control laws, that might result from subsequent analytical refinements.

Theory indicated that increasing length improved performance, so the arm length was set at the maximum practical allowed by the installation. The servovalve flow rate selected was 5 gpm. This rate was more than adequate, since the maximum flow rate needed was 2 gpm when the actuator was operating in near-stall conditions.

FLIGHT TEST PROGRAM PREPARATION

The flight test program for demonstrating the feasibility of the AAELSS was designed to use the Boeing Model 347 Advanced Technology Helicopter as the test bed. Flight testing was organized to provide comparative data of the helicopter sling load dynamics both with and without the AAELSS operating. In general, preparation for the flight testing involved:

- Rendering the Model 347 helicopter suitable for use in the program
- Developing a flight test plan and procedures document to satisfy both the contractual requirements and those of good test practice
- Conducting a safety-of-flight review
- Performing laboratory tests and calibrations of the AAELSS prior to flight
- Specification and check-out of data acquisition and recording instrumentation

AIRCRAFT CONFIGURATION

A study was made of the Model 347's maximum allowable hover gross weight with one engine inoperative (and the second engine at contingency power) for out-of-ground-effect (OGE) conditions. This was done in recognition of ground crew safety requirements during a load hookup where a power failure of one engine could be hazardous. Consideration of anticipated ambient temperatures, aircraft flight endurance time, and ballasted MILVAN weight dictated that the empty weight of the bailed Model 347 be decreased. Consequently, the equipment removals noted in Table IV were made to achieve the desired weight required for ground crew safety.

Table IV summarizes the basic Model 347 helicopter configuration used during AAELSS flight testing. This summary lists those configuration differences from the aircraft as it existed at the conclusion of Phase II of the Model 347 demonstration program. The Phase II (Winged Helicopter) configuration was identical to the Phase I (Unwinged Helicopter) aircraft except for the wing and its controls and minor gain changes in the roll SAS, roll attitude, and lateral stick pickoff. A detailed description of the Model 347 Phase I configuration is given in Reference 4.

TABLE IV. MODEL 347 ACTIVE LOAD STABILIZATION
PROGRAM, BASIC AIRCRAFT CONFIGURATION

STRUCTURE

- Phase II (winged) structure with wing removed and nonstructural fairing installed
- Wing tilt actuators removed
- Hydraulic lines capped, wire looms stowed
- End restraints for beam installed
- Right searchlight out, camera brackets installed
- Heater removed

FLIGHT CONTROLS

- Phase II cyclic trim actuators
- Schedule and operation unchanged from Phase II program
- Manual option
- Lateral control rerigged to Phase I configuration

INSTRUMENTATION, BALLAST

- Record package and TM transmitter installations as Phase I and II programs
- Right water ballast tank, water ballast dump capability removed

VIBRATION

- All self-tuning vibration absorbers removed
- Beam for pendulum flap absorbers installed in place of spacer on forward vertical shaft

SAS, AFCS

- Authorities, shaping, and gains as established for Phase II programs

AVIONICS

- Doppler removed
- Coupled navigational modes inoperative (pallet removed)
- Flight director removed
- Standard VGI installed
- Radar altimeter removed

ROTOR BLADES

- Forward head - SK 24385-5 blades
- Aft head - SK 24385-6 blades
- Standard CH-47C rotor blades with boron-reinforced trailing edges and boron skins on boxes 2, 5, and 6

FLIGHT TEST PLAN

Flight test planning resulted in the specification of the general test configurations summarized in Table V. As may be noted, the first four configurations provided compliance with the contractual requirements. The next three (Configurations 5, 6, and 7) were planned as options for consideration in the event that cost and schedule circumstances were favorable.

The general approach to testing was one of safely expanding the flight envelope. Basically, the flight envelope expansion involved an incremental airspeed buildup starting from hover and stopping at the maximum safe airspeed (V_{Limit}). At each airspeed and for each load weight, the following was prescribed:

1. Evaluation of system dynamic response due to pulse disturbance input by the pilot through his flight controls. This evaluation was required for each of the following modes of AAELSS operation:
 - a. System off
 - b. Synchronized mode
 - c. Damping mode
 - (1) Longitudinal only
 - (2) Lateral only
 - (3) Both longitudinal and lateral
2. Evaluation of system response to the simulated AAELSS failures as given in Table VI.

On-line monitoring of the system responses was required during the evaluations at each airspeed. Not until the monitored responses showed it safe to proceed to the next higher airspeed was authority granted to further expand the envelope. Similarly, when the responses became critical for any reason, these data served to define the maximum safe airspeed.

SAFETY-OF-FLIGHT REVIEW

Prior to initiating the flight test program, a formal safety-of-flight review was conducted and flight clearance obtained. Reference 5 documents the safety-of-flight review.

The AAELSS failure response data given in the Theoretical Analysis section was presented at the review. These data indicated that the bypass valve arrangement in the AAELSS would limit

TABLE V. TEST CONFIGURATIONS							
No.	Load (lb)	Riser Length (ft)	Leg Length (ft) Fwd Aft	Paralleling Cable	Flight Regime	Comment	Contract Req't
1	10,000	8	11 8	Yes	VFR		Yes
2	5,000	8	11 8	Yes	VFR		Yes
3	10,000	50	11 8	No	VFR	Hover Only	Yes
4	10,000	8	11 8	Yes	IFR	Hover & Low Speed	Yes
5	10,000	8	11 8	No	VFR	Infield, Forward	No
6	10,000	8	11 8	Yes	VFR	Passive Mode	No
7	10,000	8	11 11	Yes	VFR		No

TABLE VI. SIMULATED AAELSS FAILURES

1. Aft Longitudinal Actuator Full Forward
2. Aft Longitudinal Actuator Full Aft
3. Forward Longitudinal Actuator Full Aft
4. Forward Longitudinal Actuator Full Forward
5. Aft Lateral Actuator Full Left
6. Aft Lateral Actuator Full Right
7. Forward Lateral Actuator Full Left
8. Forward Lateral Actuator Full Right
9. Forward Lateral Actuator Full Left & Aft Lateral Actuator Full Right
10. Repeat (9) & Retract Both Longitudinal Actuators While Accelerating to Next Higher Trim Speed

the moments generated about the arm pivots to always provide a controllable MILVAN response well within the trim capability of the available control power about each axis. However, certain failures during cruise could result in MILVAN lateral motion exceeding the ± 30 -degree limit placed on load line of action from structural design criteria. For this reason, flight planning was designed to provide on-line telemetry monitoring of MILVAN motions and important structural loads. Further, by using a speed buildup technique for flight envelope exploration and expansion and by requiring AAELSS failure simulations at each of the airspeeds, a safe approach toward experimental definition of maximum safe airspeed was provided.

A second factor in the definition of maximum safe airspeed was load/airframe collision in the event of sling failure. Wind tunnel testing had provided limiting speeds as a function of MILVAN weight (see Figure 3) which were prescribed as valid for purposes of AAELSS flight testing.

LABORATORY AND PRELIMINARY HELICOPTER TESTS

The AAELSS was completely assembled and bench tested without any cargo load simulation in the Boeing engineering laboratory complex. This testing provided a checkout of the entire AAELSS except for the helicopter hydraulic and electrical power supplies, which were replaced by laboratory power supplies. The decade boxes, used in the AAELSS prototype for varying control subsystem gains and time constants, were checked for proper operation and calibrated over the range of settings given in Table III. Figure 43 pictures the AAELSS load beam mounted to its test stand in the laboratory.

The laboratory testing of the unloaded AAELSS achieved the following results:

- Check of travel range and clearance of the various components
- Sensor polarity check
- Establishment and setting of actuator position loop time constants at 0.1 second
- Polarity check of control law with cargo hook angle inputs
- Initial setting of hydraulic bypass valves

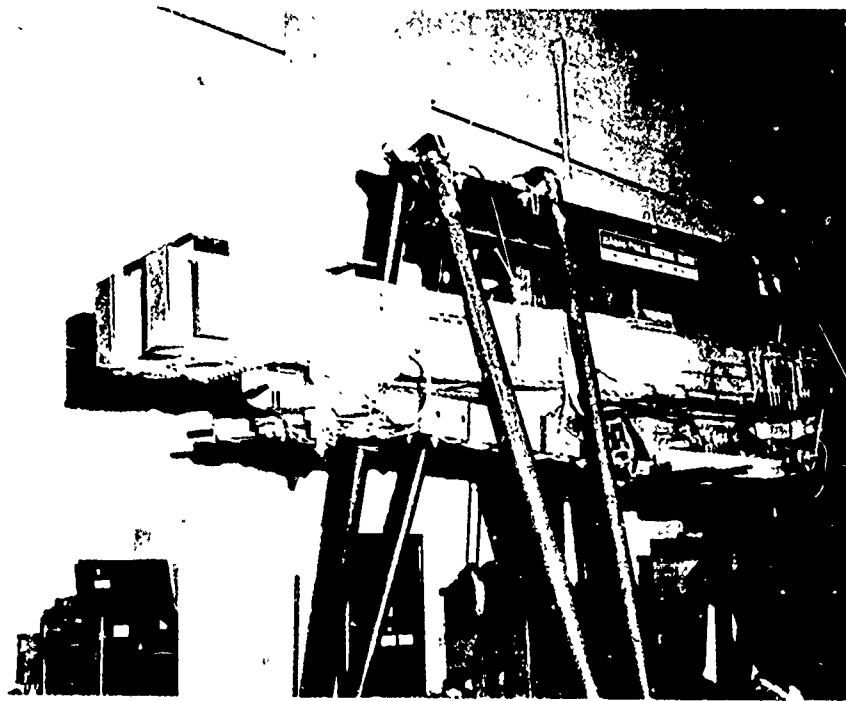


Figure 43. AAELSS Mounted on Laboratory Test Stand.

- Check of arm extension and retraction
- Check of longitudinal trail angle of arms with steady cable angle
- System pressure check

A short (2-foot-long) sling was used early in the laboratory testing to check the various operating modes of the AAELSS; namely, OFF, SYNCHRONIZED, and ACTIVE. The OFF mode removed all power to the AAELSS; the ACTIVE mode provided the normal AAELSS damping functions, and the SYNCHRONIZED mode commanded a free-swinging of the arms while under system power. In the SYNCHRONIZED mode the actuators commanded the arms to track the cable (align themselves with the cable) so that they acted like a portion of the riser cables. In the laboratory tests and later in flight tests, it was found that there was no significant difference in load pendulum damping between operation in the SYNCHRONIZED and OFF modes.

Retraction and extension cycling operations in the laboratory indicated that the system required special sequencing of its equipment switches to perform satisfactorily because the cargo hook circuits were normally effective during these operations, which gave rise to the possibility of high rates of arm operation and hard contact with the retract/stow stops.

Following the laboratory tests, the AAELSS was coupled to the Model 347 helicopter and subjected to further ground testing. These preliminary helicopter tests served to once again check AAELSS functioning and polarity. Initial tests of the integrated flight test instrumentation were also performed at that time.

A series of hover flights was then performed to check the AAELSS operation with a moderate load (approximately 500 pounds) attached to individual arms. Simulated actuator hard-over failures were injected to check both the failure input hardware and the AAELSS response. Five flights were made in this test series. The following three problems were discovered and corrected:

- The beam rolled within its elastic restraint to a degree sufficient to disengage the hydraulic quick-disconnect fitting on the return line, causing a hydraulic lock which prevented normal arm retraction. Remedial action consisted of providing more slack in the hydraulic lines, incorporating a cutoff valve in the aircraft side of the pressure line, using a check valve in the aircraft side of the return line, and providing a bleed valve on the beam side of the pressure line.

- A Dural hydraulic fitting on the hydraulic manifold failed, resulting in loss of fluid from the helicopter utility hydraulic system. All Dural fittings were replaced with stainless steel hardware.
- Synchro shaft slippage caused sensor null shifts. Retention of these shafts (accomplished by friction clamping in the initial design) was reworked to provide positive mechanical clamping.

Upon completion of the hover check flights, the system was cleared to proceed with the formal data acquisition and feasibility demonstration flight program.

INSTRUMENTATION AND RECORDED DATA

Flight test data for the AAELSS test program were gathered by an Ampex AR200 magnetic tape recording system on board the Model 347 test aircraft. Basically, this system converts physical measurements to magnetic analogs and records them on tape, allowing easy conversion to other useful forms of information.

All forms of physical measurements (accelerations, forces, motions, positions, pressures, temperatures, etc.) were converted to electrical voltages by suitable transducers, and the magnetic equivalents of these voltage outputs were recorded on magnetic tape. The Ampex AR200 tape recorder has a tape capacity of 14 tracks of data with 12 channels per track, each of which can record the output of one transducer. A broad frequency spectrum is divided into 12 subcarrier frequencies, each modulated by a transducer output. These 12 signals are combined into one composite signal by frequency shared multiplexing equipment, suitably amplified and recorded on one tape track.

The recording package for the AAELSS test program utilized one tape track for basic aircraft parameters and another track for a binary time code signal, which is the necessary accurate time reference. The remaining 11 tracks were used as required for test data recording (132 parameters available).

One track of data at a time was transmitted from the aircraft to the ground station Sanborn Pen Recorders installed in the Telemetry Van for in-flight monitoring of critical parameters. A selector switch was provided in the cockpit for data track selection. The telemetered data was also simultaneously recorded on the airborne magnetic tape along with the other parameters during data records.

Following data flights, the magnetic tape data was converted into various useful forms. Bandpass filters separated the

subcarrier frequencies of the composite signals and the information from each channel was extracted. These data, in an analog voltage form, could be readily viewed on an oscilloscope or recorded on an oscillograph for visual analysis of transducer outputs. Oscillograph strip-outs were obtained at various speeds and with various frequencies filtered to enhance waveform analysis. Most important, the analog data were capable of conversion to binary digital form and recording on a digital tape recorder. The digital tape served as the input for digital computers and graphical display units. The tabulated engineering values and plots resulting from the digital conversion were the prime output of the data system.

The parameters that were recorded during the AAELSS flight program are given in TABLE VII.

TABLE VII. AAELSS FLIGHT TEST DATA ACQUISITION

ANALOG MAGNETIC TAPE

- External Cargo Positions and Loads
 - Arm Angle - Lateral - Fwd, Aft
 - Arm Angle - Longitudinal - Fwd, Aft
 - Cable Angle - Lateral - Fwd, Aft
 - Cable Angle - Longitudinal - Fwd, Aft
 - Actuator Axial Load - Lateral - Fwd, Aft
 - Actuator Axial Load - Longitudinal - Fwd, Aft
 - Arm Axial Load - Fwd, Aft
- Aircraft Loads
 - Swiveling Actuator Axial Load - Fwd
 - Fixed Link Axial Load - Fwd Inbd, Aft Inbd, Aft Outbd
 - Rotor Shaft Torque - Fwd, Aft
- Aircraft Linear Accelerations
 - Sta. 95 Floor - Vert, Lat, Long.
 - Sta. 360 Floor - Vert, Lat, Long.
- Aircraft Angular Motions
 - Position - Pitch, Roll, Yaw
 - Velocity - Pitch, Roll, Yaw
 - Sideslip Angle
- Aircraft Control Positions
 - Lateral Stick Position
 - Longitudinal Stick Position
 - Directional Pedal Position
 - Thrust Lever Position
 - Dash Actuator Position - Upper, Lower
- Basic Aircraft Parameters
 - Outside Air Temperature
 - Airspeed
 - Altitude

EXTERNALLY MOUNTED AIRCRAFT MOTION PICTURE CAMERA

Milliken DBM4C Camera - 10MM lens
 24 fps, 200 Ft Mag - Run time - 150 sec

FLIGHT TEST RESULTS

The AAELSS was fitted to the Boeing Vertol Model 347 helicopter and test flown at Millville, New Jersey in the fall of 1972. A summary of the load damping characteristics recorded during the flight testing is presented in Figure 44. The bar height indicates the damping ratio, which is plotted separately for the longitudinal and lateral axes. Figure 44 compares the AAELSS damping characteristics at the various airspeeds, load weights, riser lengths, and control system settings used during flight testing. These characteristics are discussed in detail in this section.

The conventional external sling load (simulated by disengaging the AAELSS) displayed damping ratio (ζ) consistently near 0.05 for both the longitudinal and lateral axes for all the variations tested. Historically, with the two-point suspension, the longitudinal and lateral damping in hover has been on the order of 0.03 to 0.1, and there have occasionally been limit cycle roll-yaw oscillations that restricted maximum permissible forward-flight speeds. Thus, the present flight test results agree with past experience. The forward-flight stability of the sling load is sensitive to rigging geometry, MILVAN attitude, and riser length. It must be stressed that conclusions drawn from the present results apply only to the standard 8x8x20 MILVAN and sling configuration flown, especially for the AAELSS off (basic unaugmented) case.

Figure 44 shows that with the AAELSS turned on, the damping exceeded the minimum requirements of MIL-H-8501A for IFR operations in all cases tested. The 0.25 load modal damping ratio design objective was met except for the loaded MILVAN container in hover ($\zeta=0.22$) and the 58-foot-riser sling load ($\zeta=0.18$ to 0.22). Control system gain had a large influence on the 58-foot riser sling load dynamics, as indicated by the bar chart. Pilot comment was consistent with the damping data trends presented.

IFR flight operations with external sling loads have historically been complicated by false motion cues due to poor load dynamics. The pilot responds to these false motion cues and unknowingly moves the stick in a way that sustains oscillation. This pilot-induced oscillation often restricts IFR operations. The tendency was once again verified by this program. However, testing shows that AAELSS did eliminate it, even following a sustained oscillation which existed prior to AAELSS engagement.

A command control augmentation system using roll stick and pedal inputs was tested. The function of this system was to command the sling load to coincide with the commanded

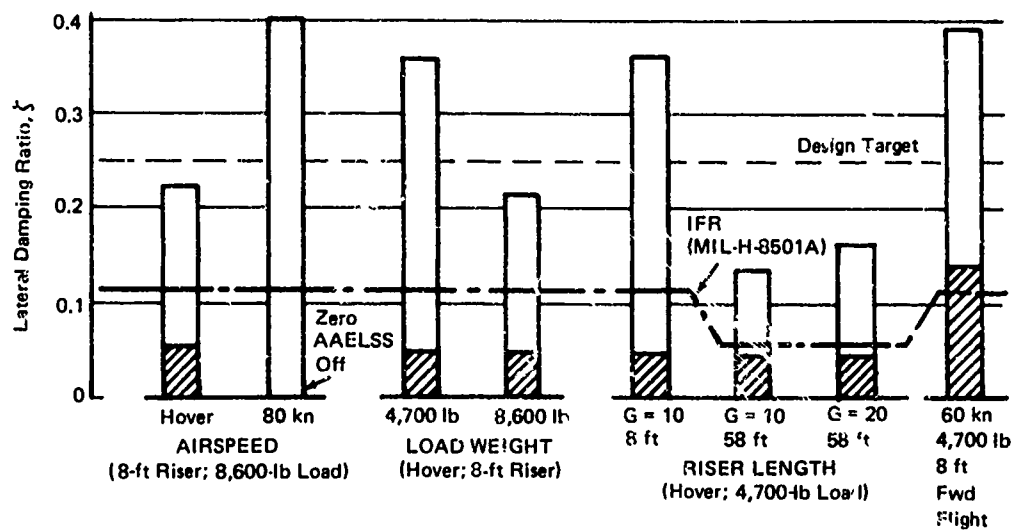
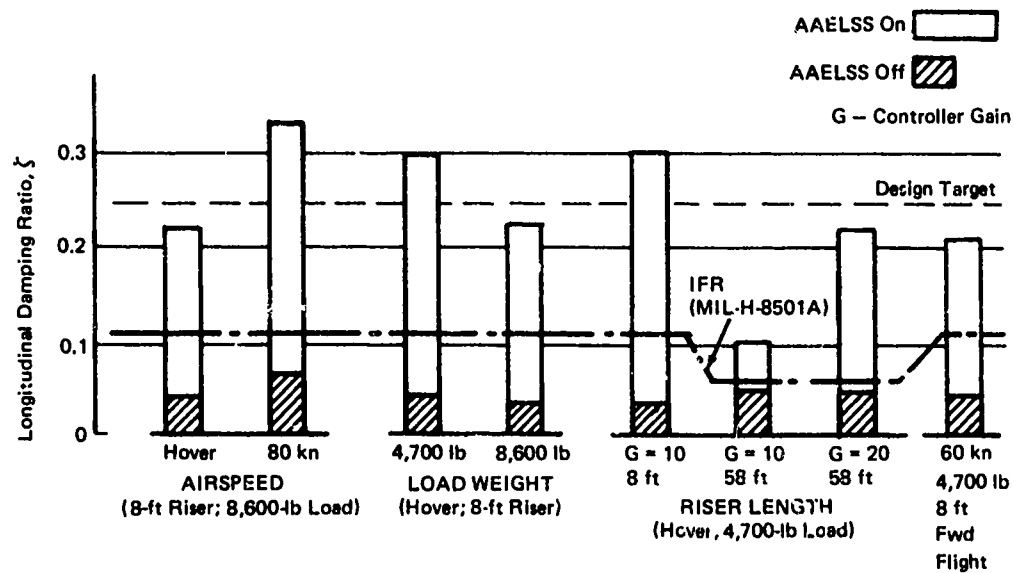


Figure 44. Summary of Load Damping Characteristics.

helicopter lateral and directional motions and thus expedite hover load placement.

The hardware used in the flight testing of this AAELSS prototype was developed solely to prove concept feasibility, and it did this. The limitations and problems associated with the prototype hardware are reviewed and summarized later in this section.

SCOPE OF TESTS AND DATA FORMAT

The test configurations explored during the flight program were Configurations 1 through 5 of Table V. In addition, pilot-induced oscillation checks for IFR capability were also performed at cruising airspeed. The loaded MILVAN condition was limited to 8,600 pounds to provide single-engine hover capability out of ground effect. The flight envelope flown assured that any hardware failures of the AAELSS actuators would be safe and that the sling failure boundary of Figure 3 would not be violated. A complete detailed accounting of the test conditions for each flight and the data record, along with pilot comments and problems/corrective action, are included in the appendixes. Essentially, all the useful engineering data can be obtained from Flights 660 through 664, and therefore only these are reviewed in depth in this report. Prior flights were devoted to initial verification and debugging of the AAELSS hardware.

A set of three pendulum angles was chosen to describe the motion of the load with respect to the helicopter. Two of these, the longitudinal and lateral pendulum angles, are illustrated in Figure 45. They describe the travel of the midpoint of the paralleling cable with respect to an axis system fixed in the helicopter. The third angle is the sling load yaw angle, defined as the heading of the load with respect to the helicopter. These angles were all synthesized from the individual cable and arm angles in the data processing. The need for this type of data presentation became apparent during flight test monitoring, where it was found to be extremely difficult to evaluate the load motion from the four arm and cable angles. All the results presented in this section use these three pendulum angles to describe load angular position. The term cable angle is used to denote the angle that the cable makes with the arm.

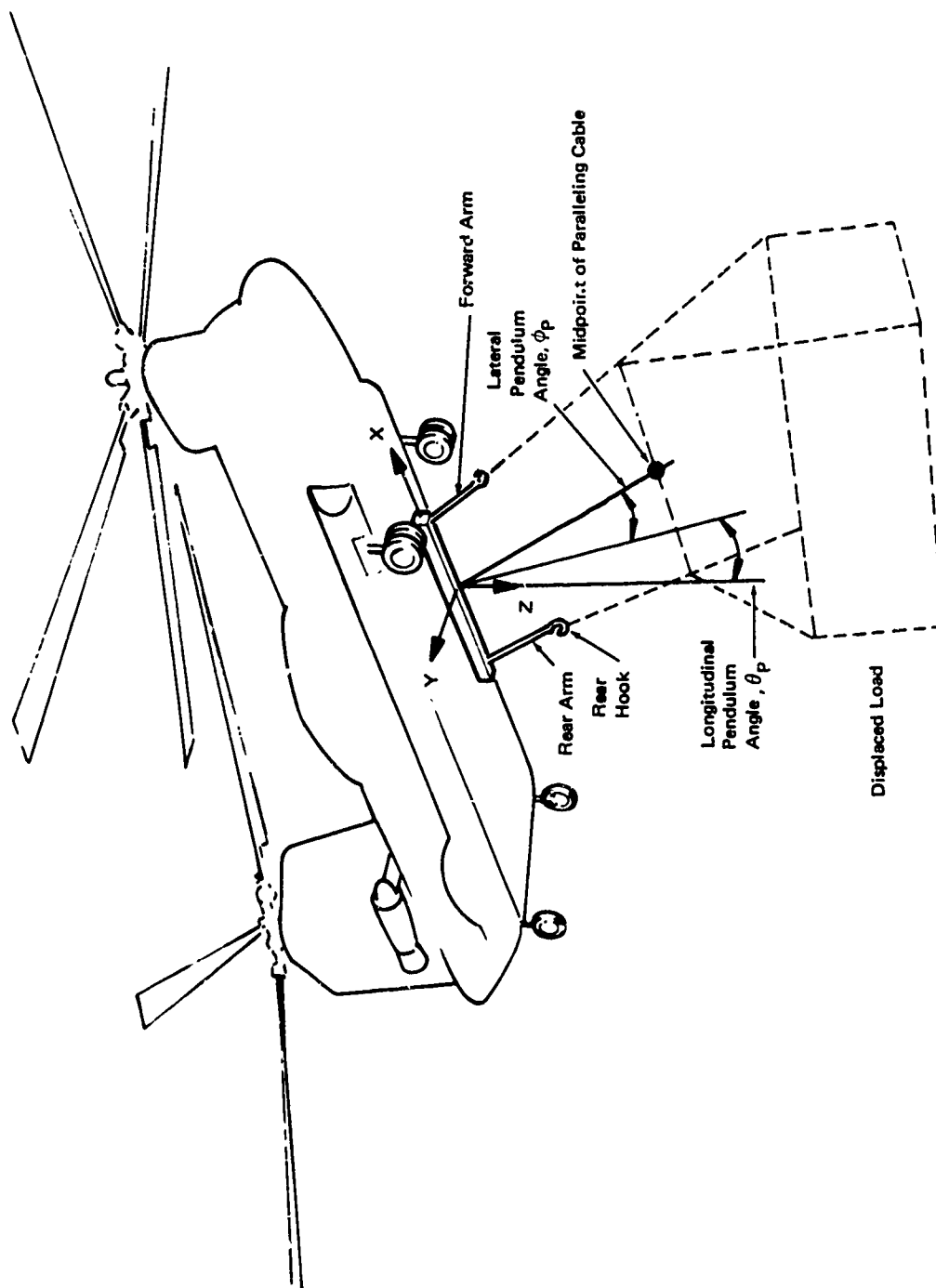


Figure 45. Angles Describing Load Motion.

AAELSS DAMPING CHARACTERISTICS

Time histories were recorded during this test program to provide a back-to-back comparison of the AAELSS active damping to that inherent in the basic uncontrolled sling for all the test conditions flown. Damping was extracted from the data by using the exponential delay from a plot of peak amplitude versus time. Care was taken not to use data where excessive nonlinear system action occurred (such as during actuator stall), and thus the reported damping approaches the best possible with all nonlinearity eliminated.

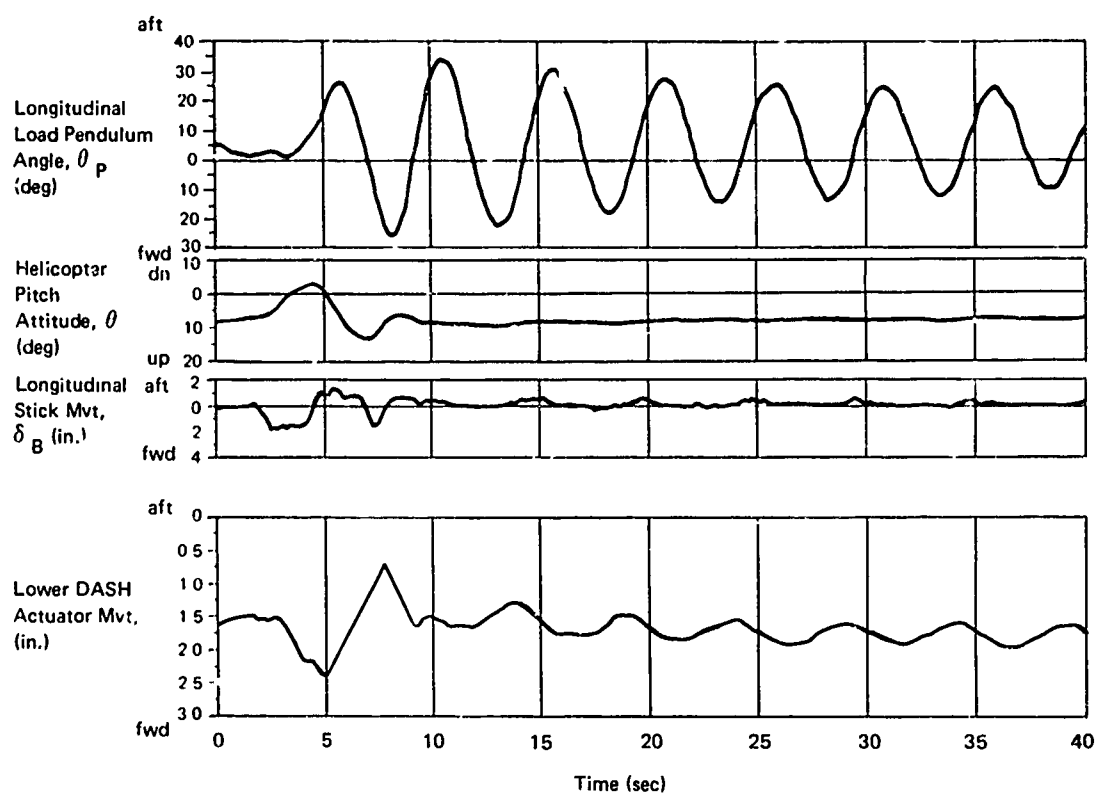
In Figure 44, the reported lateral damping was for the least damped of the several modes present. The long-period lateral drift was excluded.

Unless otherwise noted, the control system gains and lag time constant were set to their most favorable values.

Hover Characteristics, Empty MILVAN Basic Sling

The first flight data taken were for the basic sling configuration with the 8-foot riser and an empty (4,700-pound) MILVAN. The unaugmented (AAELSS off) dynamics are presented for each degree of motion freedom in Figures 46, 47, and 48. In this and all other stability tests, the pilot excited the load by a simple doublet type control input to displace the helicopter about either the longitudinal, lateral, or directional axis. The data in Figure 46 illustrate the ease with which even a moderate helicopter pitch-angle disturbance excites a lightly damped ($\zeta=0.03$) sling load longitudinal mode. Even with the DASH augmentation and pilot stick inputs, there is little damping difference from the 0.05 seen in prior testing discussed under Technical Approach. Figure 47 shows the yaw mode with a 0.05 damping ratio. It also shows two modes of MILVAN lateral motion (ϕ_p): one a well-damped ($\zeta=0.1$) roll motion, and the other a coupling with the 0.05 damped yaw mode (the latter is dominant). In Figure 48, the well-damped roll mode is dominant, thus giving the pilot the impression of good stability about this axis. In these figures it may be noted that the load motion persists to nearly 50 percent of its original magnitude even 20 to 30 seconds after the input has stopped. Such load response complicates a precision hover task even with this short 8-foot riser, since the pilot has to wait out or otherwise stop the load motion prior to placing the load.

Figure 49 is an excellent example of AAELSS active operation for the longitudinal axis. This record started with AAELSS off. The AAELSS was then turned on (evidenced where the cable angle has a large step change). During the first complete oscillation following AAELSS activation, the actuator was stalled (load saturated as indicated by the truncated actuator



Flt-Run: 660-2
 Control Sys: Off
 Excitation: Long.
 Stick
 Airspeed: Hover
 Load: 4,700 lb
 Riser: 8 ft

Figure 46. Longitudinal Damping With AAELSS Off, Empty MILVAN.

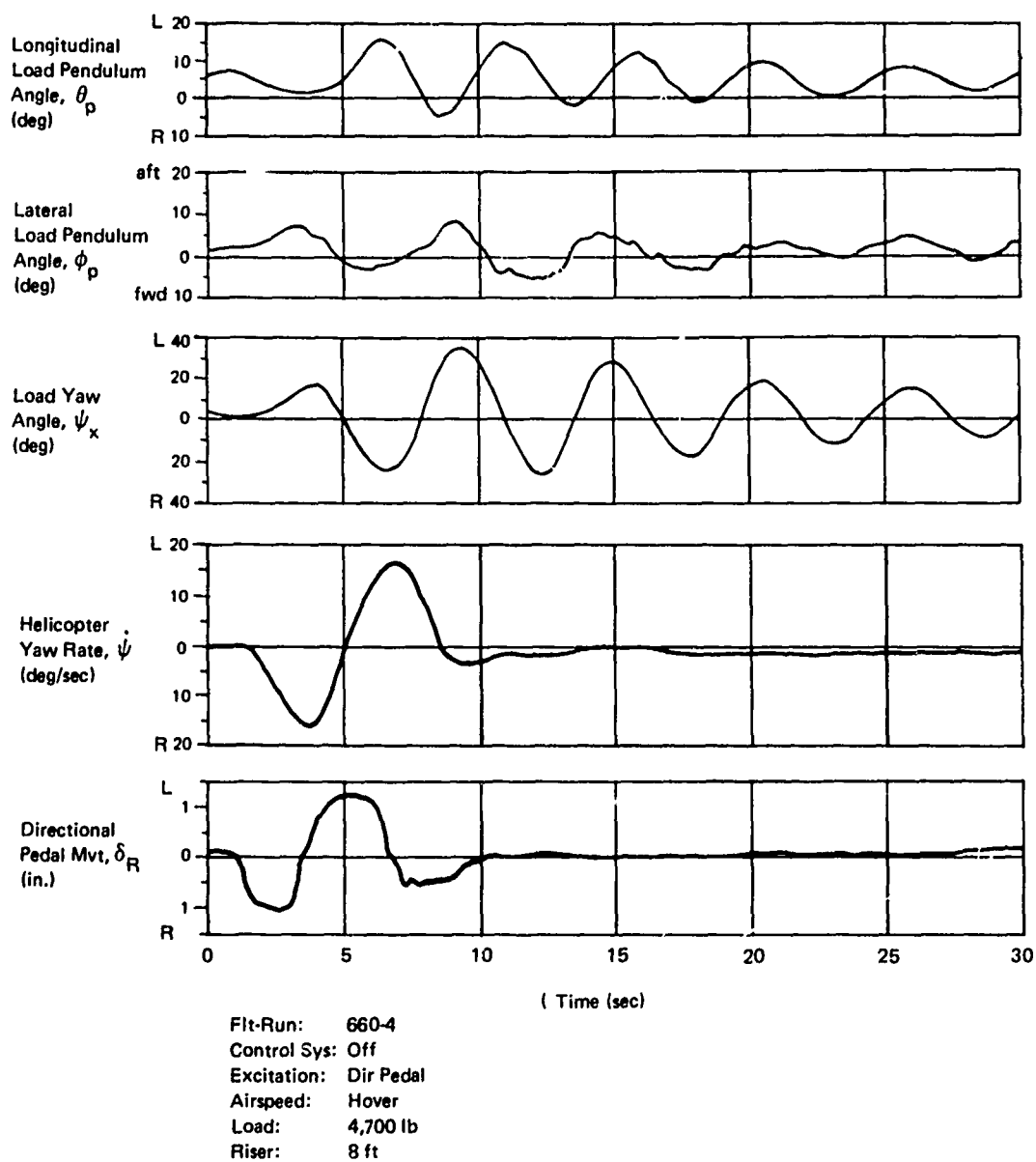
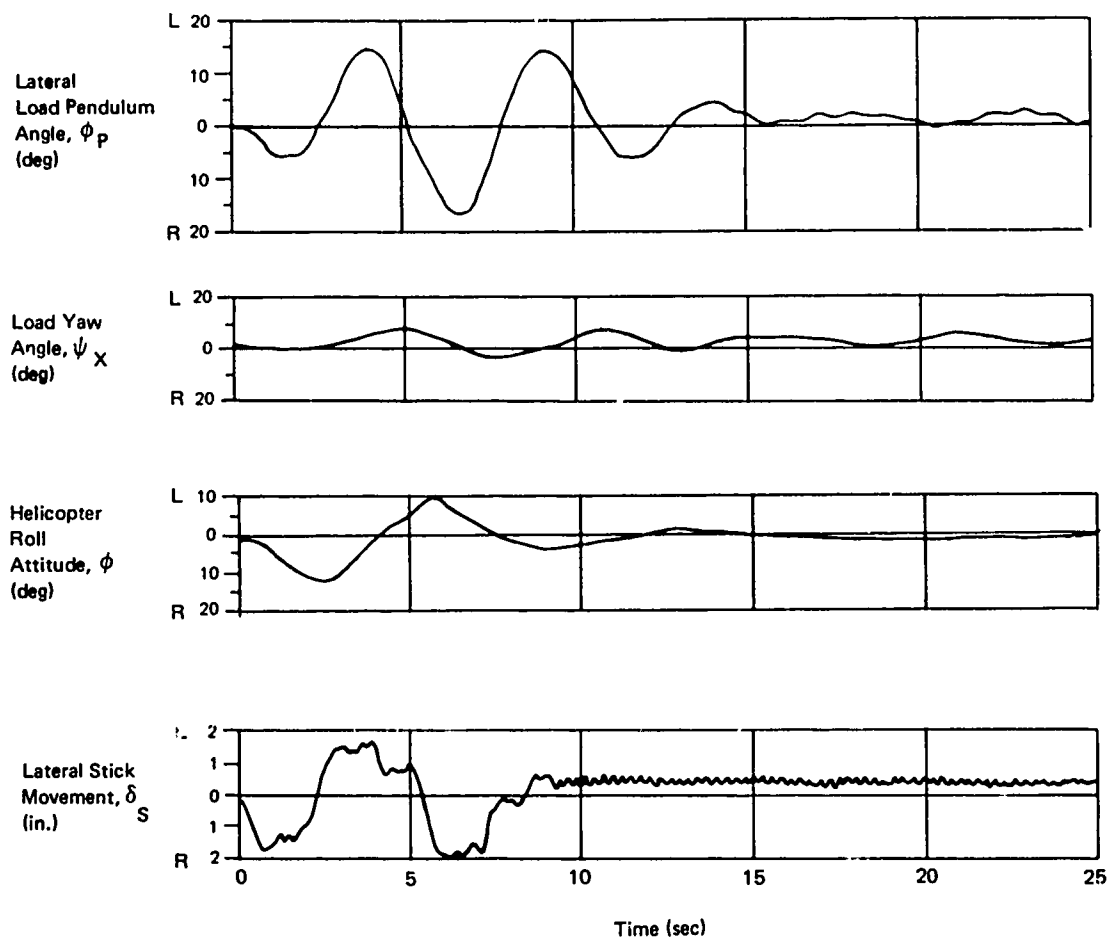


Figure 47. Yaw Damping With AAELSS Off, Empty MILVAN.



Flt-Run: 660-3
 Control Sys: Off
 Excitation: Roll Stick
 Airspeed: Hover
 Load: 4700 lb
 Riser: 8 ft

Figure 48. Roll Damping With AAELSS On, Empty MILVAN.

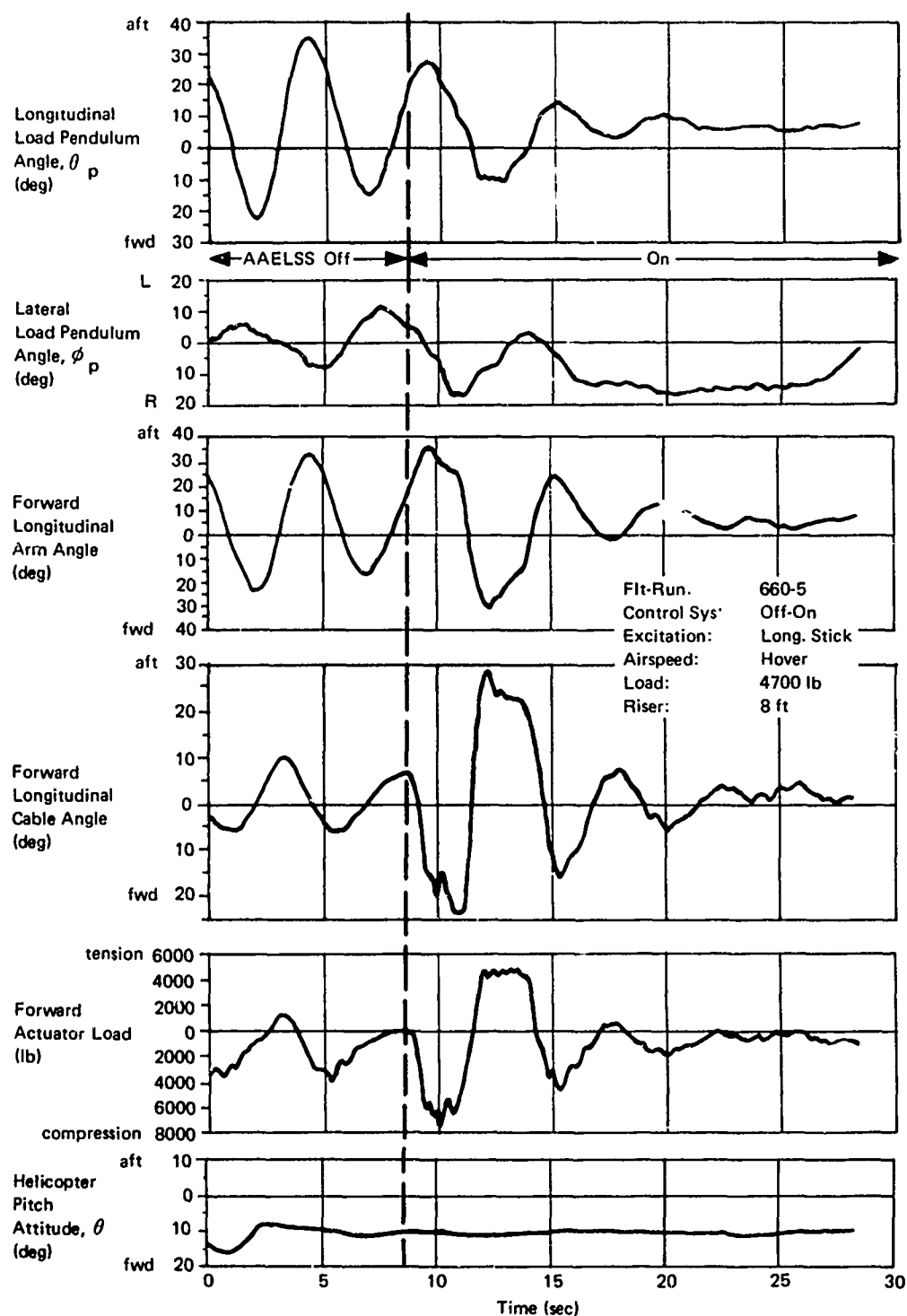


Figure 49. Longitudinal Damping With AAELSS On, Empty MILVAN.

load and cable traces). During this time, the damping action is small. For the next half cycle, there is a minimum of saturation or other nonlinear effects, and a 0.3 damping ratio is achieved. Subsequent motion appears to be poorly damped due to certain system nonlinearities which are discussed later.

With the AAELSS turned off, the arm position should track the load line of action with very little cable angle resulting. Any cable angle would indicate torque about the arm upper pivot and therefore the presence of some drag in the actuator or pivot. Such torque is evident in the longitudinal cable trace of Figure 49, but it did not appear to contribute any significant damping.

The response to roll excitation shown in Figure 50 presents a clear picture of both the strong roll and yaw damping (yaw damping ratio better than 0.3) provided by the AAELSS. Yaw damping here is significantly improved compared to the AAELSS-off case of Figure 48. Even though the roll damping for AAELSS off was fairly good to begin with, it was still markedly improved by the AAELSS active damping.

Pilot comments on the empty MILVAN indicated that the load stability with the AAELSS off was representative of a normal uncontrolled two-point suspension configuration. With the AAELSS active, the pilot noted a very dramatic increase in load damping, which he expressed as a decrease of cycles to damp, from about 5 with the AAELSS off to 1.5 with the AAELSS on.

Effect of Load Weight in Hover

Figure 51 shows that a loaded (8,600-pound) MILVAN exhibits a load damping ratio of 0.04 to 0.05 about all axes with the AAELSS off. The modulation of heading amplitude (i.e., beating) shown therein is caused by dynamic coupling between the lateral and directional load motions. This damping level is essentially identical to that shown for the empty MILVAN.

Figure 52 indicates that the damping ratio of the loaded MILVAN is increased to a value of 0.24 with the AAELSS active. Similarly, test results showed damping to be 0.22 for the lateral motion. As shown in Figure 44, these system-on damping levels were higher for the empty MILVAN than for the loaded container. This lower damping at higher load weight is caused by nonlinear effects from sensor hysteresis, which is evident in the longitudinal pendulum and cable angle time histories of Figure 52.

Control Law Verification

Hovering flight tests were conducted to select values of the control system gains and time constants by means of a parametric variation of the value of these quantities. The flight

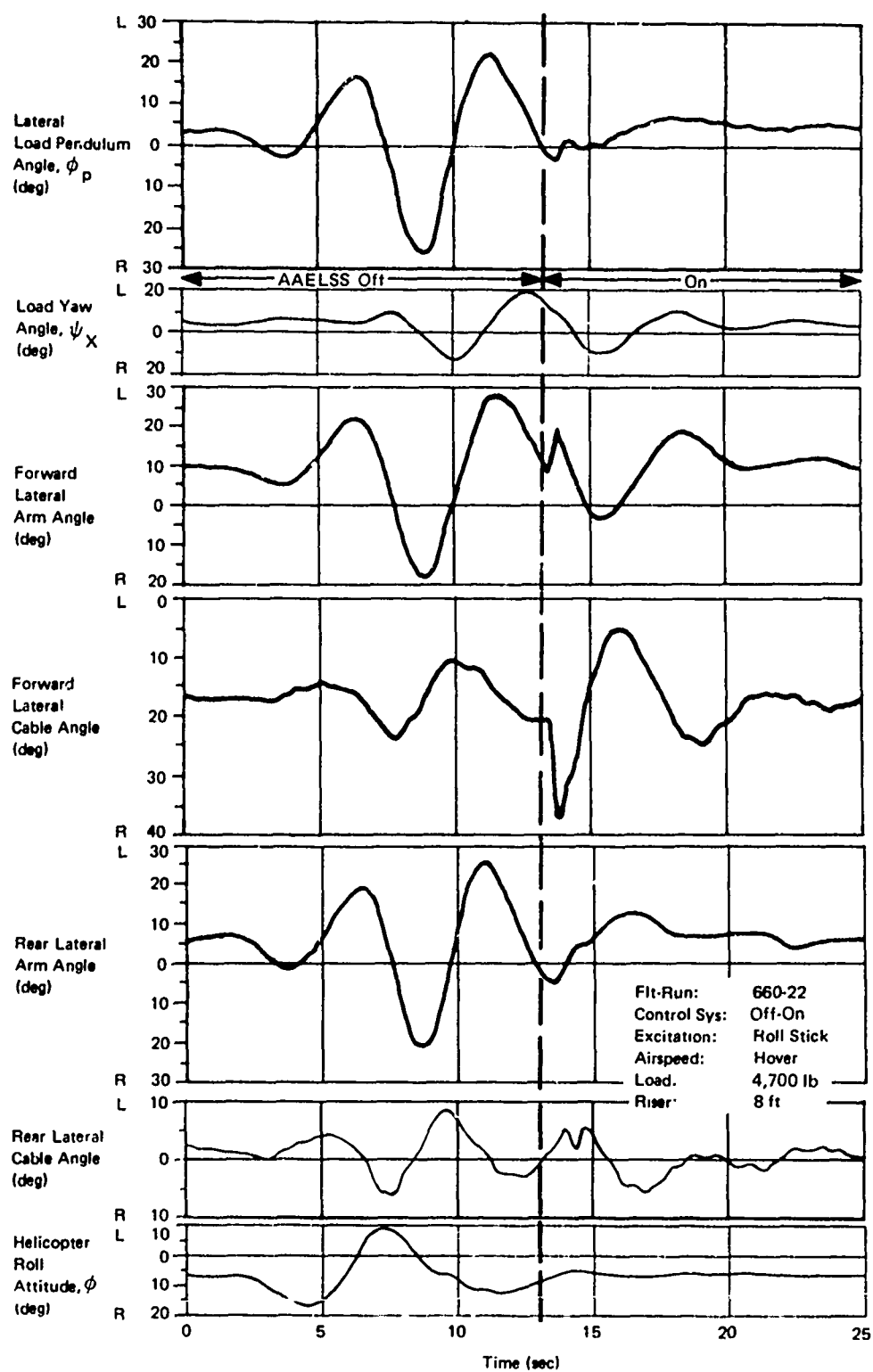
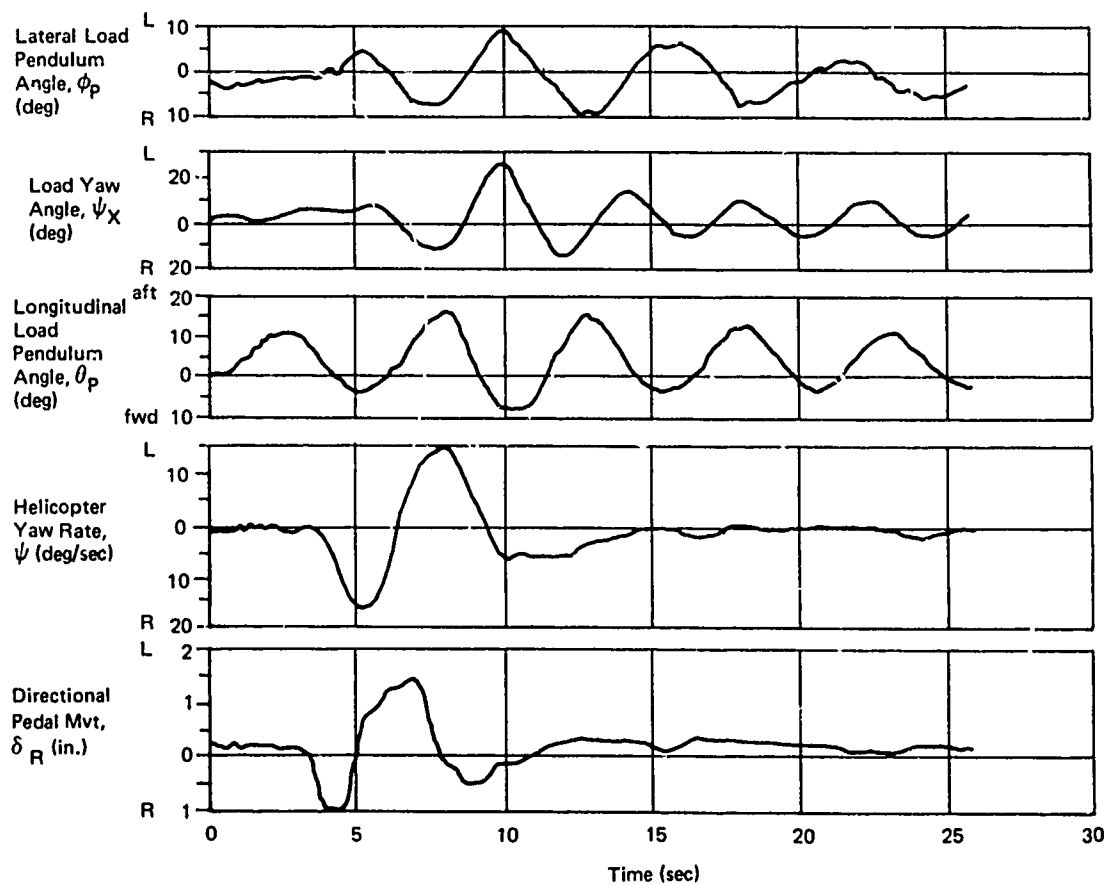
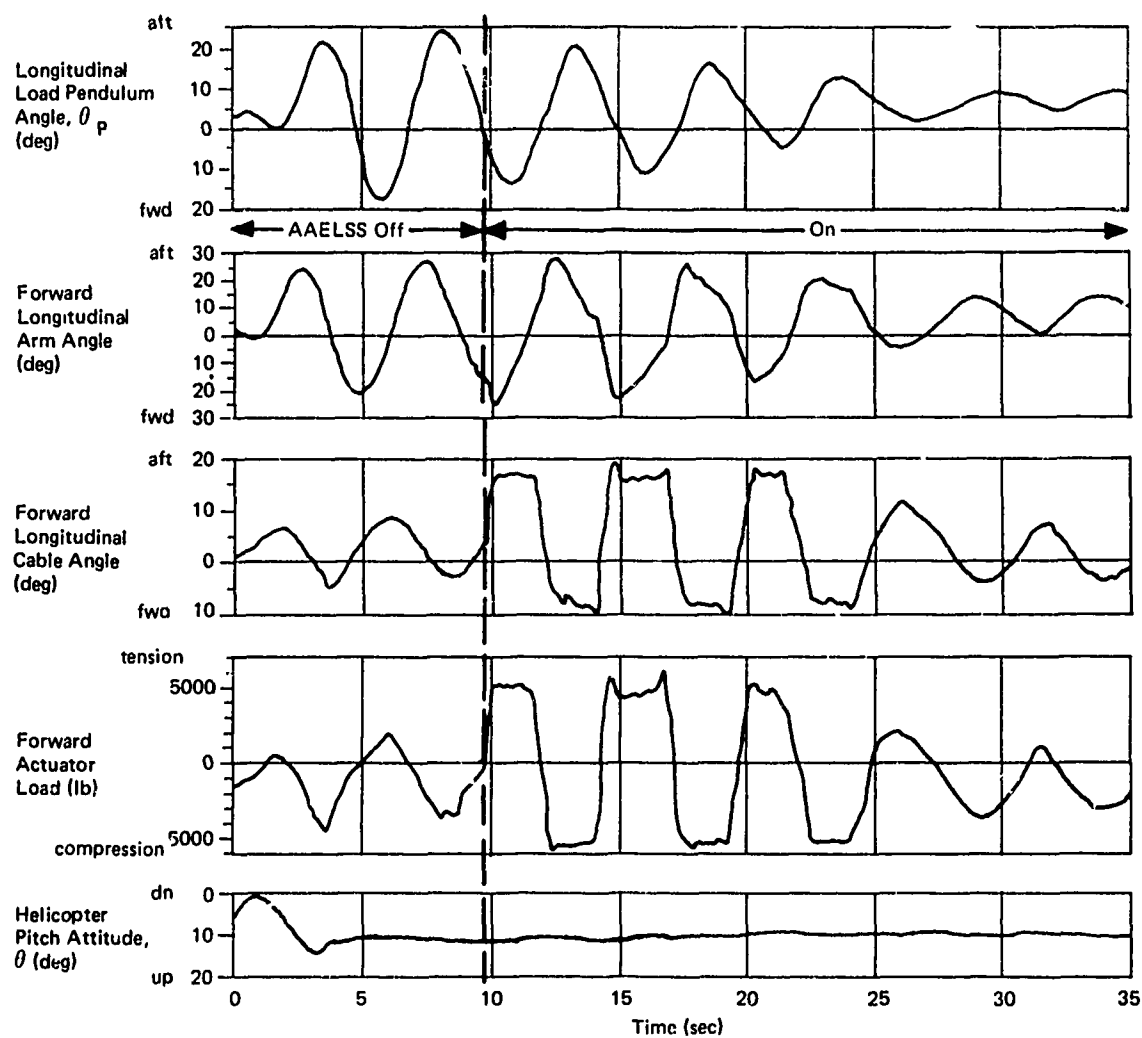


Figure 50. Lateral-Directional Damping With AAELSS On, Empty MILVAN.



Flt-Run: 661-5
 Control Sys: Off
 Axis: Yaw
 Airspeed: Hover
 Load: 8,600 lb
 Riser: 8 ft

Figure 51. Yaw Damping With AAELSS Off, Loaded MILVAN



Flt-Run:	661-10
Control Sys:	Off-On
Excitation:	Longitudinal
Airspeed:	Hover
Load:	8,600 lb
Riser:	8 ft

Figure 52. Longitudinal Damping With AAELSS On, Loaded MILVAN.

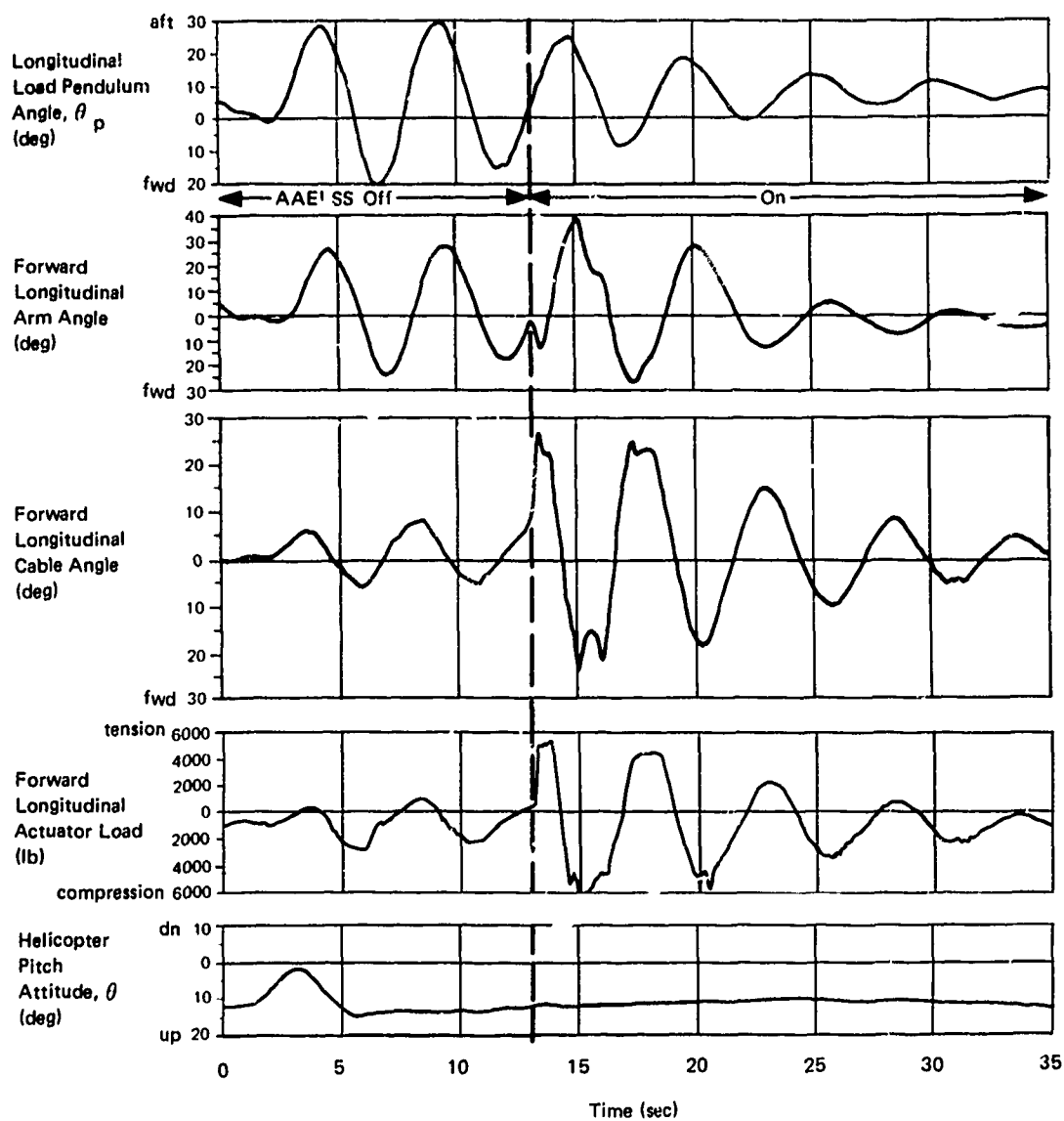
testing resulted in the selection of a 1.9-second lag time constant and a gain of 10, compared with theoretically predicted selections of 2.0 seconds and 10.

Table VIII is a comparison of flight test results with theory for the variation of load longitudinal damping with lag time constant. As may be noted, good agreement on damping exists for the optimum lag time constant. However, for long lag time constants, testing showed a larger loss of damping than theory would predict. This appears to be caused by the compounding of lags introduced by the longer lag time constant and by system sensor hysteresis. Figures 49 and 53 illustrate time histories of system responses at optimum lag time constant (1.9 seconds) and the large lag time constant (2.8 seconds), respectively.

Gain settings of 5 and 10 were tested with the empty MILVAN. Although either gain setting provided satisfactory damping in the lateral axis, a value of 5 was finally selected to minimize a low-frequency oscillation that was noted. Longitudinally, damping appeared nearly proportional to gain, resulting in the

TABLE VIII. DAMPING/TIME CONSTANT TRENDS, LONGITUDINAL AXIS		
Lag Time Constant, τ (Sec)	Damping	
	Test	Theoretical Prediction
1.9 (Optimum)	0.3	0.34
2.8	0.1	0.25
<u>Notes</u> Gain - 10 Washout - 10 sec		

selection of the higher value (10) for this axis. No attempt was made to adjust gains or time constants in forward flight, since adequate damping was displayed by the AAELSS in cruise.



Flt-Run: 660-13
 Control Sys: Off-On
 Excitation: Long. Stick
 Airspeed: Hover
 Load: 4,700 lb
 Riser: 8 ft

Figure 53. Longitudinal Damping With Large Lag Time Constant.

Hover Stability With a 58-Foot Riser

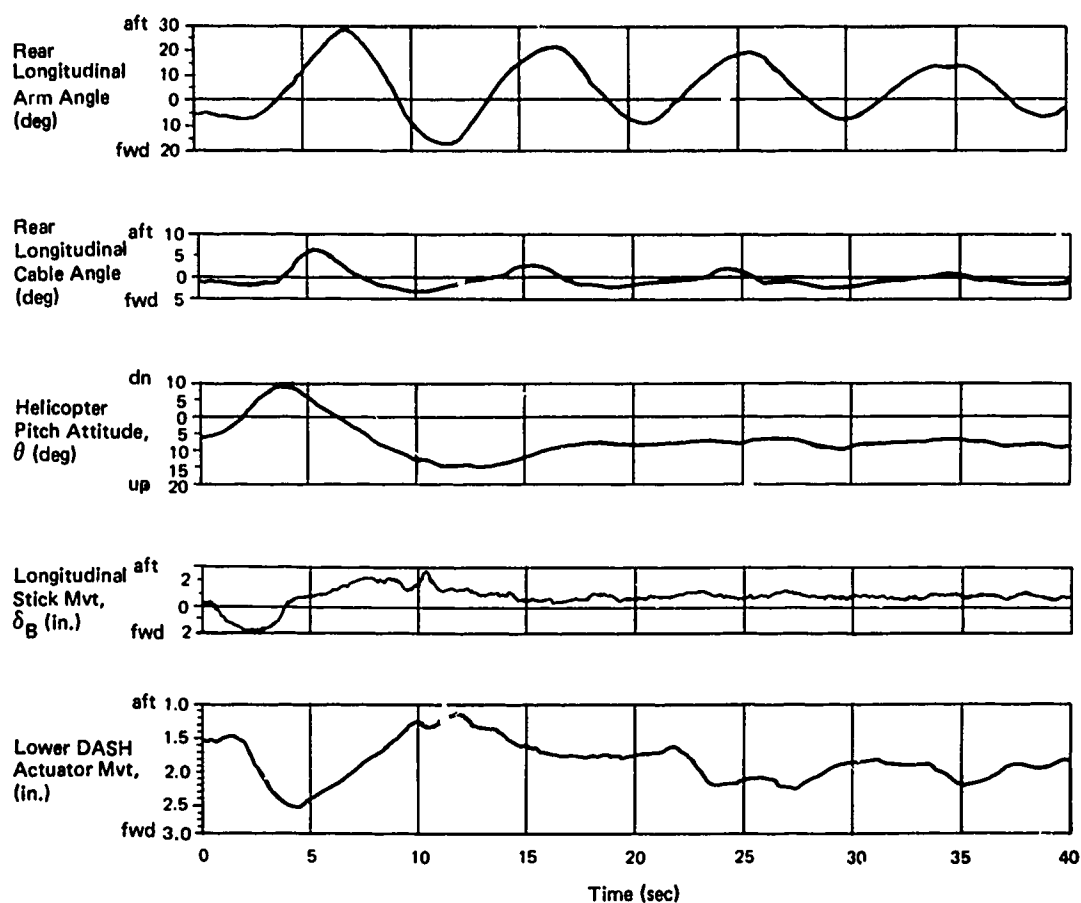
Testing with the long (58-foot) riser was limited to hover flights, which happened to occur on a day of high steady winds with gusts. Longitudinal tests were flown in a crosswind and lateral tests in a headwind. These heading conditions were found to provide the least load damping and were therefore the most critical. Response time histories for the empty MILVAN with AAELSS disengaged are shown in Figure 54 and 55. These tests indicated approximately a 0.04 damping ratio about all axes, agreeing with prior tests of 50-foot riser suspensions, as shown in Figure 4.

The motion excitation for the responses shown for the lateral-directional modes in Figure 55 occurred prior to the starting time shown in the figure; it was a pilot lateral cyclic control input. In spite of this roll excitation, the figure shows a strong yaw response which appears to be growing in magnitude. This response is the result of roll and yaw motions coupling and beating, probably due to the nose-down attitude rigging of the MILVAN. The dominant single mode of motion displayed by the arm angle traces was used to determine system damping for these AAELSS-off dynamics.

Again the difficulty of precision hover is seen in both of the AAELSS-off time histories (Figures 54 and 55). The peak amplitude in both cases is approximately $\pm 25^\circ$, which means that the load is traversing ± 25 feet with the 58-foot riser. For this disturbance, and even with smaller ones, it would still take more than 20 seconds to reduce the initial amplitude by 50 percent.

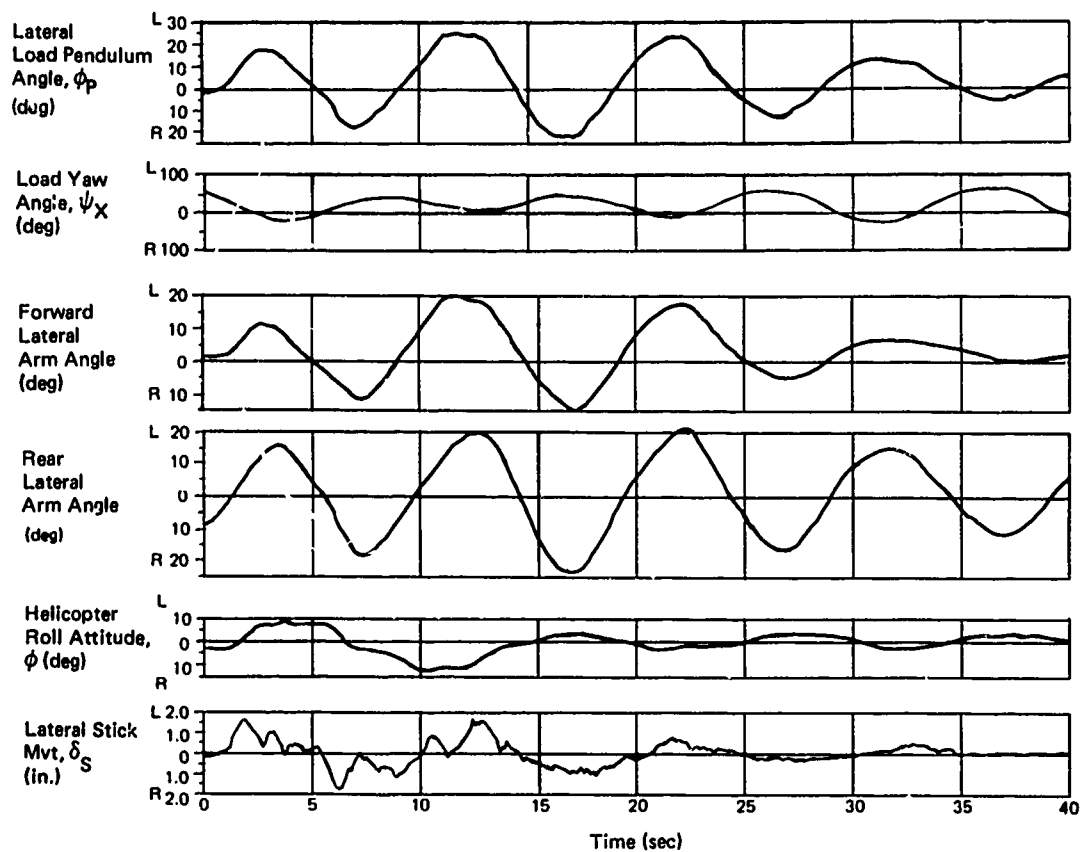
The improvement of longitudinal damping with the AAELSS on at a gain of 10 with the 58-foot riser is shown in Figure 56. After 15 seconds, where actuator stalling (indicated by the truncated cable-angle trace) ceases, the damping is slightly greater than 0.10. Later in the trace, the motion appears to become a constant-amplitude oscillation due to sensor hysteresis. Figure 57 shows that high gain is beneficial with the 58-foot riser, increasing the damping to 0.20. The high-frequency motion in these traces is associated with local sling motion and should be ignored.

The lateral dynamics with AAELSS on at high gain (20) evidence several cycles where the actuator is stalled (see Figure 58); only moderate damping results at first, followed by rapid damping. However, a very long period lateral oscillation causes an offset of the arm. Therefore, using a gain which varies with load lateral displacement (i.e., cable angle signal) may be beneficial. For example, use of a lower gain at the large cable angles would decrease chances of actuator stall and improve the damping for these large motions. Likewise, maintaining high



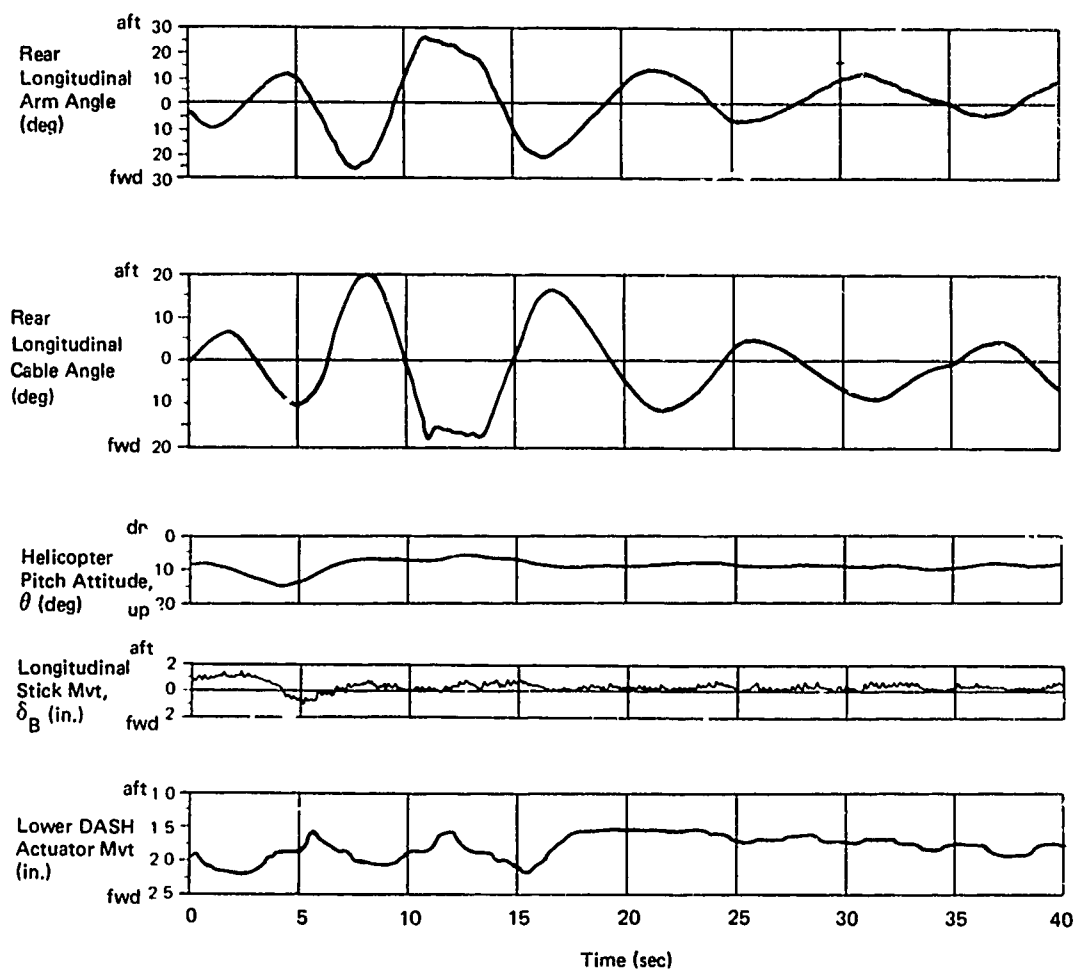
Flt-Run: 662-3
 Control Sys: Off
 Excitation: Longitudinal
 Airspeed: Hover
 Load: 4,700 lb
 Riser: 58 ft

Figure 54. Longitudinal Damping With 58-Foot Riser, AAELSS Off.



Flt-Run: 662-5
 Control Sys: Off
 Excitation: Lateral
 Airspeed: Hover
 Load: 4,700 lb
 Riser: 58 ft

Figure 55. Lateral Damping With 58-Foot Riser, AAELSS Off.



Flt-Run: 662-25
 Control Sys: On
 Excitation: Longitudinal
 Airspeed: Hover
 Load: 4,700 lb
 Riser: 58 ft
 Gain: 10

Figure 56. Longitudinal Damping With 58-Foot Riser, AAELSS on Low Gain.

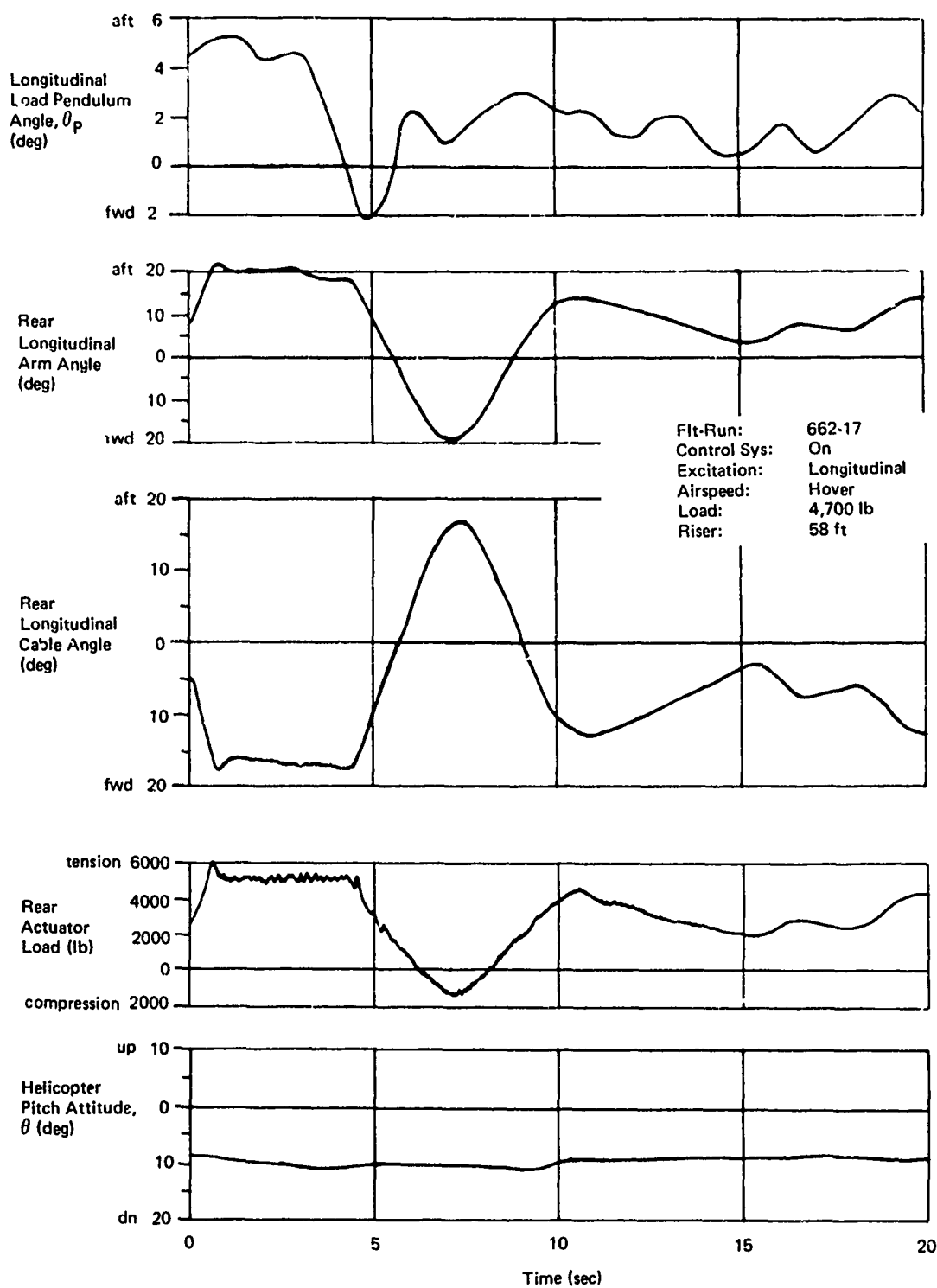
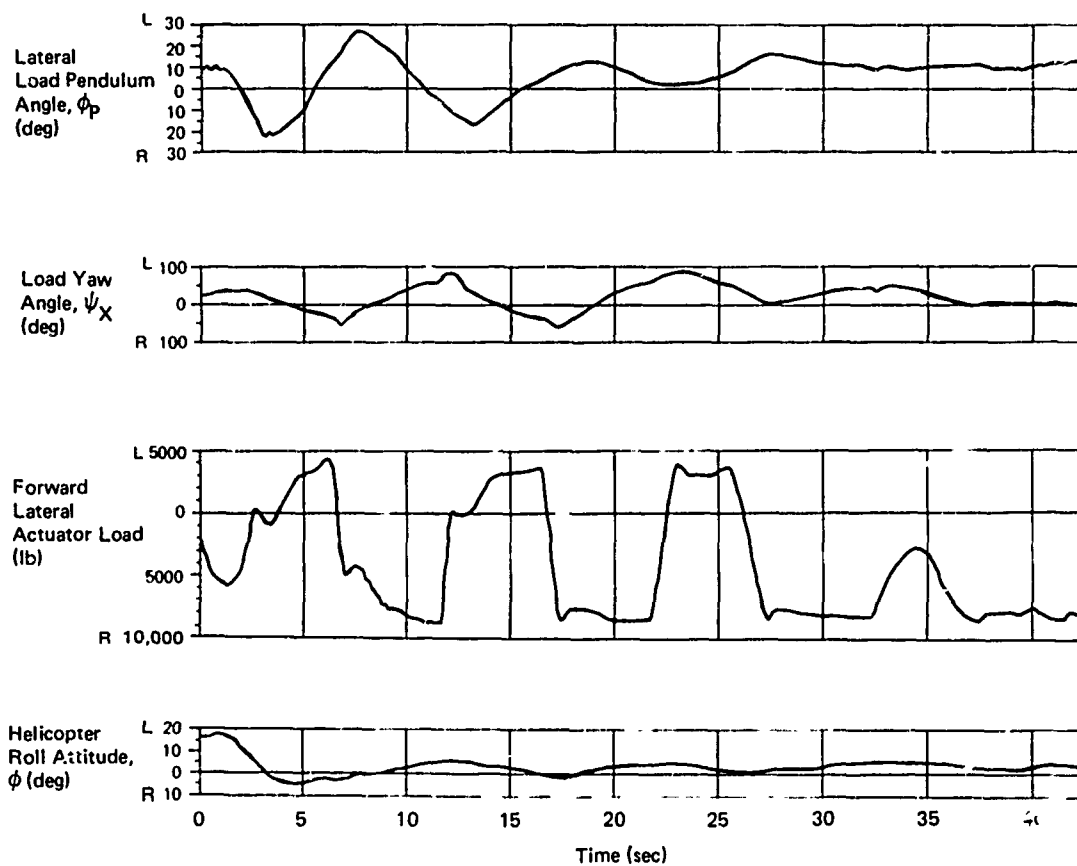


Figure 57. Longitudinal Damping With 58-Foot Riser, AAELSS on High Gain.



Flt-Run: 662-14
 Control Sys: On
 Excitation: Lateral
 Airspeed: Hover
 Load: 4,700 lb
 Riser: 58 ft
 Gain: 20

Figure 58. Lateral Damping With 58-Foot Riser, AAELSS On.

gain for small displacements provides good damping in the precision hover task. However, the data for the long riser do indicate the capability of the AAELSS control concept and its potential for providing high damping.

Forward Flight Stability With AAELSS Off

Tests at 60 knots with AAELSS disengaged show a longitudinal damping ratio of 0.04 with the empty container. This ratio is essentially identical to the damping ratio in hover.

Similarly, responses for the loaded MILVAN (8,600 pounds) at 80 knots displayed a damping ratio of about 0.07, slightly greater than the hover result. Stick-fixed dynamics were stable up to the 100-knot maximum safe speed limit.

With the AAELSS off and with the MILVAN empty, the lateral axis exhibited surprisingly high damping at 60 knots, as illustrated by the responses in Figure 59. Here, distinct roll and yaw modes appear. Damping of the roll mode is about 0.16, while the yaw is above 0.30. The slight pedal motion present had little influence on damping, as verified in other similar tests.

At airspeeds above 60 knots, a variety of sustained lateral-directional oscillations were recorded for AAELSS-off operation (see Figure 60) depending upon airspeed and MILVAN weight. The upper portion of this figure portrays responses for an empty MILVAN at 80 knots; a distinct two-frequency roll-yaw oscillation is shown. Also shown are the responses of the loaded MILVAN at 80 knots and 100 knots. For the loaded MILVAN, the yaw oscillations at both airspeeds showed nearly identical frequency, but the motion amplitude was significantly larger at 80 knots than at 100 knots. At 80 knots, the pilot controls were fixed; thus the yaw oscillation is self-sustaining. Pilot lateral-stick activity was present at 100 knots and may have caused the reduced yaw oscillation amplitude. However, since no controls-fixed data were taken at 100 knots, the pilot-in-the-loop influence cannot be conclusively established. It appears advisable for future tests to include both controls-fixed and pilot-in-the-loop evaluations to preclude such assessment difficulties.

Figure 60 shows that the motion of the loaded MILVAN at both 80 and 100 knots generally occurs about the nose of the MILVAN, with the box yawing left as it rolls right and vice versa, in somewhat of a dutch-roll motion. This dutch-roll motion is more pronounced at 80 knots than at 100 knots. The scope of this program did not permit extensive mapping of this problem. It would appear that the dynamics must be evaluated by a speed sweep in small speed increments to record the degradation of dynamics with airspeed and magnitude of any limit cycle oscillations.

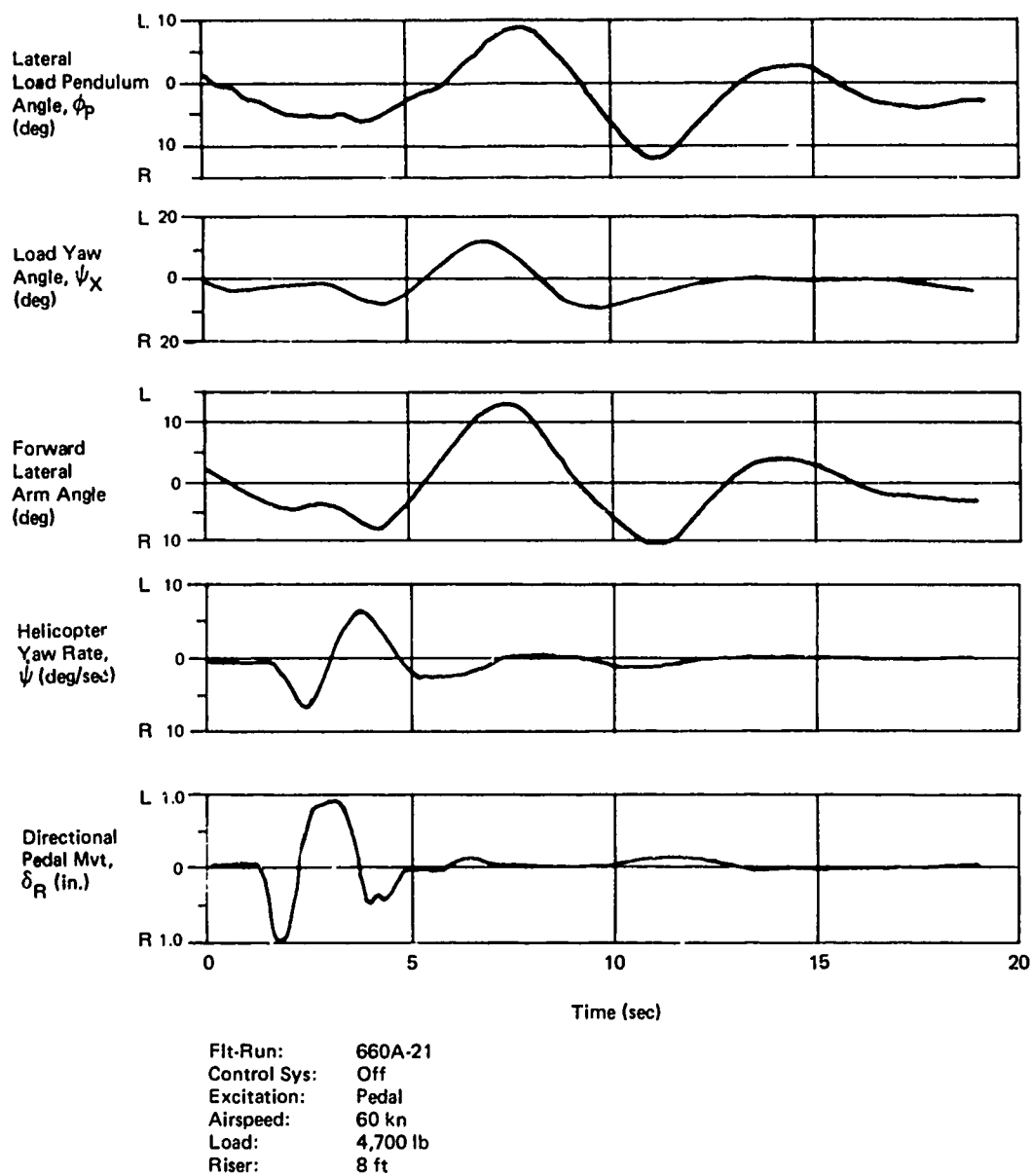


Figure 59. Lateral Stability at 60 Knots With AAELSS Off, Empty MILVAN.

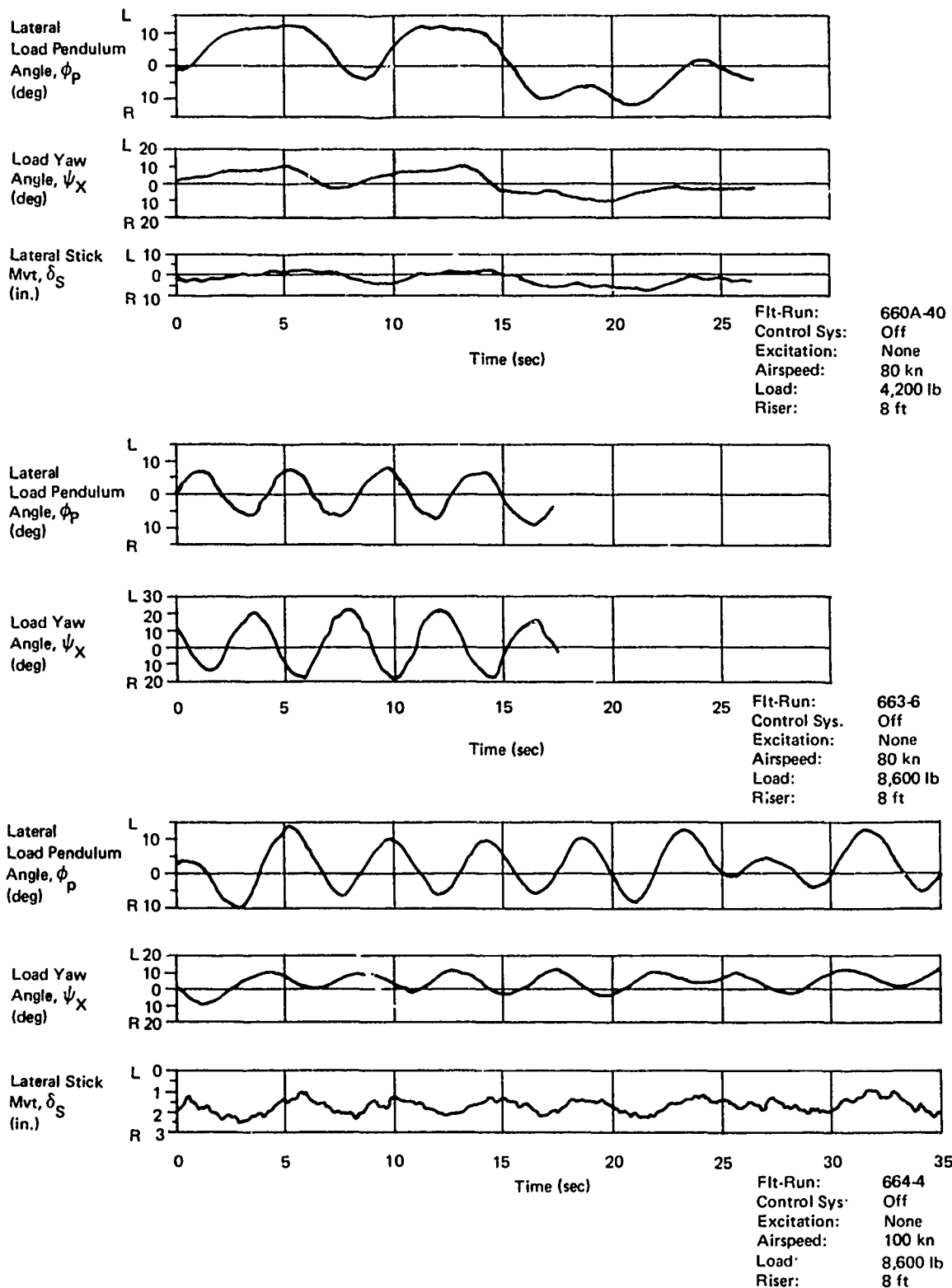


Figure 60. Yaw Oscillation With AAELSS Off.

The experience summarized in Figure 3 indicated the presence of sustained lateral oscillations only with the empty (4,700-pound) MILVAN. The present flight test program has given the first indication of sustained oscillations with a heavy load. This may be attributed to the lower yaw spring rate of the 12-foot effective riser and the paralleling cable. Past tests used an effective riser length of 8 feet. The fact that the damping deteriorates so rapidly from 60 to 80 knots with the empty MILVAN and the fact that the loaded MILVAN appears most unstable at 80 knots suggests that existence of a resonant condition at this airspeed. Such resonance could be caused by vortices shed from the MILVAN at a frequency approaching the lateral-directional sling load natural frequency. An initial check of the vortex frequency using a two-dimensional Strouhal number showed coincidence with sling frequency at 40 to 60 knots. Further study appears warranted. At first, the additional nose-down attitude change with airspeed was thought to be causing the improvement. However, this was later discounted since the attitude of the MILVAN did not change by more than 1.5 degrees between 80 and 100 knots.

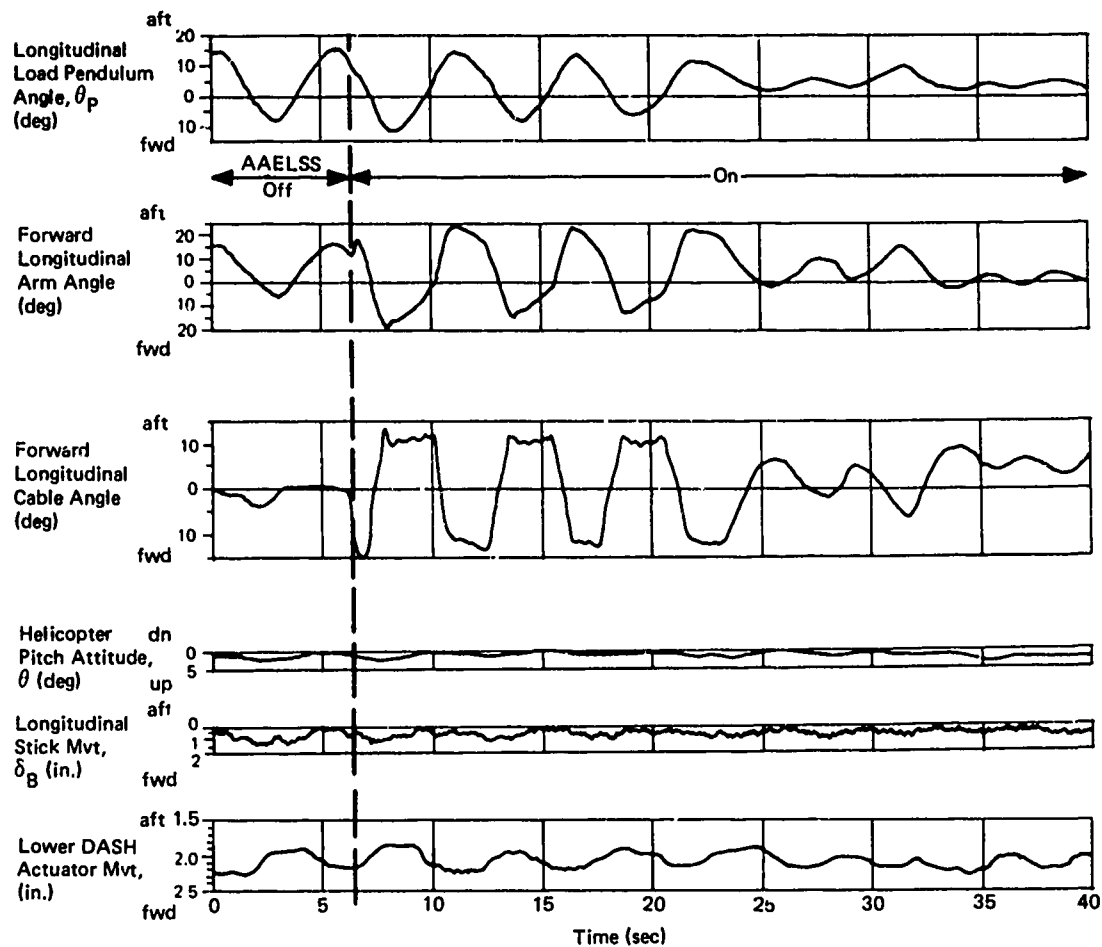
Forward-Flight Stability With AAELSS On

Flight tests showed that the AAELSS functioned properly during cruise in its ability to align the arms with the trim trail angle of the riser cables. This alignment was always within 5 degrees. Further, as shown by Figure 44, the damping augmentation provided by the AAELSS was adequate for accomplishing cruise mission operations without problems.

Figure 61 illustrates load longitudinal dynamic responses typical of cruise with the loaded MILVAN. The data shown contain an element of pilot-induced oscillation representative of cruising flight under IFR conditions. As may be noted, with AAELSS engagement at about the 7-second time reference, the AAELSS damping is effective in diminishing load motion, particularly after actuator stall ceases.

The left-hand portion of Figure 62 shows the sustained lateral-directional load oscillation typical of cruising flight with the AAELSS off. This motion has a period of nominally 5 seconds. The effectiveness of the AAELSS in damping this motion is clearly evident by the rapid decay of lateral pendulum angle and load yaw angle once the AAELSS is engaged. The damping ratio with AAELSS active is about 0.30. The test pilot described this characteristic as a most significant demonstration of the AAELSS capability and stated that upon the subsequent return to the AAELSS-off mode, the yaw oscillation quickly developed once again.

Figure 62 also indicates the buildup of a long-period lateral oscillation subsequent to the AAELSS engagement and the damping



Flt-Run: 664-13
 Control Sys: Off-on
 Excitation: Simulated IFR
 Airspeed: 80 kn
 Load: 8,600 lb
 Riser: 8 ft

Figure 61. Longitudinal Pilot-Induced Oscillation, Loaded MILVAN.

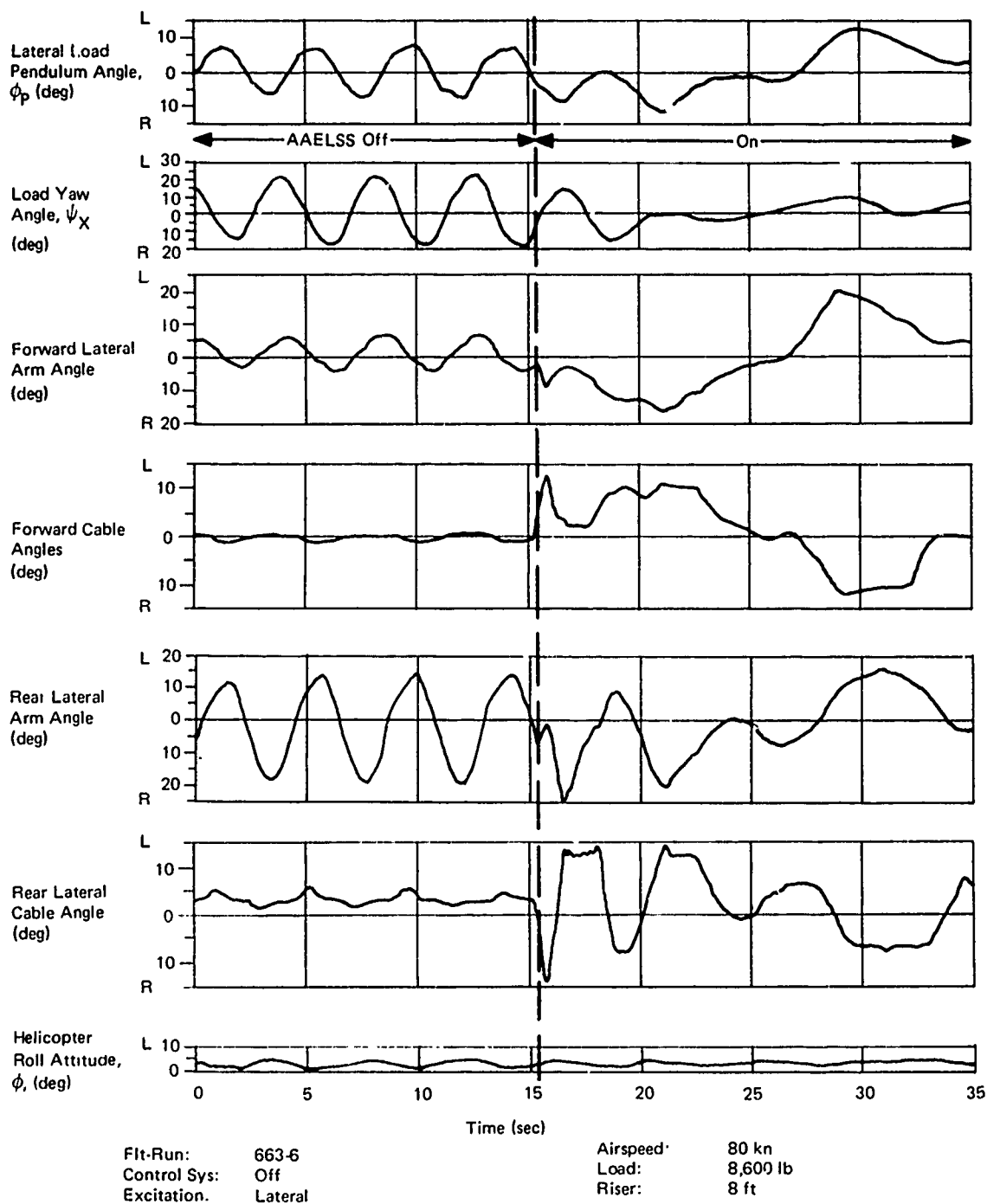


Figure 62. AAEELSS Stops Sustained Oscillations of Loaded MILVAN.

of the short-period lateral oscillation. This same long-period oscillation has previously been noted in hover flight, but only to a minor degree. The period of this oscillation was 20 seconds or longer, and it was apparent throughout the whole test program no matter what the sling configuration. This long-period oscillatory response is predominant in the results shown in Figure 63. Here the short-period damping was good in both heading and lateral motion. The pilot stated that the arm and load appeared to drift with aircraft sideslip; this is evident in the traces, where left slip resulted in a right roll of the load. Which motion came first is questionable, but the oscillation characteristics are typical of a very poorly damped long-period mode. Most of the resulting motion was just arm movement (+25 degrees) with small load swing (+10 degrees). Elimination of this behavior is necessary since the arm offset can limit proper AAELSS performance.

This long-period lateral oscillation had shown some minor improvement with reduced gain. Since the problem exhibits the characteristics of a specific lightly-damped mode, it should be readily amenable to analysis and resolution in future studies.

Single-Arm Operation in Cruising Flight

The possibility exists for using only one arm of the AAELSS to provide the required load damping in cruising flight. Although evaluation of single-arm operation was not within the intended scope of this program, circumstances did produce some insight into this situation. At one point during the flight test program with the loaded MILVAN at 80 knots, a system failure had occurred which caused the forward arm to go hardover when the AAELSS was engaged; the rear arm remained normally operative. Figure 64 illustrates the results gathered under this condition. As shown, the AAELSS did stabilize the yaw oscillation in the 9-second period during which it was active.

Although not conclusive, the results shown in Figure 64 imply the feasibility of using only an active rear arm to stabilize the load in cruising flight. It must be recognized, however, that other load or sling configurations may require that the forward arm be active, rather than the rear arm as suggested by the results of this program. Further, it is to be expected that single-arm AAELSS operation in precision hovering tasks will afford less effective load damping than a dual-arm AAELSS.

AAELSS FAILURE TESTING

Test were conducted to duplicate the effects of failures in the AAELSS power controls. Load motions were observed and recorded for each potentially unsafe condition. Simultaneous longitudinal failure of both arms with the empty MILVAN

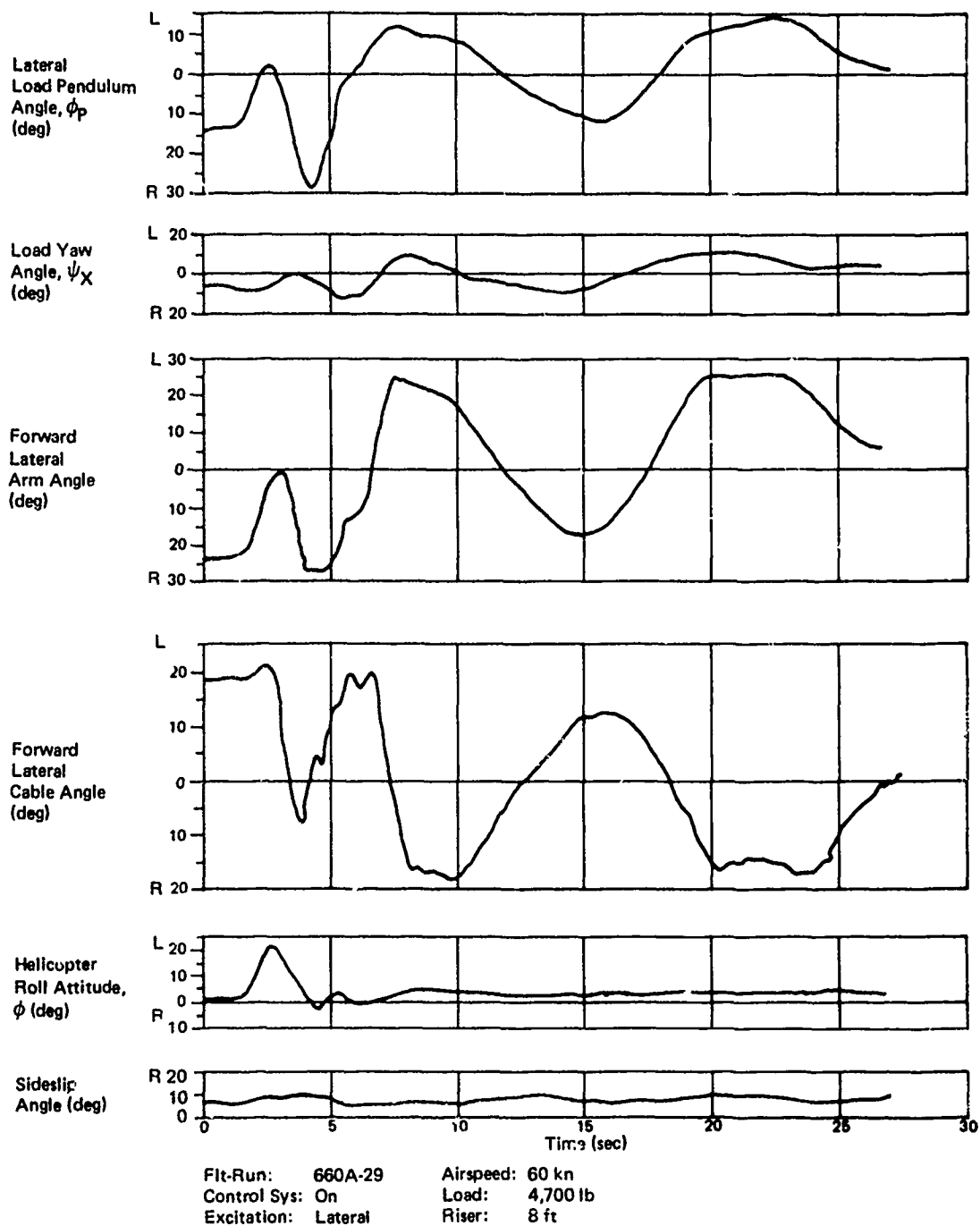


Figure 63. Lateral Oscillation With AAELSS On, Empty MILVAN.

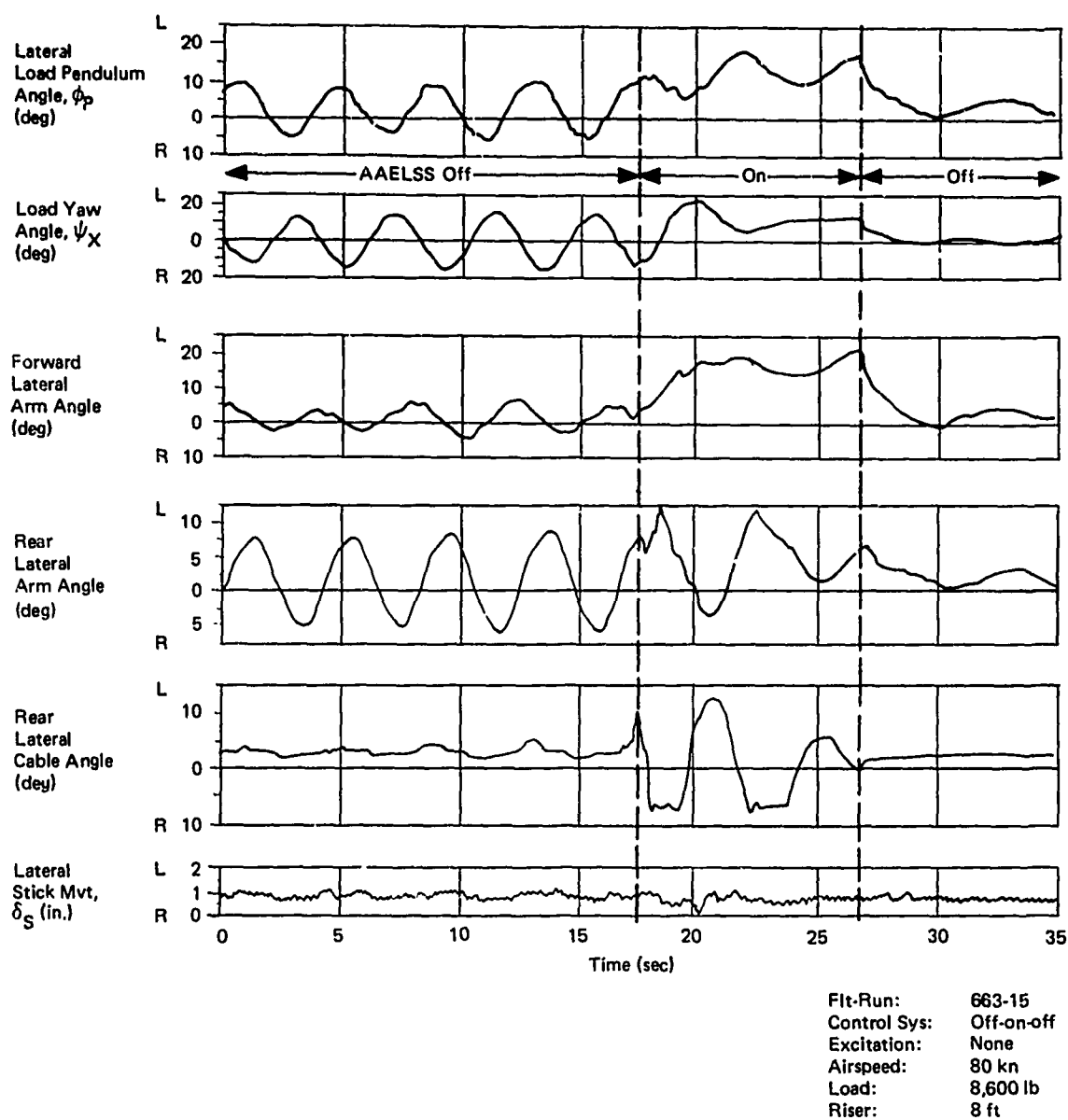


Figure 64. Single-Arm Oscillation, Loaded MILVAN.

resulted in a 28-degree arm travel, which produced a mild response that required no pilot control correction for the 15-second test duration.

Since there were AAELSS control circuits which allowed the possibility of the forward and rear actuators to fail in a yaw mode (i.e., differential lateral arm motion), this condition was tested. This failure mode proved to be most critical. Such a failure with the empty MILVAN at 80 knots is illustrated in Figure 65. This left yaw failure drives the forward lateral arm to a left stall condition and the rear actuator to a right stall (as seen by the arm and cable angle traces). The final load trim position after failure is 30 degrees left roll. No attempt was made to establish the time that the pilot could delay this control input following failures, and small pilot inputs were always present. It is interesting to note that the external load indicates very reasonable stability even while in this failure mode. However, since the cable angle reached the 30-degree structural limit, this speed (80 knots) was established as the maximum safe airspeed for the empty MILVAN.

Longitudinal failure testing for the loaded MILVAN at 80 knots (see Figure 66) showed a mild longitudinal response with only a 15-degree motion of the arm and no noticeable pitch attitude change in the aircraft; no pilot control inputs were required. The yaw failure, as shown in Figure 67, was conducted at 90 knots and the AAELSS turned off after the failure yawed the container only 10 degrees from its initial trim position.

LONGITUDINAL PILOT-INDUCED OSCILLATION

The susceptibility of this external load configuration to pilot-induced oscillation under IFR conditions is widely known and was again demonstrated with AAELSS off. The basic source of the problem is that the swing of the external load creates a longitudinal acceleration force on the helicopter proportional to the load-to-helicopter weight ratio. The pilot, if not diligently monitoring instruments, interprets acceleration as a speed change and responds with a corrective longitudinal stick input. Experience has shown that this stick input reinforces or sustains the oscillation. Test results given in Figure 61 for the 8,600-pound load show one cycle of a pilot-induced oscillation (the first 7 seconds of the plot) that had been sustained for greater than 30 seconds prior to AAELSS activation. In the next three cycles (7 seconds to 22 seconds), the actuator is stalling intermittently; but once out of stall, the system rapidly stabilizes both the load motion and the helicopter pitch attitude. The pilot reported that the AAELSS provided positive load damping and eliminated any pilot-induced oscillation. It must be recognized that, to date, this type of testing of pilot-induced oscillation has been limited to load/aircraft weight ratios of 0.25, whereas ratios of 1 and

greater are possible. The influence of the high weight ratio (and therefore greater longitudinal acceleration) on the requirements for load damping is not well known.

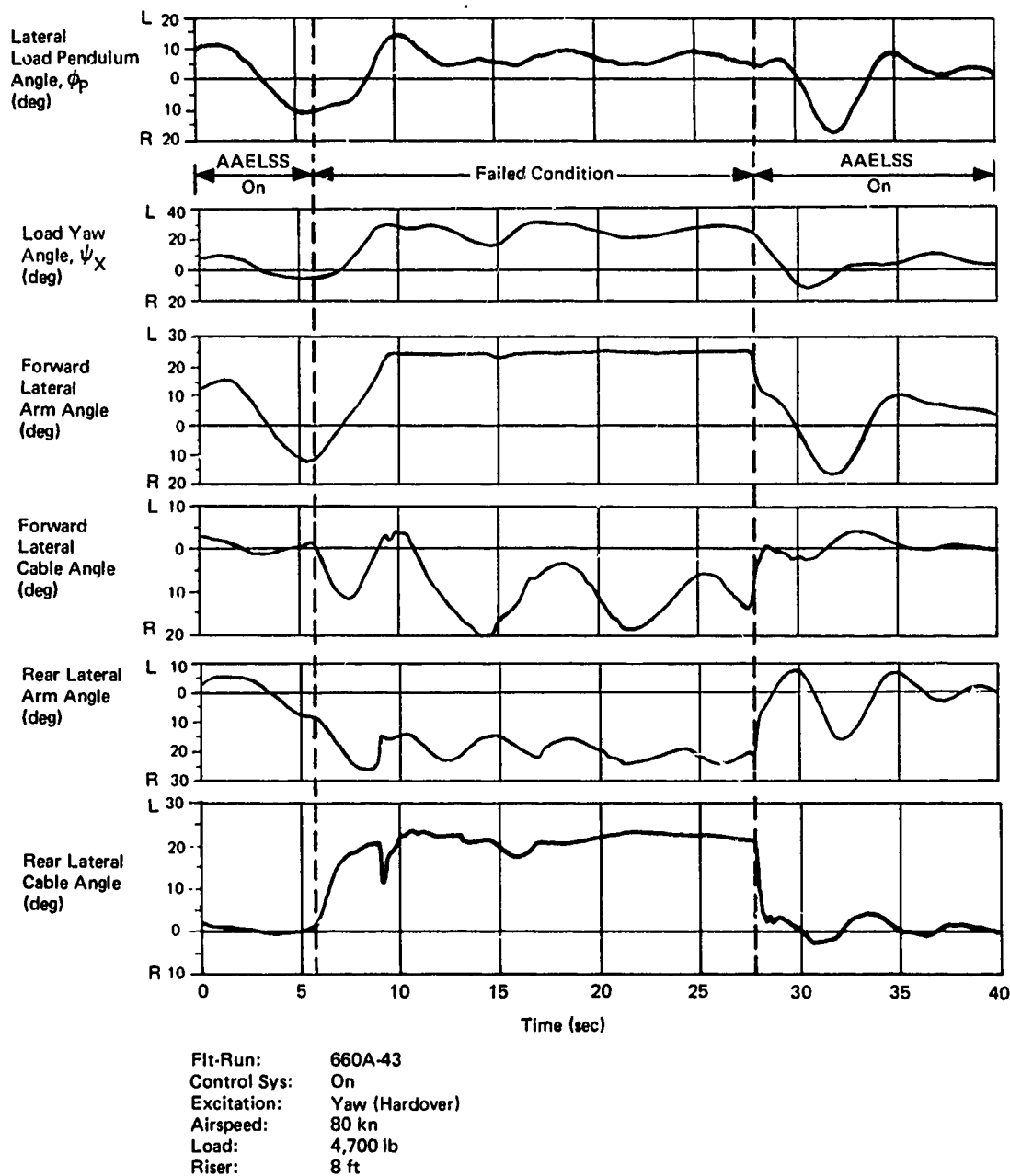
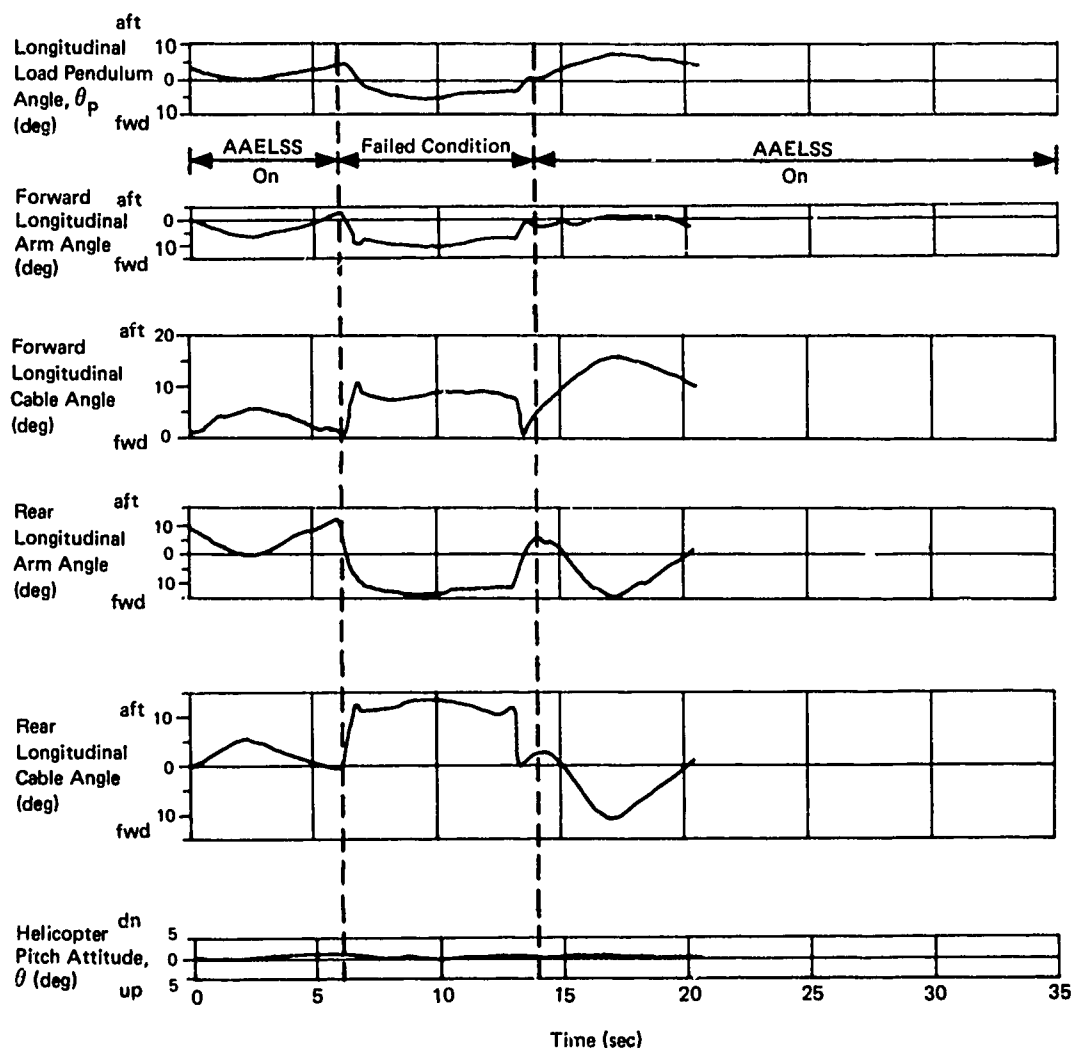


Figure 65. Yaw Actuator Failure at 80 Knots, Empty MILVAN.



Fit-Run: 663-11
 Control Sys: On-off
 Excitation: Longitudinal
 Airspeed: 80 kn
 Load: 8,600 lb
 Riser: 8 ft

Figure 66. Longitudinal Damping With AAELSS On, Loaded MILVAN.

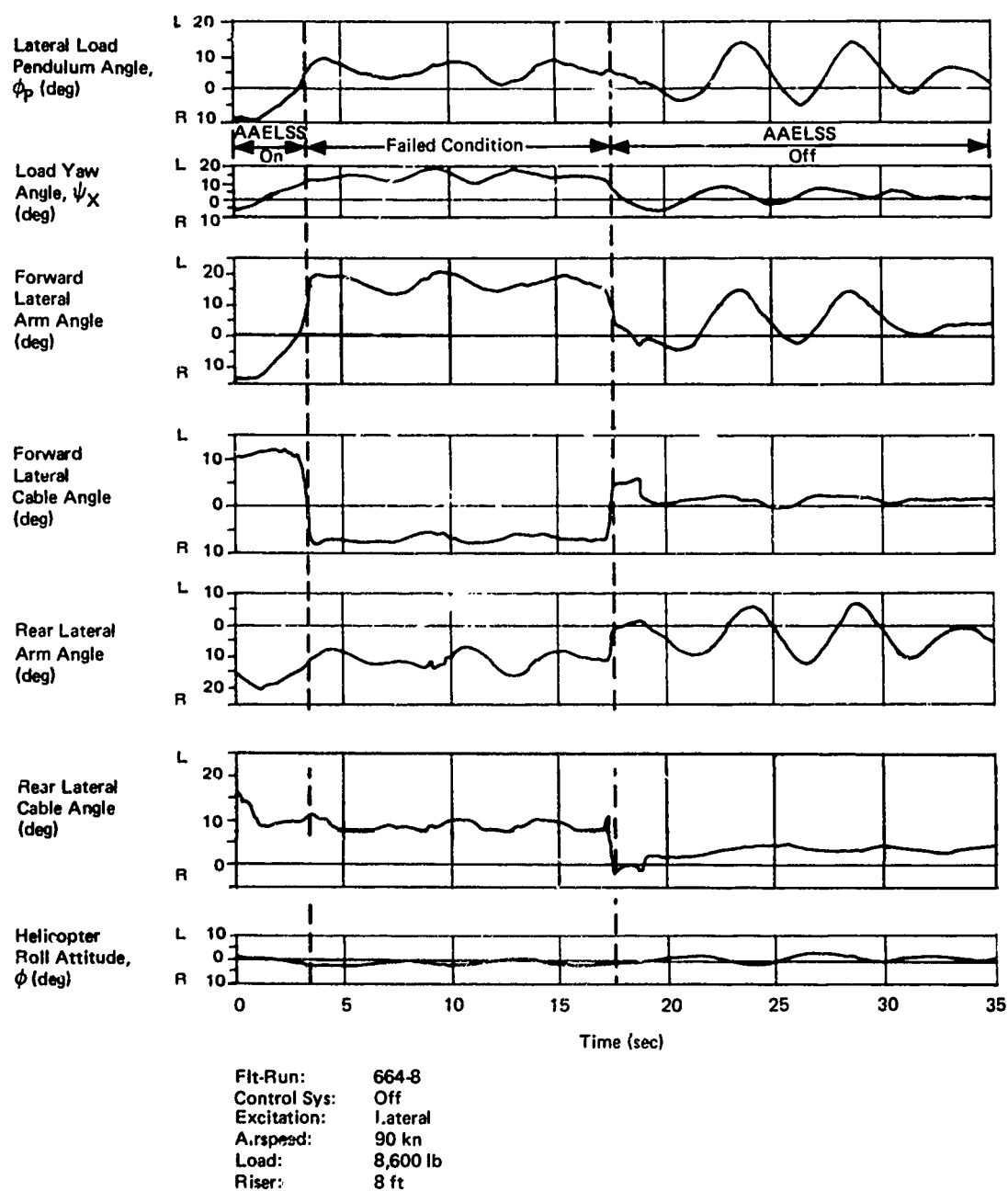


Figure 67. Yaw Actuator Failure, Loaded MJLVAN.

COMMAND AUGMENTATION

Part of the AAELSS uses lateral cyclic stick and directional pedal pickoffs to detect the commanded helicopter maneuver and to move the arms to force the external load to move along with the helicopter. An example of AAELSS command augmentation performance in yaw is seen in Figure 68. Tests at three different gain settings are presented. Normal gain and zero gain augmentation results had very similar inputs (except for polarity), and the magnitude of yaw error (ψ_x) is halved when using augmentation. The above test used 8-foot riser cables. Testing conducted with 58-foot risers was generally troubled by the arm drifting hardover. On one occasion, however, a reasonable response to a roll stick input was obtained with the 58-foot riser. These results are shown in Figure 69, where it can be seen that the load lateral pendulum angle generally followed the helicopter roll attitude.

In all cases where the control augmentation was tried, the lack of a well-developed sensor produced inaccurate results, which prohibited a good assessment of its effectiveness. Since control augmentation will be used only to refine and expedite load placements in precision hover, its use is dependent on accurate low-hysteresis sensors.

EXPERIMENTAL AAELSS WEIGHT

The removable part of the AAELSS hardware (substantially the beam and arms) was weighed and found to be 1318 pounds. Electronics and wiring associated with this system amounted to no more than 10 pounds. Approximately two-thirds of the total AAELSS weight is in the beam and the balance attributed to the arms, actuators, hooks, hydraulic components, and other components. The design of the test article emphasized simplicity of fabrication over weight savings, and therefore in a production design, a marked weight reduction could be expected, especially in large fittings of the arms. Two weight-effective designs are possible in future designs:

- Arm directly mounted to the airframe
- Beam mounting designs which are more structurally efficient

Either of the choices requires varying degrees of modifications to airframe structure for increased airframe strength, and so the approximately 800-pound weight of the beam alone can not be totally eliminated.

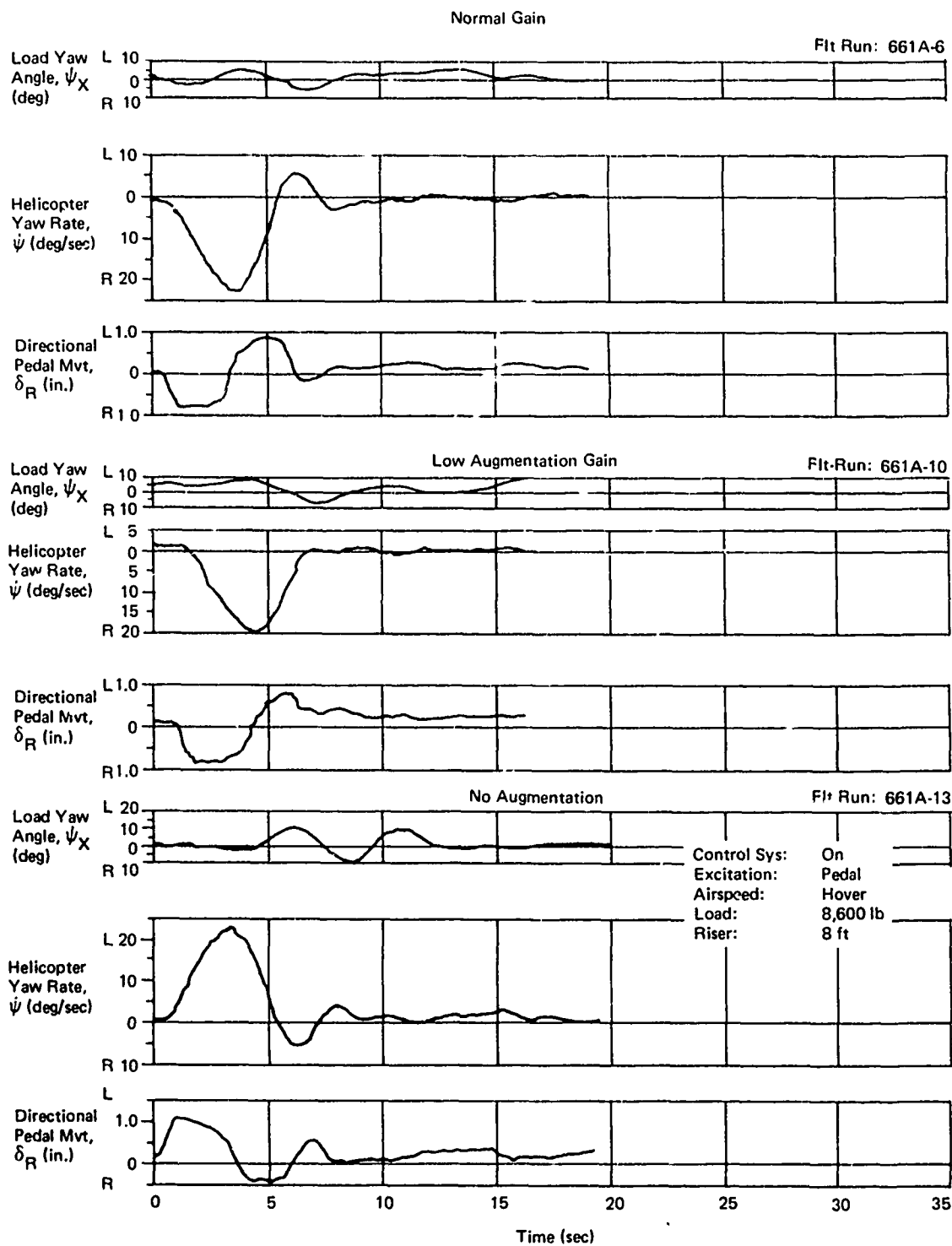
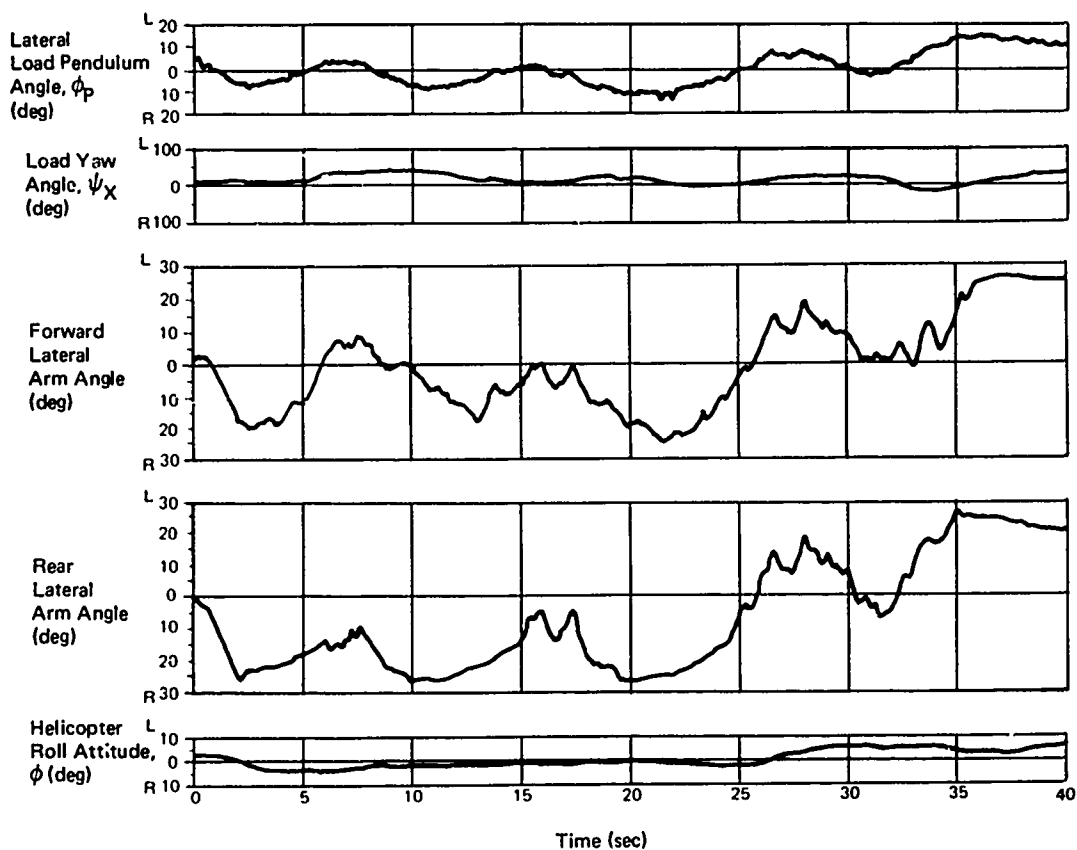


Figure 68. Normal Control Augmentation Gain.



Flt-Run: 662-27
 Control Sys: On
 Excitation: Roll
 Airspeed: Hover
 Load: 4,700 lb
 Riser: 58 ft

Figure 69. Roll Command Augmentation With 58-Foot Riser.

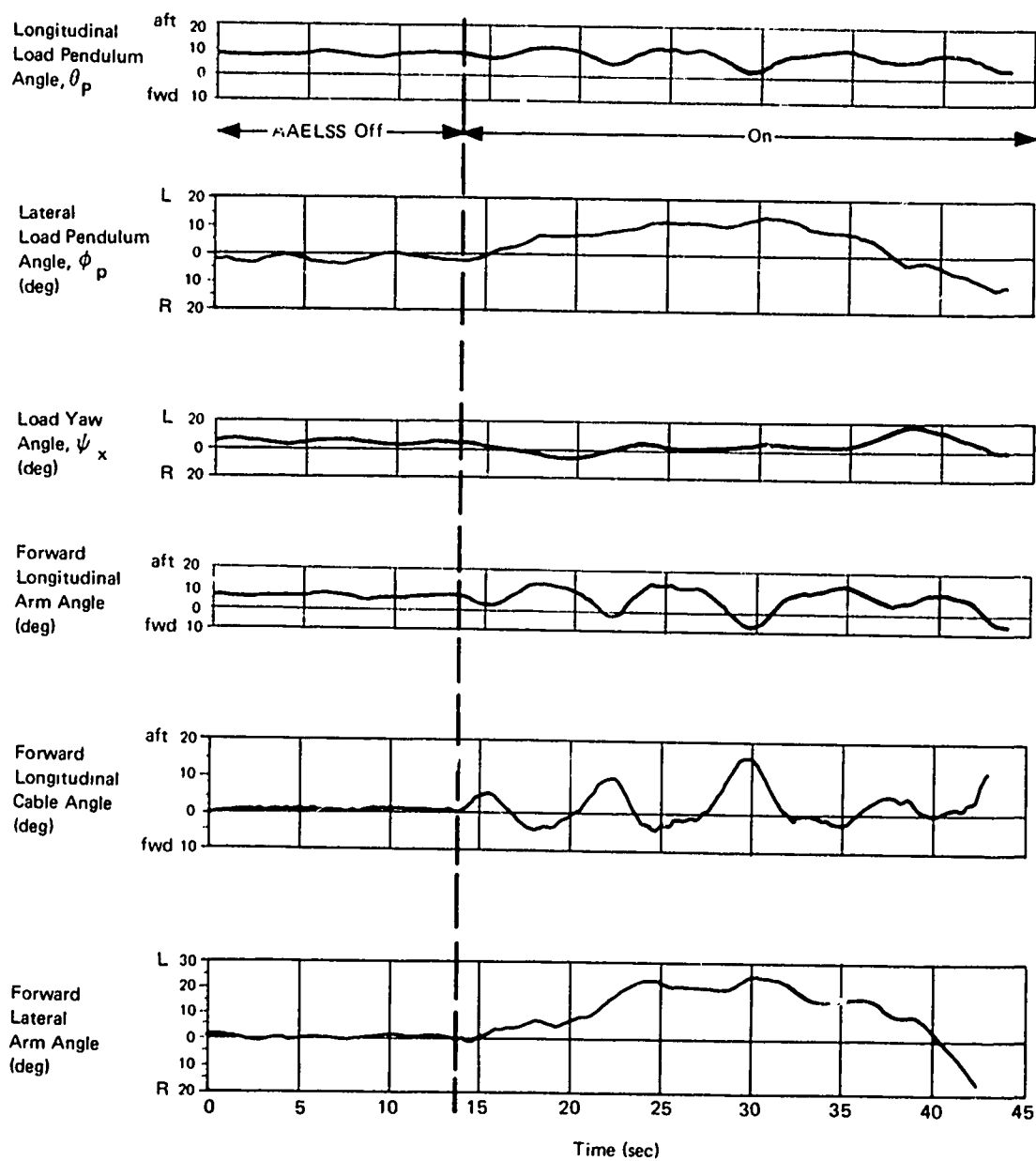
HYDRAULIC POWER REQUIREMENTS

The power required is proportional to the hydraulic flow supplied to the actuator and in turn proportional to the actuator or arm velocity. A review of the data to estimate this supply requirement shows the maximum arm rotary velocity in both the lateral and longitudinal axes to be 25 degrees per second. The rating is chosen from the data at the time when the actuator stall conditions terminate. The velocity during stall often peaks to 40 degrees per second when the load is aiding the arm motion, but this should not be a design condition as system capacity has been exceeded. This 25 degrees per second is equivalent to 2.5 gpm to be supplied to each actuator. The maximum supply flow required is 10 gpm if all arms are at a peak velocity simultaneously. In future systems, the supply demands could be reduced by reducing the gain at large amplitudes and therefore reducing the maximum velocities of the arms. The electrohydraulic servo valves used in this experimental system had a 5.0-gpm rating, which is excessive. Reducing this valve flow capacity might have a beneficial effect and should be studied in the future.

PROTOTYPE AAELSS LIMITATIONS

Two types of oscillations occurred in testing: very-low-frequency lateral drift and sensor hysteresis-induced limit cycle oscillation. The former will have to be solved, since the drift of the arm to hardover limits causes loss of operation and poor damping; its cause is a lightly damped response mode which is amenable to analysis and correction.

The limit cycle oscillation was undoubtedly caused by the friction of the hook pivot under load imparting a hysteresis in the cable angle feedback signal, since it is the only significant nonlinearity in the system. It is well known that any hysteresis in a control system acts to cause phase error, which in turn causes poor resolution and/or limit cycle oscillations. At the long riser length (58 feet), this was much more critical than for the standard 8-foot riser, since the system was operating over smaller load angles, and therefore the hysteresis effect was more dominant in the sensor output. Figure 70 shows that starting from a quiet condition in hover with the empty MILVAN and turning the system on resulted in higher levels of motion and a sustained longitudinal arm oscillation. Also, there is evidence of lateral drift. Another way of looking at the hysteresis problem is to consider the damping change with arm amplitude as plotted in Figure 71. Here, data from both 8-foot and 58-foot riser tests on the empty container are presented. These data show that, in both cases, the best damping occurs when the arm is required to move about one foot. Then, as the motion decays, the effective damping suddenly drops off and



Flt-Run: 660-8
 Control Sys: Off-On
 Excitation: None
 Airspeed: Hover
 Load: 4700 lb
 Riser: 8 ft

Figure 70. AAELSS-On Oscillation.

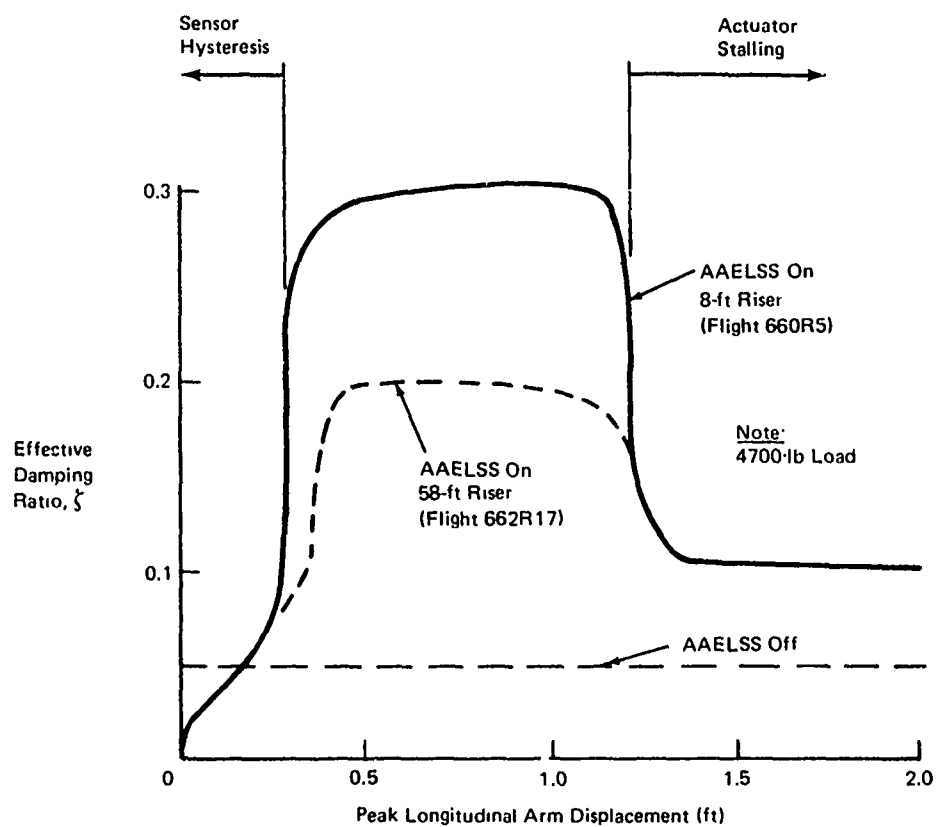


Figure 71. Nonlinear Damping.

in fact decreases below the AAELSS-off damping level. A sensor is needed that detects the line of action in the sling tension members with moderate accuracy but with a minimum of hysteresis. Improvements in the sensor will allow control augmentation and damping to be effective in a precision hover task, which involves maneuvers requiring less than a foot of arm travel.

Figure 71 also indicates the loss of damping as the amplitudes of motion get large and the actuator operates largely in a stalled condition. Evidence of this stalling has been frequent in the time histories presented here. The test results show that the load damping ratio is decreased to about 0.1 (twice the AAELSS-off value) when stall is present. This condition is not serious except with heavy loads where possibly there would not be enough effective damping to prohibit pilot-induced oscillation tendencies. Some relief could be obtained by reducing gain as the amplitude increases, as was mentioned earlier in this report.

Other problems occurring during the flight test that were significant to system operations were jitter in the controls and arm when the pilot transmitted on VHF due to radio frequency interference, and chattering of the hydraulics during bypassing, which happened every time the actuator stalled. The latter problem can easily be avoided by designing the system to permit a hydraulic relief setting above system supply pressure. The radio frequency interference problem was bypassed, since its solution was not within the scope of this program.

CONCLUSIONS

The following conclusions are drawn from the analysis, design, and testing of an experimental AAELSS. The flight testing used the Boeing Model 347 helicopter for transporting an 8x8x20-foot MILVAN container with a tandem dual hook sling suspension.

1. The AAELSS is a feasible external load stabilization concept which demonstrated its capability for improving the productivity, enhancing the load placement capability, and permitting IFR operations of external load-carrying cargo helicopters.
2. The AAELSS improves the load pendulum damping in each motion axis by a factor of 4 to 6 over that existing with an unstabilized load. Specifically, the AAELSS provided damping ratios of at least 0.20 and 0.30 over the entire test flight envelope for the ballasted (8,600-pound) MILVAN load and the empty (4,700-pound) MILVAN, respectively, using 8-foot riser cables.
3. Flight under simulated IFR conditions demonstrated that the AAELSS permits satisfactory IFR flight operations. This resulted from the load damping augmentation afforded by the AAELSS and its ability to eliminate any pilot-induced oscillation tendencies.
4. Load placement time is reduced with use of the AAELSS as a result of both the improved load damping and the pilot command control augmentation functions designed into the system.
5. No excessive power is required by the AAELSS.
6. No unsafe flight conditions are produced by the AAELSS.
7. The AAELSS concept permits increased maximum operational airspeeds, thereby increasing cargo-helicopter system productivity. The AAELSS did not impose any airspeed restriction on the ballasted (8,600-pound) MILVAN. The empty (4,700-pound) MILVAN was restricted to 80 knots during the flight program - the speed where coincidentally a structural limit on lateral load swing (30 degrees for the prototype AAELSS) and a sling failure limit based on load/airframe proximity occurred simultaneously. In a production version of the AAELSS, all speed restrictions can be removed by providing redundancy in the AAELSS control subsystem and the sling members.

8. The system is stable; no system instabilities arose over the full range of AAELSS gains and time constants tested.
9. Simple root locus analysis methods provide good predictions both of the required AAELSS control gain and time constant settings and of the system response variations with changes in these gains and time constants.
10. The prototype AAELSS control law, which operates to control the rate of load motion, can be improved by designing it to control load position. Included in this report is a candidate control law that is expected to be capable of decreasing the hover position hold error of the load by a factor of 10 from that of the prototype AAELSS control law.
11. Design improvements to reduce pivot joint friction and consideration of other sensor concepts are desirable in future developments. Precision hover performance of the AAELSS was degraded somewhat by sensor system hysteresis, which caused some limit cycling of arm motion for small load displacements.
12. The AAELSS provides improved damping ($\zeta=0.15$ to 0.20) for the precision hover task even with the long (58-foot) riser cables, although performance with small load motions is compromised by sensor hysteresis nonlinearities.
13. The use of nonlinear gain (high gain for small load motions and low gain for large motions) appears to offer increased AAELSS performance for a given system capacity (or conversely, to maintain performance with less system capacity).

RECOMMENDATIONS

Based on the results of this program, the following recommendations are made for future study and application of the AAELSS concept:

1. The AAELSS control law developed in this study should be modified to:
 - a. Eliminate the long-period lateral oscillation of the arms that resulted in intermittent actuator stall;
 - b. Control load position rather than load motion rate to improve precision hover load placement operations and to eliminate load steady-state side-slip angle conditions during cruising flight; and
 - c. Improve system performance or reduce system hardware capacity by incorporation of system gain changes as a function of load cable angle (i.e., use of nonlinear gain).
2. An improved load position sensor design should be developed to sufficiently minimize hysteresis effects for elimination of the sustained arm oscillations that occurred for small load displacement disturbances.
3. Additional system logic should be installed to permit:
 - a. Extension and retraction of the arms by single switch control, and
 - b. Disarming of the system when hook loads are small. (A safety hazard to ground crewmen exists in the prototype AAELSS because rapid arm movements are possible if an unloaded hook is disturbed when the system is active.)
4. The AAELSS capability for eliminating pilot-induced oscillation at higher ratios of load weight to helicopter gross weight should be investigated. The experimental system demonstrated this capability, but the maximum load weight flown was restricted by engine-out hover capability, and the piloted flight simulator evaluations suffered from inadequate cueing.
5. Redundant AAELSS controls and sling members should be provided in any production version to permit safe flight operation up to power-limited airspeed with lightweight loads.

6. Revisions should be made to the system hardware design as follows:
 - a. The commanded arm moment about its upper pivot should be regulated by selecting the appropriate combination of arm actuator effective piston area and system pressure, thereby removing this function from the bypass valve.
 - b. The load beam end restraint should be improved to reduce the movement of the beam within the end restraint boxes and to reduce wear in this area.
 - c. Greater actuator travel should be provided to avoid actuator bottoming prior to stall under large load displacements or hardover failures.
7. The knowledge of arm and sensor pivot design gained during the AAELSS flight program should be incorporated. In the design of arm pivot bearings, bearing misalignment tolerances and lubrication requirements must be carefully considered. The arm pivots must be treated as oscillating rather than rotating bearings. Sensor elements should be designed for positive mechanical locking, since the friction locking used initially in the prototype permitted synchro null shifts due to slippage.
8. Future flight tests should incorporate a demanding precision hover task (such as MILVAN stacking or containership loading and unloading) to accurately assess the AAELSS benefits to precision load placement operations. Such flying will require a load controlling crewman or a visual presentation of the load for the pilot.

LITERATURE CITED

1. Midget, J., and A. J. Hutto, FLIGHT TEST EVALUATION OF A TWO-POINT EXTERNAL LOAD SUSPENSION SYSTEM CONCEPT ON A CH-47 HELICOPTER, The Boeing Company, Vertol Division, 114-FT-035-1, December 1969.
2. Harvath, L., and R. Wiesner, ANALYSIS OF DUAL CARGO HOOK WIND TUNNEL TEST, The Boeing Company, Vertol Division, D210-10514-1, 30 August 1972.
3. McKercher, D., HEAVY LIFT HELICOPTER ADVANCED TECHNOLOGY COMPONENTS PROGRAM, FIRST QUARTERLY SUMMARY REPORT, The Boeing Company, Vertol Division, D310-10100-1, 20 October 1971.
4. Yamakawa, George, M., et al, TECHNICAL EVALUATION OF BOEING-VERTOL MODEL 347 ADVANCED TECHNOLOGY HELICOPTER, PHASE I, FINAL REPORT, USAASTA Project No. 70-38, U.S. Army Aviation Systems Test Activity, Edwards Air Force Base, California, January 1972.
5. Kendall, R., MODEL 347 - ACTIVE EXTERNAL LOAD STABILIZATION PROGRAM - SAFETY OF FLIGHT CONFERENCE, The Boeing Company, Vertol Division, Memorandum 8-5760-1-149, 18 September 1972.

APPENDIX I
FLIGHT TEST LOG

The data recorded during Flights 660 through 664 were used in the final analysis of the AAELSS characteristics. Flights preceding No. 660 were used to check out and debug the system.

This appendix presents flight configuration and test condition logs for flights 660 through 664.

Table VII is the AAELSS flight configuration log. It presents a descriptive summary of the following for each test flight by flight number:

- Aircraft weight and center-of-gravity position,
- External load configurations in terms of MILVAN weight and sling configuration, and
- General purpose of the flight in terms of flight mode and airspeed.

Tables VIII through XIII are test condition logs for each flight. They describe the following by flight number:

- Identification of primary axis being evaluated,
- AAELSS control system configuration in terms of system gains and time constants,
- Damping ratio for the best data records, and
- General comments on the data.

TABLE IX. MODEL 347 FLIGHT CONFIGURATION LOG									
Flight	Date (1972)	Gross Weight* (lb)	CG** Location (in.)	Riser Length (ft)	Paral- leling Cable	Sling Length (ft)	Container*** Weight (lb)	Purpose	
660	6 Nov	41,893	11.5 fwd	8	Yes	11 fwd 8 aft	4,700 (Unloaded)	AAELSS in hover	
660A	6 Nov	41,893	11.5 fwd	8	Yes	11 fwd 8 aft	4,700 (Unloaded)	AAELSS in field transition and out of field, forward flight	
661	7 Nov	45,885	15 fwd	8	Yes	11 fwd 8 aft	8,600 (Loaded)	AAELSS in hover	
661A	7 Nov	45,885	15 fwd	8	Yes	11 fwd 8 aft	8,600 (Loaded)	AAELSS in hover and out of field	
661B	7 Nov	45,885	15 fwd	8	Yes	11 fwd 8 aft	8,600 (Loaded)	AAELSS in hover	
662	9 Nov	41,983	15 fwd	8 (Nylon) plus 50 (cable) then 8 (Nylon)	NO	11 fwd 8 aft	4,700 (Unloaded)	AAELSS in hover	
663	10 Nov	45,885	15 fwd	8	Yes	11 fwd 8 aft	8,600 (Loaded)	AAELSS out of field, forward flight	
664	10 Nov	45,885	15 fwd	8	Yes	11 fwd 8 aft	8,600 (Loaded)	AAELSS out of field, forward flight	
* 37,277 lb unloaded ** Unloaded - 8 in. forward *** 8x8x20-ft MILVAN									

TABLE X. TEST CONDITIONS FOR FLIGHT 660

Record Number	Maneuver Or Input Axis	Control System Configuration				Damping Ratio	Comments on Data
		Longitudinal Gain	Longitudinal τ_{lag}	Gain	Lateral τ_{lag}		
1	Long.	0	9.4	0	10.4	0.04	Update instrumentation
2	Lat	0				0.04	AEELSS off
3	Lat	0				0.1	AEELSS off
4	Lat	0				0.04	AEELSS off
5	Long.	10	1.8	10	1.8		Synchronized to on (S-A)
6	Lat	10	1.8	10	1.8		
7	Long.	10	1.3	10	1.4		Same
8	Lat	10	1.3	10	1.4		
9	Lat	10	1.3	10	1.4		
10	Lat	10	2.3	10	1.4		
11	Long.	10	2.3	10	1.4		Very poor damping, less than off
12	Lat.	10	2.3	10	1.4		Good in linear range
13	Long.	10	2.8	10	2.4		Turned on when motion was stopped
14	Lat	10	2.8	10	3.18		Poor damping
15	Lat	10	2.8	10	3.18	~0.4	
16	Lat	10	2.8	10	3.18		Good data
17	Lat	10	2.8	10	1.8		Synchronized to on (S-A)
18	Long.	10	2.8	10	1.8		
19	Long.	10	2.8	10	1.8		On (S-A)
20	Long.	10	2.8	10	1.8		Sync good damping AEELSS off
21	Lat	10	2.8	10	1.8	~0.36	
22	Lat	10	2.8	10	1.8		On
23	Lat	10	2.8	10	1.8		Sync
24	Lat	10	2.8	10	1.8		S-A
25	Lat	10	2.8	10	1.8		A
26	Lat	10	2.8	10	1.8		Initial trials of control augmentation
27	Lat	10	2.8	10	1.8		
28	Lat	10	2.8	10	1.8		
29	Lat	10	2.8	10	1.8		
30	Lat	10	2.8	10	1.8		
31	Lat	10	2.8	10	1.8		
32	Lat	10	2.8	10	1.8		Long. act. failure 1/2 rate hardover
33	Failure	10	2.8	10	1.8		Long. act. failure full rate hardover

Container - 8x8x20-ft MILVAN
 Weight - 4,700 lb
 Riser - 8 ft
 Date - 6 Nov 72
 Hover flight only

TABLE XI. TEST CONDITIONS FOR FLIGHT 660A

Record Number	Airspeed (Kn)	Maneuver Or Input	Control System Configuration						Damping Ratio	Failures			Comment on Data
			Gain	Longitudinal		Lateral	Lag	Wo		Long.	Roll	Yaw	
				I	Lag								
1	Hover		10.0	1.8	9.4	5	2.9	5.4					Update
2		Failure								Fwd			
3										Aft			
4											L		
5											R		
6												L	
7												R	
8	Hover	Failure											Cn
9	0 to 60		10.0			5							Sync
10	0 to 60	Failure	10.0			5				1/2 Aft			
11										Aft			
12											1/2L		
13											L		
14											R		
15													
16										Fwd			
17											1/2L		
18		Failure									L		
19		Long.									R		
20		Lat							0.3				Off
21		Yaw					2.9		0.04				Off
22		Long.							0.16				Sync
23		Lat					1.8						S
24		30° R turn											S
25		Yaw											S
26		Long.							0.2				S - A Sync to on
27		Lat							0.4				S - A
28		Yaw							0.4				S - A
29		Lat											A (AAELSS-on) Very high damping short period
30		Long.							0.22				On
31		Yaw											On
32		30° L turn											On
33		R											On
34		L											On
35		R											On
36		L											On
37		Climb											On
38		Climb											On
39	60	PPD 1500 fpm											System off sustained oscillation
40	80												
41	80	Failure											
42	80	Failure								1/2			
43	80	Failure	10.0	1.8	9.4	5	1.8	5.4		Fwd			1/2 Excellent failure data

Container - 8x8x20- ft MILVAN

Weight - 4,700 lb

Riser - 8 ft

Date - 6 Nov 72

Container - 8x8x20- ft MILVAN
 Weight - 4,700 lb
 Riser - 8 ft
 Date - 6 Nov 72

Flight Number	Record Number	Airspeed (Kn)	Maneuver Or Input	Control Augmentation			Damping Ratio	Comments on Data
				Gain Roll	Gain Yaw	τ_{wo}		
661	1	Hover	Long.	0	0	0	0.22	Update instrumentation
	2		Lat					Update instrumentation
	3		Lat					Sys off
	4		Lat					Sys off
	5		Lat					Sys off
	6		Lat					Long. on lat off
	7		Lat					Sync
	8		Lat					S
	9		Lat					S
	10		Lat					Sync to on (S - A)
	11		Lat					S - A
	12		Lat					S - A
	13		Lat					AAELSS on*
	14		Lat					A*
	15		Lat					A*
	16		Lat					A*
	17		Lat					A*
	18		Lat					A*
	19		Lat					A*
	661A		1	Long.	0	0		0
661B	2	Lat	0	0	0	A		
	3	Lat	0	0	0	A		
	4	Lat	0	0	0	A		
	5	Lat	18°/in.	6°/in.	1.3	Contr 1 augmentation tests		
	6	Lat	19°	6°/in.	1.3	Contr. augmentation tests		
	7	Lat	24°	9°/in.	1.3	Contr. augmentation tests		
	8	Lat	24°/in.	9°/in.	1.3	Contr. augmentation tests		
	9	Lat	9°/in.	~4°	~1	Contr. augmentation tests		
	10	Lat	9°/in.	~4°	~1	Contr. augmentation tests		
	11	Lat	30°/in.	~4°	~1	Contr. augmentation tests		
	12	Lat	18°/in.	~4°	~1	Contr. augmentation tests		
	13	Lat	18°	~4°	~1	Contr. augmentation tests		
	14	Lat	18°	~4°	~1	Contr. augmentation tests		
	15	Lat	18°	~4°	~1	Contr. augmentation tests		
	16	Lat	18°	~4°	~1	Contr. augmentation tests		
	17	Lat	18°	~4°	~1	Contr. augmentation tests		
	18	Lat	18°	~4°	~1	Contr. augmentation tests		
	19	Lat	18°	~4°	~1	Contr. augmentation tests		
	20	Lat	18°	~4°	~1	Contr. augmentation tests		
	661A	1	Long.	0	0	0	Update 661A	
661B	2	Lat	0	0	0	A		
	3	Lat	0	0	0	A		
	4	Lat	0	0	0	A		
	5	Lat	18°/in.	6°/in.	1.3	Contr 1 augmentation tests		
	6	Lat	19°	6°/in.	1.3	Contr. augmentation tests		
	7	Lat	24°	9°/in.	1.3	Contr. augmentation tests		
	8	Lat	24°/in.	9°/in.	1.3	Contr. augmentation tests		
	9	Lat	9°/in.	~4°	~1	Contr. augmentation tests		
	10	Lat	9°/in.	~4°	~1	Contr. augmentation tests		
	11	Lat	30°/in.	~4°	~1	Contr. augmentation tests		
	12	Lat	18°/in.	~4°	~1	Contr. augmentation tests		
	13	Lat	18°	~4°	~1	Contr. augmentation tests		
	14	Lat	18°	~4°	~1	Contr. augmentation tests		
	15	Lat	18°	~4°	~1	Contr. augmentation tests		
	16	Lat	18°	~4°	~1	Contr. augmentation tests		
	17	Lat	18°	~4°	~1	Contr. augmentation tests		
	18	Lat	18°	~4°	~1	Contr. augmentation tests		
	19	Lat	18°	~4°	~1	Contr. augmentation tests		
	20	Lat	18°	~4°	~1	Contr. augmentation tests		
	661A	1	Long.	0	0	0	Update 661A	
661B	2	Lat	0	0	0	A		
	3	Lat	0	0	0	A		
	4	Lat	0	0	0	A		
	5	Lat	18°/in.	6°/in.	1.3	Contr 1 augmentation tests		
	6	Lat	19°	6°/in.	1.3	Contr. augmentation tests		
	7	Lat	24°	9°/in.	1.3	Contr. augmentation tests		
	8	Lat	24°/in.	9°/in.	1.3	Contr. augmentation tests		
	9	Lat	9°/in.	~4°	~1	Contr. augmentation tests		
	10	Lat	9°/in.	~4°	~1	Contr. augmentation tests		
	11	Lat	30°/in.	~4°	~1	Contr. augmentation tests		
	12	Lat	18°/in.	~4°	~1	Contr. augmentation tests		

TABLE XIII. TEST CONDITIONS FOR FLIGHT 662

Record Number	Maneuver Or Input	Control System Configuration												Type Test A-Active S-Sync	Damping Ratio	Comment on Data	
		Longitudinal						Lateral									
		Gain	Lag	Wo	Gain	Lag	Wo	Gain	Lag	Wo	Gain	Lag	Wo				
1	Instr update	0			0			0			0			0		Off	Into wind increases damping
2	Long. into wind																Use this for basic data
3	Long. crosswind																Lat crosswind increases damping
4	Lat crosswind																Shows roll-yaw beating
5	Lat into wind	0															Input too large
6	Long. crosswind	10	2.8	9.4													Input too large
7	Long. crosswind		1.8														Input too large
8	Long. crosswind		2.8														Input too large
9	Long. crosswind	10	4.3														Input too large
10	Lat into wind	0						0									Fair damping but drift
11	Lat into wind																Fair to poor
12	Lat into wind																Too large input
13	Lat into wind																Too large input
14	Lat into wind	0															Good data actuator stalling
15	Long. crosswind	10	4.3					0									Good data low damping
16	Long.	20	3.6					0									Actuator stalling
17	Long.	20	3.6					0									Run 17 better than 18
18	Long.	20	4.6					0									
19	Long.	10	4.3					10									
20	Long.																
21	Lat															A	Poor data stick motion
22	Lat															S to A	Poor data stick motion
23	Lat															S to A	Fair
24	Lat															S to A	Fair
25	Lat															S to A	Fair
26	Lat															A	Fair
27	Lat															A	Good data
28	Lat															A	Data bad
29	Lat															3N	Arm moves with stick
30	Lat															N	Arm lat drift negates system
31	Lat															N	Arm lat drift negates system
32	Lat															N	Arm lat drift negates system
33	Lat															3M	Arm lat drift negates system
34	Lat															0	Fair
35	Lat															0	Off
36	Lat															0	Off
37	Lat															0	Good data +35° yaw oscillation
38	Lat															0	Arm drift negates system
39	Lat															0	
40	Lat															0	
41	Lat															0	
42	Lat															0	
43	Lat															0	
44	Lat															0	
45	Lat															0	
46	Lat															0	
47	Lat															0	
48	Lat															0	
49	Lat															0	
50	Lat															0	
51	Lat															0	
52	Lat															0	
53	Lat															0	
54	Lat															0	
55	Lat															0	
56	Lat															0	
57	Lat															0	
58	Lat															0	
59	Lat															0	
60	Lat															0	
61	Lat															0	
62	Lat															0	
63	Lat															0	
64	Lat															0	
65	Lat															0	
66	Lat															0	
67	Lat															0	
68	Lat															0	
69	Lat															0	
70	Lat															0	
71	Lat															0	
72	Lat															0	
73	Lat															0	
74	Lat															0	
75	Lat															0	
76	Lat															0	
77	Lat															0	
78	Lat															0	
79	Lat															0	
80	Lat															0	
81	Lat															0	
82	Lat															0	
83	Lat															0	
84	Lat															0	
85	Lat															0	
86	Lat															0	
87	Lat															0	
88	Lat															0	
89	Lat															0	
90	Lat															0	
91	Lat															0	
92	Lat															0	
93	Lat															0	
94	Lat															0	
95	Lat															0	
96	Lat															0	
97	Lat															0	
98	Lat															0	
99	Lat															0	
100	Lat															0	

Container - 8x8x20-ft MILVAPN

Weight - 4,700 lb

Riser - 58 ft

Date - 9 Nov 72

Hover flight only

Forward longitudinal arm angle instruments out

TABLE XIV. TEST CONDITIONS FOR FLIGHT 663

Record Number	Airspeed (Kn)	Maneuver Or Input	Failures		Damping Ratio	Comments on Data
			Long.	Roll Yaw		
1	Hover	Update				On
2		Long.				On
3		Lat				On
4		Yaw				
5	Hover to 60					
6	80					
7			1/2 Aft		0.4	Yaw osc on to off to on Yaw osc off to on Lat off after this run
8		Failure				On
9		30° Turn				On
10		Failure	Aft		0.07	Off
11		Failure	Fwd		0.33	(S to A)
12		Long.				On
13						Off
14		Long.				On
15		Lat				Off
16		Yaw				Off to on
17	80					Off to on
18	90					On
19	80	30° Turn				Sync dash off PIO evaluation
20		IFR-PIO				(S to A) Dash off
21						AAELSS off dash off to on
22		IFR-PIO				AAELSS on at end eliminates PIO
23		1000 fpm PPD				Off
24	80	1500 fpm PPD				Off

Container - 8x8x20-ft MILVAN
Weight - 8,600 lb
Riser - 8 ft
Date - 10 Nov 72
Control gains same as in Flight 661

TABLE XV. TEST CONDITIONS FOR FLIGHT 664

Record Number	Airspeed (Kn)	Maneuver Or Input	Failures			Damping Ratio	Comments on Data
			Long.	Roll	Yaw		
1		Rotor Start					
2	Hover to 60						
3	85	Yaw osc					(S to A) good damping - stops yaw osc
4	100	Yaw osc					Not as strong damping as above
5	100	Yaw osc					On
6	90						
7	90						
8	90						
9	95-100	30° turn					Removed failure with sys off
10							
11	90	Yaw osc					
12	80	IFR					Sys off to on
13	80	IFR					PIO-IFR checks off to on
14	80	PPD					
15	80	Turn yaw osc					
<p>Container - 8x8x20-ft MILVAN Weight - 8,600 lb Riser - 8 ft Date - 10 Nov 72 Control gains same as in Flight 661</p>							

APPENDIX II
PILOT COMMENTS FROM ACTIVE EXTERNAL LOAD
STABILIZATION FLIGHT TEST PROGRAM

The pilot's comments concerning his evaluation and assessment of AAELSS performance characteristics as determined during the flight test phase of the investigation were as follows:

FLIGHT 656

The flight was initiated with a lift of the empty 8x8x20-foot MILVAN container from the MILVAN transporter to the load holding area.

The ballasted (8,600 pound) container was then lifted from the transporter, and testing commenced with an evaluation of load behavior following pilot-induced longitudinal and lateral oscillations. A ± 1 inch of control applied in a sine wave pattern in approximately a 4-second period was used to induce load swing. With the AAELSS off, a load swing amplitude of approximately ± 20 degrees in longitudinal and lateral was excited. The longitudinal oscillation exhibited light damping; however, the lateral oscillation was well damped and required only 1.5 to 2 cycles to stop swinging.

The AAELSS functioned correctly in the SYNC mode, and results were similar to those with the system off.

The ACTIVE mode was evaluated by exciting longitudinal, lateral, and directional load oscillations with the system off and immediately switching to the ACTIVE mode. An increase in load damping was apparent with the ACTIVE system on.

The flight was terminated at this point due to an instrumentation wiring failure. The qualitative assessment of system operation and load behavior revealed the following:

- At this weight and sling configuration, the load appeared fairly well damped in longitudinal oscillation and well damped in lateral and directional oscillations.
- The AAELSS appeared to provide an increase in damping; however, the effect was less evident due to the system-off damping.
- The heavy load caused hydraulic bypassing of the pendant actuators at low angles, thereby reducing the potential effectiveness of the AAELSS.

These factors indicated the desirability of utilizing the empty MILVAN for the AAELSS optimization tests.

Binding of the forward arm required retraction to be performed manually by the ground crew.

FLIGHT 657

The empty container was used on this flight. Pilot-induced load oscillations produced a significant amplitude (± 25 degrees). Load oscillations with the AAELSS off were not as well damped laterally and were more effectively damped longitudinally than was the case with the ballasted MILVAN. The improved longitudinal damping is thought to be due to a binding in the forward longitudinal arm and the deteriorated lateral damping due to the decreased load weight.

The ACTIVE mode provided better damping longitudinally with the light load and a very dramatic improvement in lateral and directional load damping.

An evaluation of damping with a range of lag time constants revealed the previously selected nominal value to be most effective. During this investigation, a long-period oscillation was observed in the arms. This oscillation was reported by the telemetry (TM) observers and was not initially recognized by the flight crew.

The washout time constant was adjusted in an attempt to eliminate the long-period oscillation, but without success.

The arm actuator hardover failures were evaluated to check out the system, revealing that the forward arm was bound in the half-retract position and that the lateral hardover control circuitry was reversed.

The flight was terminated due to binding of the forward arm.

Qualitatively, the ACTIVE mode exhibited a dramatic improvement in lateral load stability. The empty MILVAN configuration appears best for use in AAELSS optimization because it allows greater freedom in aircraft maneuvering and greater amplitudes of load oscillation.

The forward arm was completely bound in the stowed position, and the aircraft was returned to Philadelphia for rework of the pendant longitudinal bearings.

FLIGHT 658

The aircraft was flown from Millville, N.J., airport to Boeing Vertol Center 3E in Philadelphia.

FLIGHT 659

This flight was conducted to ferry the aircraft to Millville from Center 3E and to check TM reception in the desired test area. The flight was routine, and TM reception appeared to be adequate for the conduct of the intended tests. The lead from the TM van to the antenna had been changed following the check made on Flight 655.

FLIGHTS 660 AND 660A

During hover tests, pilot-induced load oscillations produced lightly damped response with AAELSS off. The load stability with the system off was representative of the normal two-point suspension configuration, indicating that the results of previous tests were adversely affected by arm bearing friction.

The ACTIVE mode provided a very dramatic increase in load damping as evidenced by the following qualitative comparisons:

	<u>Cycles to Damp</u>	
	<u>AAELSS Off</u>	<u>AAELSS Active</u>
Longitudinal	5-6+	1-1.5
Lateral	2-5	0.5 - 1.5
Directional	2-5	1 - 1.5

Optimization of shaping of the AAELSS ACTIVE mode was completed.

Qualitatively, the ACTIVE mode eliminated any tendency to excite the load in normal hover maneuvering. A typical load lift, shuttle, and deposit were performed with a rearward lift-off and 180-degree heading change in the shuttle prior to load deposit. The maneuver was performed both with AAELSS off and ACTIVE, and the technique was intentionally abrupt with an attempt at minimum time for the maneuver. The load was very stable in the ACTIVE mode; however, lightly damped load oscillations were excited with the system off, and hover time was required to allow the load to damp prior to touchdown.

The arm actuator hardover tests were completed as scheduled with proper functioning.

Transitions from 0 to 60 knots and back to 0 knots were performed over the airport with acceptable load behavior.

In forward-flight tests, the aircraft was flown to test altitude at 60 knots and arm actuator hardover failure tests were conducted. Hardovers in all axes were evaluated, and directional failures were considered most significant due to the side lift and lateral swing of the load, which increased drag angle. This maneuver is equivalent to an abrupt entry into a sideslip and is envisioned as the worst case at high speeds.

Pilot-induced disturbances in longitudinal, lateral, and directional axes produced load oscillations with AAELSS off that were representative of a two-point sling configuration. With AAELSS off, longitudinal oscillations were fairly well damped due to drag; lateral oscillations were also fairly well damped; directional oscillations were lightly damped and coupled the familiar lateral swing and increased drag angle previously described into a dutch-roll behavior.

The ACTIVE mode provided very dramatic positive damping to all load motions during turn maneuvers, climbs, and descents, which were conducted with the system both ACTIVE and off.

The aircraft was accelerated to 80 knots, where the directional dutch-roll behavior was observed. The ACTIVE mode effectively damped this oscillation; however, there was a long-period directional pendant drift which excited or allowed the load to oscillate or drift ± 5 to 10 degrees at a 20-second plus period.

In forward flight, an RFI problem excited by the VHF transmitter caused the arms to jerk each time a transmission was made from the helicopter.

The flight was terminated before 80-knot data could be collected due to a low fuel state; however, 80 knots appears to be the maximum safe speed to sustain an arm actuator directional hardover at this load weight.

FLIGHT 661

The AAELSS was tested in hover with a loaded container. Manual pulse flight control longitudinal, lateral, and directional inputs of an approximate sine wave pattern with control amplitudes of approximately 1-1/2 inches to induce swinging of the load were made:

- System Off
- In SYNC mode
- In SYNC mode going to ACTIVE mode during load oscillation
- In ACTIVE mode

Load behavior following pilot excitation with the system off was a lightly damped oscillation requiring approximately four to five cycles to damp and a slightly better damped lateral oscillation requiring two to four cycles to damp. The ACTIVE mode was quite effective in damping the load from longitudinal and directional inputs, with damping achieved in one to one and one-half cycles. It also performed well from lateral inputs,

with damping achieved in one-half to one cycle, but it was as impressive because damping in this axis was good even with the system off. Lateral inputs with control augmentation were made, but results were difficult to assess because a broken wire to the aft arm prevented movement of this arm. Forward arm reaction was normal.

FLIGHT 661A

AAELSS testing in hover with the loaded container was conducted. Manual flight control system pulses to induce swinging of the load were applied in the longitudinal, lateral, and directional axes with the system in the ACTIVE mode at optimum gains with positive damping demonstrated.

Control augmentation was checked in lateral and directional axes with nominal, high, and low gains (time constants) to determine the optimum circuitry characteristics. Results of the control augmentation evaluation indicated no significant or noticeable difference in load behavior from a qualitative point of view; therefore, quantitative data must be analyzed to determine the effect of control augmentation.

Transition out of the field was accomplished in the ACTIVE mode. No testing was accomplished because the TM traces indicated a longitudinal restriction on the aft arm hook movement. The detent pin fell from this arm hook while the hook was being checked by the ground crew with the aircraft hovering. There was no restriction in the hook during a ground check following shutdown.

FLIGHT 661B

AAELSS checks in hover with the loaded container were performed to complete the hover testing with 8-foot risers. Manual flight control system longitudinal pulses to induce load swinging were performed with the system off, in the ACTIVE mode, and in SYNC to ACTIVE mode with lag time constants of 1.8, 1.3, and 2.8 seconds.

During these hover checks, there was noticeable clipping of the TM traces of both forward and aft pendant hook longitudinal positions. This was attributed to shifting of the null of the position synchro risers. The flight was terminated without leaving the field.

FLIGHT 662

This was a hover evaluation of the system with an empty MILVAN container suspended on a 50-foot cable riser plus an 8-foot nylon riser. This test was commenced with longitudinal and

lateral pilot-induced control excitations to start the longitudinal and lateral pendulum oscillation in the load. The surface winds were approximately 15 knots, gusting to 40 knots, on this flight, and a significant damping to load oscillations was noted when the plane of the pendulum oscillation was into and away from the surface wind.

Subsequent to initial checks, all excitations were accomplished for longitudinal excitations with the aircraft oriented with a right crosswind and lateral oscillations with the aircraft headed into the wind. With the AAELSS off, pilot-induced control oscillations excited the long-period pendulum oscillation, with approximately five to six cycles required to damp the load. With the AAELSS in the ACTIVE mode, oscillations were damped very effectively in one and one-half to two and one-half cycles.

In normal hover maneuvering with the load on the 58-foot riser, there was no tendency to excite long-period oscillations with the AAELSS in the ACTIVE mode. An investigation of a range of lag time constant values and gain values was completed, and apparent optimum values were identified. The control augmentation was evaluated with pilot-induced steps in lateral and directional control. Once again the operation of control augmentation was confirmed, in that the arms were following the control inputs; however, a qualitative assessment of control augmentation indicated no significant improvement in load control.

A typical load transport maneuver was conducted for comparison of aircraft and load behavior with the AAELSS on and off. This maneuver consisted of a load lift-off with rearward transitioning into sideward flight with a 180-degree heading change from the original heading and lift-off. An acceleration to approximately 30 knots was accomplished during the 180-degree turn; then the aircraft was decelerated to a hover, the load oscillations were allowed to damp, and the load was deposited. With the AAELSS in the ACTIVE mode, there was less tendency for load oscillations to be excited and a minimum time was required to stabilize the load prior to load touchdown. The 58-foot suspension system tests were completed as planned, with all data appearing representative of this configuration, and the load was landed and reconfigured with 8-foot risers to complete the empty container tests with short suspension configuration. System performance to damp pilot-induced oscillations was evaluated in longitudinal, lateral and directional axes with the apparent optimum lag time constant and gain values as determined on previous flights. The typical load transport maneuvers described in the 58-foot suspension tests were repeated in this configuration with the system off and on in the ACTIVE mode. With the ACTIVE system, a minimum of load oscillation was noted, and the most efficient flight maneuvering was possible.

The short riser evaluation on this flight was conducted with no paralleling cable at the top of the nylon slings. Therefore, this data is representative of the simple two-point sling system configuration.

FLIGHT 663

This flight was conducted to collect data in forward flight on the loaded MILVAN container ballasted to 8,600 pounds on a short sling configuration consisting of 8-foot risers, 11-foot forward slings, and 8-foot aft slings with a paralleling cable. The load was acquired, and a hover evaluation of system operation indicated that the system was functioning normally. In the transition to forward flight, the system operated properly, and the aircraft was flown to test altitude.

In the climbout to test altitude at approximately 70 knots, a moderate neutral yaw oscillation was noted with the AAELSS off. This oscillation was approximately ± 7 to 10 degrees of container yawing, which appeared to be the aft end of the MILVAN oscillating about the forward attaching point. This induced a yawing oscillation in the aircraft and constituted a very uncomfortable environment. The AAELSS was placed in the ACTIVE mode, and the neutral yaw oscillation was immediately damped. This was a most significant demonstration of ACTIVE AAELSS operation. The system was turned off, and the neutral yaw oscillation quickly developed again; and again, it was effectively damped when the AAELSS was returned to the ACTIVE mode.

The aircraft was accelerated to the initial test speed of 80 knots at altitude, and the planned tests were commenced with AAELSS arm actuator hardover checks, with arms forward, aft, left, and right investigated. These tests indicated the directional hardover failure to be most critical, as this induced a yawing of the container which coupled to a sideward motion and increased the lateral and drag angle of the load. All indications were that this particular hardover failure would be most critical at maximum speed, as the dynamics of the container produced a fairly heavy lateral and aft longitudinal swing following the hardover. AAELSS operation was assessed in load damping following pilot-induced excitations in longitudinal, lateral, and directional axes with the system off and then in the ACTIVE mode. In all cases, the stabilization system provided a very positive and impressive damping to any load motion in the ACTIVE mode. Early in the testing, the forward arm failed hardover laterally. The lateral system was disabled, and the flight continued in an effort to collect data on the longitudinal system.

An IFR evaluation was conducted at 80 knots with the pilot controlling the aircraft under an instrument hood. Tests included

flight control with DASH off and on and with pilot-in-the-loop going to pilot-cut-of-the-loop with the AAELSS off and then on in the ACTIVE mode. With the pilot-in-the-loop in smooth air conditions, there was a tendency to excite a longitudinal load oscillation at the pendulum frequency of the load and sling combination. This longitudinal excitation was identical to that reported in previous two-point suspension system testing, wherein the pilot responds to the longitudinal acceleration induced by the load on the aircraft. This pilot-controlled excitation closes the load oscillation loop and excites a fairly heavy neutral longitudinal swinging. This oscillation of pilot-in-the-loop excitation could be broken if the pilot either referred to his visual horizon to sort out and separate the load-induced accelerations from the normal maneuvering cues, or went out of the control loop and allowed the DASH to provide attitude and speed stability. The system was switched to the ACTIVE mode during a pilot-in-the-loop control excitation situation, and it provided a very positive damping of this longitudinal load oscillation; it eliminated the tendency of the pilot to excite the longitudinal oscillation in approximately one-half to one cycle. Due to the previously reported lateral arm failure, the flight was aborted following the check of the pilot-induced longitudinal oscillation excitation tendencies at 80 knots.

FLIGHT 664

This flight was conducted to collect the remainder of the required data on the loaded container in cruise flight conditions. The aircraft and load were accelerated to 100 knots, and the tests commenced with AAELSS pendant actuator hardover checks. Again, the most critical hardover failure appeared to be the directional failure which induced the yawing, lateral swinging, and aft swinging of the load.

AAELSS operation to damp pilot-induced longitudinal, lateral, and directional oscillations was considered to be very impressive, with all induced oscillations damped in from one-half to one cycle. At the higher speeds, pilot-induced oscillations resulted in greater load longitudinal swinging due to the drag loads at the higher speeds, and accelerations in the airframe caused by load swinging were heavier. The improved damping provided by the ACTIVE system was more significant and qualitatively more appreciated at this high-speed condition.

Tests conducted included system response to pilot-induced excitations, 30-degree banked turns to the left and right, partial-power descents, and a pilot-in-the-loop check of simulated IFR conditions. Again, at this speed with pilot-in-the-loop, a longitudinal excitation developed. This excitation was very effectively damped by placing the AAELSS in the ACTIVE mode. One hundred knots was identified as the limit speed with

this configuration due to the dutch-roll motion of the load following directional system excitations. This motion occurred occasionally at random with the AAELSS turned off.

The typical behavior of this MILVAN container in forward flight at high speeds is to trail very nicely under the aircraft in a zero-sideslip, smooth-air situation; however, when disturbed by gusts or slight sideslips in the aircraft, the load tends to yaw and swing out to one side and remain there. This lateral positioning of the load increases the drag of longitudinal trail angle and tends to induce a slipping condition in the aircraft.

The IFR evaluation indicated that with the pilot out of the loop, the DASH and AFCS could provide good cruise condition hold with no excitation of load oscillation. However, with the pilot in the control loop, any load oscillation or swinging induces linear accelerations in the aircraft to which the pilot immediately, and unknowingly, responds with a control displacement. The AAELSS actively damped all load response and therefore eliminated the pilot-induced oscillations.

APPENDIX III
LOAD STABILIZATION SYSTEM PROBLEMS

Progress of the test program was frequently interrupted by system component failure or deterioration which prevented optimum system performance. Problems, flight of occurrence, and corrective action are summarized below.

FLIGHT 650

Problem

Hydraulic leakage from longitudinal arm actuators caused by disconnect of quick-disconnect fitting in AAELSS hydraulic return line. With this line disconnected, the arms could not be retracted hydraulically. Manual retraction by ground crew was very difficult because of hydraulic lock.

Corrective Action

Added fitting to lengthen flex hydraulic return line between dual point suspension beam and aircraft. Added a manual pressure bleed valve to AAELSS hydraulic return line.

FLIGHT 651

Problem

Hydraulic leak from AAELSS because of a broken fitting at a pressure relief valve.

Corrective Action

Replaced Dural fitting in AAELSS actuator control valve assemblies with steel fittings. Installed solenoid shutoff valve in AAELSS hydraulic pressure line upstream of quick-disconnect fitting and a check valve in return line downstream of quick-disconnect fitting to prevent fluid loss in case of a broken line between aircraft and shutoff valve on dual point suspension beam.

FLIGHT 652

Problem

Forward arm went hardover forward during retraction.

Corrective Action

Renulled longitudinal synchro potentiometer for forward arm.

FLIGHT 653

Problem

Control augmentation inoperative. Arms moved in wrong direction during actuator hardover checks. Arms not centered during retraction.

Corrective Action

Increased gains in AAELSS control box for control augmentation. Hardover box relabeled for input direction. Lateral bolts for both arms drilled and pinned to prevent slippage which moved synchros. Installed shim in forward arm to eliminate lateral play which broke synchro coupling. Renulled longitudinal and lateral synchro potentiometers for both arms.

FLIGHT 654

Problem

AAELSS arm actuator hardover motion not apparent on aircraft indicators or on TM.

Corrective Action

Changed AAELSS actuators hardover failure box output from linear to rate.

FLIGHT 656

Problem

Longitudinal binding of forward arm. Restricted lateral movement of aft arm hook.

Corrective Action

Freed forward arm longitudinal binding by reshimming and retorquing attachment bolts of pillow blocks. Freed locked detent pin of aft arm hook.

FLIGHT 657

Problem

Severe longitudinal binding of forward arm. Excessive lateral motion of dual point suspension beam.

Corrective Action

Installed alum-bronze bushings in longitudinal pillow blocks for both arms. Aligned pillow blocks with machined shims and line bored bushings. Installed steel bushings over bearing surfaces of longitudinal trunnions of forward arm. Installed pressure-feed grease reservoirs for pillow blocks of forward arm. Replaced aluminum-faced rubber lateral restraint blocks on dual point suspension beam with solid aluminum blocks. Replaced rubber lateral restraint wedges with rubber-faced aluminum wedges.

FLIGHT 660

Problem

Hydraulic leakage because of a loose "B" nut in AAELSS.

Corrective Action

Tightened "B" nut.

FLIGHT 660A

Problem

High-frequency longitudinal arm oscillation during VHF transmissions.

Corrective Action

RFI problem minimized by utilizing a portable UHF transceiver in chase airplane so test transmissions out of field could be made on UHF instead of VHF.

FLIGHT 661

Problem

Aft arm inoperative.

Corrective Action

Repaired two broken synchro signal wires on aft arm.

FLIGHT 661A

Problem

Restricted longitudinal movement of aft arm hook.

Corrective Action

Hook detent pin fell out during hover check, relieving movement restriction.

FLIGHT 661B

Problem

Clipping of both arm hooks longitudinal TM traces caused by synchros shifting.

Corrective Action

Spot-welded synchro drive pins in bolts for longitudinal motion of arm hooks to prevent movement. Added shimming washers to prevent end play of bolts. Replaced synchro coupling for forward arm hook longitudinal motion. Renuled arm hook synchros.

FLIGHT 663

Problem

Forward arm hook immobile laterally. Hydraulic leakage because of a loose "B" nut in AAELSS.

Corrective Action

Reconnected loose wire on forward arm hook lateral motion synchros. Retightened and safety-wired loose "B" nut.

FLIGHT 664

Problem

TM trace indicated no longitudinal movement of aft arm hook (synchro attachment ears broken). Excessive lateral movement of dual point suspension beam (rubber faces came off lateral restraint wedges).

Corrective Action

No corrective action taken. Program was terminated.